

Reconstitution of bacterial cytokinesis: the Z-ring

DISSERTATION

**Zur Erlangung des akademischen Grades
Doctor of Philosophy
(Ph.D)**

vorgelegt
der Fakultät Mathematik und Naturwissenschaften
der Technischen Universität Dresden

von

Senthil Arumugam

Geboren am September 7, 1983 in Surat, India

July 2012

Reviewers: **Prof. Petra Schwille** and **Prof. David Sherratt**

Date of Defense: **07.11.2012**

Date of Submission: **11.08.2012**

*Dedicated to
Prof. Veronica Rodrigues
(1953-2010)*

Abstract

Prokaryotic cell division is one of the most fundamental processes in biology, but the dynamics and mechanics are far from being understood. In many bacteria, FtsZ, a tubulin homologue assembles into a ring-like structure – Z-ring at precisely the middle of the cell. This accurate site selection is dependent on the Min proteins. Min D and MinE self-organise into waves *in vitro*, and oscillate pole to pole *in vivo*. MinC is thought to couple the Min oscillations to FtsZ by direct interaction. The mechanism of inhibitory action of MinC on FtsZ assembly is not known. Critical to the understanding of regulation of FtsZ by MinC and other proteins and its probable role in force generation is the organisation, structure and the dynamics of the Z-ring. Current models of the FtsZ filament organization in the Z-ring argue between two different structures – (i) short overlapping protofilaments with lateral interactions and (ii) few long annealed protofilaments with or without lateral contacts.

Our observations of the characteristics of polymerization and turnover studies using fluorescence microscopy suggest that the FtsZ filament is a continuous and irresolute bundle. The results are consistent with a structure where the turnover happens throughout, and any specialised structure resulting in a GTP cap like structure can be ruled out. We show that the turnover rates and hydrolysis rates are similar arguing for a model in which subunit leaves as soon as it hydrolyses GTP. On the basis of crystal structures, we cloned the N-terminal of FtsZ, which acts as a C-terminal end capping fragment and is able to interact with monomers. The end-capping fragment, NZ can disassemble the FtsZ polymers, without influencing the GTPase activity, offering a comparable standard for the activity of MinC. On the basis of our observations, we propose a model on how MinC can disassemble FtsZ polymers. Furthermore, our data shows that the Min CDE system is sufficient to cause spatial regulation of FtsZ provided FtsZ is dynamic.

How the Z-ring takes the form of a functional helical or ring-like structure remains unclear. Extensive modelling approaches have tried to explain the ring formation and force generation. Previous studies have qualitatively shown bending of liposome membranes by FtsZ filaments. We hypothesised that the presumably intrinsically curved filaments should respond to pre-curved substrates, and the alignment should be quantifiable. This should ascertain whether or not FtsZ has intrinsic curvature and/or actively induces any force. Thus, we investigated how FtsZ filaments respond to a range of curvatures, which mimic different stages of the division process.

Our results show that the FtsZ filaments possess intrinsic curvatures as well as spontaneous twist. This facilitates the formation of Z-ring by utilizing geometrical cues. Our results are in agreement with consistent helical FtsZ polymers observed *in vivo* by Cryo-EM or super resolution microscopy. The alignment of filaments over a range of curvature suggests that the filaments have considerable flexibility, which strongly suggests reconsidering possible

mechanisms of force generation. Moreover, the developed assay constitutes a valuable platform to further study proteins involved in modifying curvature of FtsZ filaments.

In summary, by reconstituting the FtsZ filament *in vitro*, we have elucidated the nature of FtsZ filaments. The dynamics of FtsZ filaments allows them to be inhibited by MinC, thus cooperating with the Min waves. The presence of intrinsic curvature and twist facilitates their formation into a ring necessary for the cell to carry out cytokinesis.

Zusammenfassung

Die Zellteilung bei Prokaryoten ist ein elementarer biologischer Vorgang, dessen Dynamik und Mechanik jedoch noch nicht verstanden sind. Bei vielen Bakterien fñgt sich das Protein FtsZ, ein Homolog zu Tubulin, zu einer ringartigen Struktur (Z-Ring) zusammen, die exakt in der Mitte der Zelle positioniert ist. Die genaue Positionierung an dieser Stelle hñngt von den Min-Proteinen ab. MinD und MinE bilden *in vitro* von sich selbst aus Wellen, und oszillieren *in vivo* von Pol zu Pol. Es wird vermutet, dass diese Min-Oszillationen durch direkte Interaktion über MinC mit FtsZ gekoppelt sind. Der Inhibitionsmechanismus von MinC auf FtsZ ist nicht bekannt. Das Wissen über die Organisation, Struktur und Dynamik des Z-Rings ist notwendig für das Verständnis sowohl darüber, wie FtsZ von Min C und anderen Proteinen reguliert wird, als auch über seine vermutete Rolle in der Krafterzeugung. Momentan existieren mehrere Modelle, welche die Organisation der FtsZ-Filamente beschreiben, so einerseits eines mit kurzen, überlappenden, oder aber mit langen, aneinandergefügten Protofilamenten.

Unsere Beobachtungen zur Charakterisierung der Polymerisierung mithilfe von Fluoreszenzmikroskopie deuten darauf hin, dass das FtsZ-Filament aus einem kontinuierlichen und amorphen Faserbñdel besteht. Diese Ergebnisse stimmen mit der Annahme einer Struktur mit rñumlich gleichmässigen Umsatz überein, somit kann eine spezialisiertere Struktur in der Art eines GTP-„capping“ *ausgeschlossen* werden. Wir zeigen, dass die Umsatz- und Hydrolisierungsraten ähnlich sind, was darauf hindeutet, dass eine Untereinheit die Struktur verlässt, sobald sie GTP hydrolysiert hat. Basierend auf der Kristallstruktur klonierten wir den N-Terminus von FtsZ, welcher als Deckel für den C-Terminus fungiert und mit Monomeren interagieren kann. Dieses „capping“ Fragment kann FtsZ-Polymere zerlegen, ohne die GTPase-Aktivität zu beeinflussen, was einen vergleichbaren Standard für MinC-Aktivität anbietet. Aufgrund unserer Beobachtungen stellen wir einen Modellmechanismus für die Depolymerisierung von FtsZ-Polymeren durch MinC auf. Zusätzlich zeigen wir, dass das MinCDE-System ausreicht, um FtsZ rñumlich zu regulieren, unter der Voraussetzung, dass FtsZ dynamisch ist.

Wie genau sich der Z-Ring zu einer helix- oder ringartigen Struktur formt, ist ungewiss. Umfassende Modelle beschreiben die Erzeugung des Z-Rings und die anschliessende Krafterzeugung, und qualitative Studien konnten die Krñmmung von Liposommembranen durch FtsZ-Filamente zeigen. Wir vermuten, dass intrinsisch gekrñmmte Filamente auf gekrñmmte Substrate reagieren, und dass diese Ausrichtung quantifizierbar ist. Dies lässt uns feststellen, ob FtsZ eine intrinsische Krñmmung besitzt und/oder aktiv Kraft ausñbt. Dementsprechend untersuchten wir, wie FtsZ-Filamente auf verschiedene Substratkrñmmungen reagieren, die verschiedene Phasen des Zellteilungsvorgangs darstellen.

Die Resultate zeigen, dass die Filamente sowohl intrinsische Krñmmung als auch spontanen Torsion besitzen. Dies erleichtert die Bildung des Z-Rings durch geometrische Signale.

Unsere Resultate stimmen mit dem Modell von einheitlichen helixförmigen Polymeren überein, wie sie *in vivo* durch Cryo-EM oder Superresolutionsmikroskope beobachtet wurden. Die Anordnung der Filamente auf Substraten mit unterschiedlichen Krümmungen deutet darauf hin, dass diese Filamente sehr flexibel sind, was wiederum verschiedene Kraftgenerierungsmechanismen wahrscheinlich macht. Weiterhin bietet die entwickelte Probe eine hilfreiche Technik, um weitere Proteine, welche die Krümmung von FtsZ beeinflussen könnten, zu untersuchen.

Anhand der Rekonstitution der FtsZ-Filamente *in vitro* konnten wir die Beschaffenheit dieser Filamente aufklären. Die Dynamik der FtsZ-Filamente ermöglicht eine Inhibition durch MinC, wodurch sie mit den Min-Wellen wechselwirken können. Ihre intrinsische Krümmung und Torsion erleichtert die Bildung eines für die Zellteilung notwendigen Rings.

Table of Contents

1. Introduction	1
1.1 The Eukaryotic Cytoskeletons.....	1
1.2 The Prokaryotic Cytoskeletons.....	1
1.2.1 <i>The Tubulin/FtsZ/TubZ family</i>	2
1.2.2 <i>The Actin/MreB/ParM/FtsA family</i>	4
1.2.3 <i>Intermediate filament like family</i>	4
1.2.4 <i>MinD/ParA/ParF/Soj (WACAs)</i>	5
1.3 On the evolution of cytoskeletons.....	6
1.4 Bacterial cell division.....	8
1.4.1 <i>FtsZ and the Z-ring</i>	9
1.4.2 <i>Positioning of the Z-ring – Nucleoid Occlusion and Min system</i>	12
1.5 Objective of this work.....	16
2. Materials and Methods	19
2.1 Constructs.....	19
2.2 Expression and purification of proteins.....	20
2.2.1 <i>Growth and harvest of bacteria</i>	20
2.2.2 <i>Purification of proteins</i>	20
2.2.3 <i>Protein labelling with fluorescent dyes</i>	22
2.3 GTPase activity assays.....	23
2.4 Microscopy.....	23
2.4.1 <i>Confocal Laser Scanning Microscopy</i>	23
2.4.2 <i>Total Internal Reflection Fluorescence Microscopy</i>	23
2.5 Fluorescence Correlation Spectroscopy.....	24
2.6 Fluorescence Intensity Distribution Analysis.....	24
2.7 Lipid membrane systems.....	25
2.7.1 <i>Supported lipid bilayer as model membranes</i>	25
2.7.2 <i>Supported lipid bilayer formation</i>	25
2.7.3 <i>Curved support substrate preparation</i>	25
2.7.4 <i>Giant Unilamellar Vesicles</i>	27
2.8 AFM imaging and data processing.....	27

3. Results I: The FtsZ filaments are a disordered dynamic bundle with constant turnover throughout the length.	29
3.1 Preface	29
3.2 The Z-ring in vivo – Assembly and Dynamics	30
3.3 Filaments assemble on the membrane by annealing/ disassemble by fragmentation ...	31
3.4 The FtsZ filaments are an irresolute bundle devoid of dynamic instability	35
3.5 Exchange of nucleotides in FtsZ bundles	36
3.6 NZ binds to the FtsZ filaments, disassembles by sequestration of monomers	38
3.7 Conclusions	40
4. Results II: Dimeric MinC disassembles FtsZ	43
4.1 Preface	43
4.2 MinC-GFP is a strong dimer	44
4.3 Dimeric MinC depolymerises FtsZ filaments by occupying binding sites	45
4.4 Trapped FtsZ-GDP with binding site occupation by MinC model.....	50
4.5 MinCDE waves spatially regulate FtsZ polymers	53
4.6 Conclusions	55
5. Results III: Z-ring forming FtsZ filaments are intrinsically curved with a twist.....	57
5.1 Preface	57
5.2 FtsZ bends the membrane towards its own intrinsic curvature	59
5.3 FtsZ filaments respond to the curvature of supported bilayers	60
5.4 FtsZ polymers on membrane curvatures higher than $1 \mu\text{m}^{-1}$	61
5.5 Spontaneous curvature and twist in FtsZ filaments.....	64
5.6 Conclusions	65
6. Outlook: Towards a 3-dimensional reconstitution of bacterial cell division..	69
7. Concluding remarks and additional research directions..	71
Appendix	75
Abbreviations	83
Bibliography	85
List of Publications	94
Acknowledgements	95
Declaration.....	97

Chapter 1

Introduction

1.1 The Eukaryotic Cytoskeletons

Cytoskeletons are dynamic structures that result from self-assembly of proteins. Cytoskeletons or cell frameworks or scaffolds exhibit a rich dynamical behaviour and are involved in various essential functions. The eukaryotic cytoskeletal elements are built around different molecular components, namely, **actin**, **microtubules** and **intermediate filaments** (Fig.1.1). These three cytoskeletal elements display completely different architecture and dynamics. Mechanical strength is an inherent feature of these multi-stranded protein polymers. Coupling of the building units of these polymers to nucleotide hydrolysis makes the polymerization cycles energy dissipating. This allows rapid dynamics, inherently and by other regulating proteins and for force generation. Together with the mechanical strength and the rich dynamics, the eukaryotic cytoskeletons are involved in functions like chromosome segregation or cell division. Together with these cytoskeletal proteins, other proteins which highly regulate the dynamics, stability, length, geometry and number have evolved. In concert with these proteins, the cytoskeletal elements are able self-organise into large-scale complex structures like the mitotic spindle or the lamellipodia.

1.2 The Prokaryotic Cytoskeletons

Historically, lack of cytoskeletal elements was thought to be one of the defining distinctions between prokaryotes and eukaryotes. Before 1990, cytoskeleton was presumed to have only evolved in eukaryotes; although there have been sporadic reports of bacterial actin and tubulin in 1970s and 1980s. The first strong suggestions of prokaryotic cytoskeleton came in the form of bacterial homolog of tubulin from three independent groups. Subsequently, further studies have discovered actin homologues which are not only restricted to cytoskeletal forms.

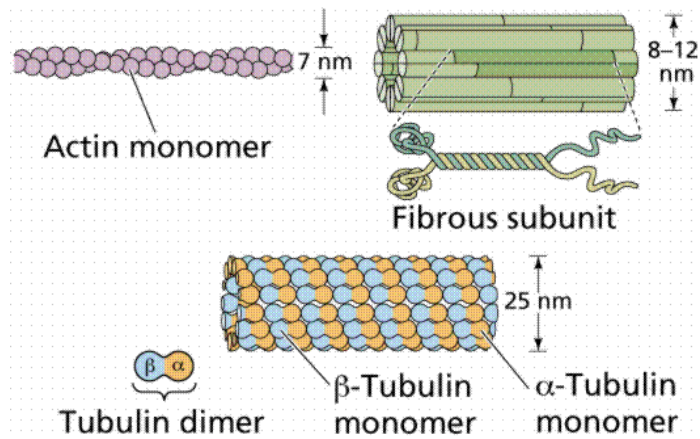


Fig.1.1 The eukaryotic cytoskeletal system consisting of Actin, Microtubules and the intermediate filament systems.

The absence of eukaryotic motor protein – like entities in the prokaryotes have resulted in the prokaryotes evolving independent mechanisms using the filaments to move cellular contents like plasmids or other proteins around. Therefore, many filaments in prokaryotes may be referred to as ‘cytomotive’ than ‘cytoskeletal’ [1]. As with the eukaryotic Actin, Tubulin and Intermediate filaments, the prokaryotic cytomotive/skeletal proteins can be divided into four classes – the Actin like, the Tubulin like, the Intermediate filaments like and the Walker A cytoskeletal ATPases (WACAs). The WACAs are an additional group of cytoskeletal proteins, structurally unrelated to actin, tubulin and intermediate filaments, but also capable of filament assembly [1].

1.2.1 The Tubulin/FtsZ/TubZ family

FtsZ was shown to form ring-like structures at the division septum of *E.coli* cells [2]. In 1991, it was the first bacterial protein suggested to have a cytoskeletal function. Various studies found that the tubulin homolog FtsZ bound and hydrolysed GTP similar to tubulin and that it had a seven amino acid sequence, GGGTGTG [3-5], virtually identical to the ‘tubulin signature sequence’. Other groups also showed that FtsZ assembles into filamentous structures and forms different conformations depending on the bound nucleotide [6, 7].

The Tubulin and Tubulin-like proteins appears to have a conserved longitudinal contact between adjacent subunits (Fig.1.2). The subunits consist of two conserved domains with the N-terminal domain providing the nucleotide binding and one interface of the active contact, whereas the C-terminal provides the other. With filament assembly, contacts between the two interfaces are made. The ability of second interface to activate the nucleotide hydrolysis links nucleotide hydrolysis to polymerization. The similarity of FtsZ with tubulin was shown by the determination of its crystal structure [8, 9].

In tubulin, filament assembly is thought to cause a conformational change that in turn increases the hydrolysis rate in subunits other than the end one. This enables the filament to trap the nucleotide in the lattice with no exchange, resulting in dynamic instability [10, 11].

Apart from FtsZ, several tubulin-like proteins exist in prokaryotic cells [1], e.g. **TubZ** and **BtubAB**. However, these proteins do not assemble into a ring-like structure. TubZ is a bacterial plasmid-borne protein which assembles filaments to push plasmids apart in the cell for segregation [12]. TubR, an adaptor protein might link the growing TubZ and the plasmids. BtubAB was found in some deep-branching *Verrucomicrobia* and forms longitudinal protofilaments with alternating A and B subunits [13-15]. However, unlike tubulin heterodimers, every longitudinal interface forms a fully active GTPase. The sequences and the structures of BtubAB are very similar to eukaryotic $\alpha\beta$ tubulin. This fact and the fact that no other genes in these organisms are so closely related to any eukaryotic ones prompted the hypothesis that the BtubAB genes were transferred from eukaryotes by horizontal gene transfer [14].

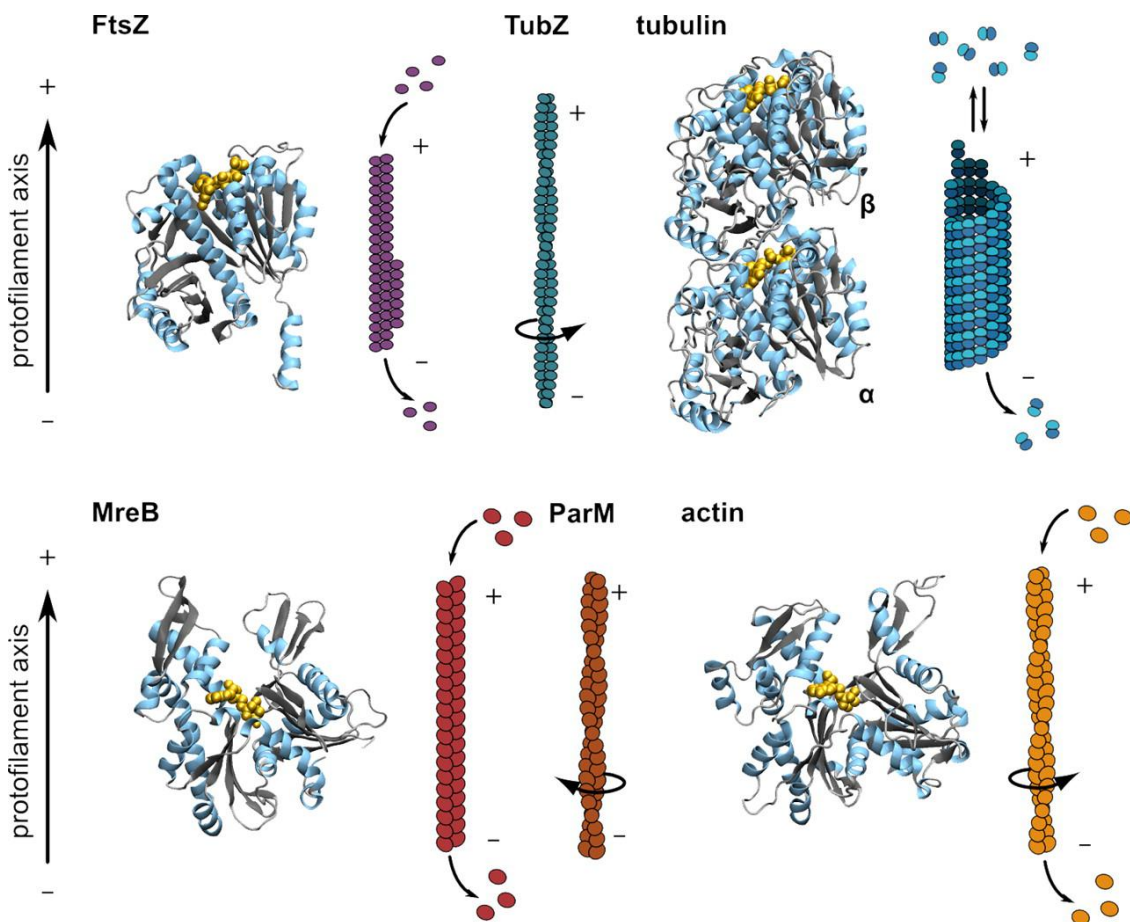


Fig.1.2 Homology between prokaryotic and eukaryotic cytoskeletal filaments: Despite the low levels of sequence similarity, the homologous cytoskeletal proteins have considerable conservation of folding longitudinal interactions. (taken from [16]).

1.2.2 The Actin/MreB/ParM/FtsA family

The second class of cytoskeletal filaments are thought to have evolved from a gene duplication of the RNase-H fold [17]. The actin fold is not restricted to cytoskeletal filaments but also extends to several classes of enzymes and heat-shock proteins as well. Currently, the most reliable picture of longitudinal contacts in filaments comes from two actin homologues from bacteria – **MreB** and **FtsA**. MreB is widespread in bacteria and has been shown to be associated with peptidoglycan synthesis machinery and moves across the circumference on peptidoglycan synthesis paths [18, 19]. Because of biochemical difficulties with this protein, details of properties and filament dynamics are yet to be completely understood.

On the basis of its fold, FtsA was originally classified as a member of the actin/HSP70 family of proteins, alongside actin and prokaryotic actin-like MreB[20]. FtsA from *T. maritima*, *E. coli* and *B. subtilis* all form filaments in *E. coli* cells when overexpressed. FtsA has been proposed to form a discontinuous A-ring attaching the Z-ring to the circumference of the cell. How exactly FtsA aids the Z-ring in cell division is an open question. FtsA has been shown to assemble into filaments and lie along the FtsZ filaments *in vitro* [21]. However, the domain variations in the FtsA compared to other actin-like proteins show that FtsA is most distant of these proteins. It will be compelling to find out whether the last common ancestor of actin and FtsA is more ‘actin-like’ or ‘FtsA-like’.

ParM is probably the best studied actin homologue. It functions to segregate low copy number plasmids to the extremes of the cell before cell division. This partitioning system consists only of three components – ParM, showing dynamic instability [22], ParR, the adaptor protein and *ParCDNA* [23, 24]. Interestingly the ParM forms left handed helix compared F-actin [25]. ParM are probably the simplest models of dynamic instability shown by cytoskeletal elements. The ParR has formin-like activity, participating in addition of new ParM subunits to the end.

1.2.3 Intermediate filament like family

In *Caulobacter crescentus*, a protein **Crescentin** was identified which shares structural characteristics of intermediate filament proteins[26]. Although poorly conserved on primary-sequence level, intermediate filament proteins and Crescentin show a similar three-dimensional architecture: a long central coiled-coil region flanked by variable head and tail domains. Crescentin assembles into long filaments *in vitro*, similar to its eukaryotic homologues. The polymerization occurs spontaneously and does not require nucleotides. In *C.crescentus* cells, depletion of Crescentin results in the loss of the crescentoid shape of the cells and grows in the form of straight rods. This indicates that Crescentin is responsible for the curved shape of the *C.crescentus* cells. Crescentin is thought to mediate the curvature by redirecting peptidoglycan synthesis. The physical strain borne by the Crescentin structure

anisotropically alters the kinetics of cell wall growth leading to curved cells [27]. However the exact mechanism for this process remains unidentified and needs further investigation.

1.2.4 *MinD/ParA/ParF/Soj* (WACAs)

There is potentially a fourth class of cytoskeletal filaments, though not necessary performing cytoskeletal functions. These are structurally unrelated to the intermediate filament, actin or tubulin like filaments: Walker A cytoskeletal ATPases (WACA). The defining characteristic of WACA is a deviant walker A motif, which is required for nucleotide binding[28]. Exact homologues seem to be lacking in eukaryotic genomes, but they may be related to eukaryotic **Septins**. Septins have been shown to have a related fold and form similar sandwich dimers and polymerise [29]. Because of the lack of information about WACA filaments, it is currently impossible to compare them with Septins at polymer level.

MinD is part of the **MinCDE** system for septum inactivation at the poles of bacteria [30]. MinD binds to the membrane through an amphipathic helix. MinE activates the hydrolysis of MinD [31]. The interplay of MinD and **MinE** on the membrane produces self-organising waves that are thought to increase the concentration of **MinC** at the poles inhibiting of FtsZ at the poles [32, 33]. The moving waves of MinCDE have been reproduced *in vitro* on flat membranes [34]. The Min system is described in detail in section.1.4.2.

ParA is a common bacterial plasmid-borne WACA which acts synergistically with **ParB**, ParB binds a specific DNA sequence **ParS**. This arrangement is similar to the **ParMRC**, actin-like systems [35, 36]. How exactly ParA affects partitioning is not known, but does involve filament formation [37, 38].

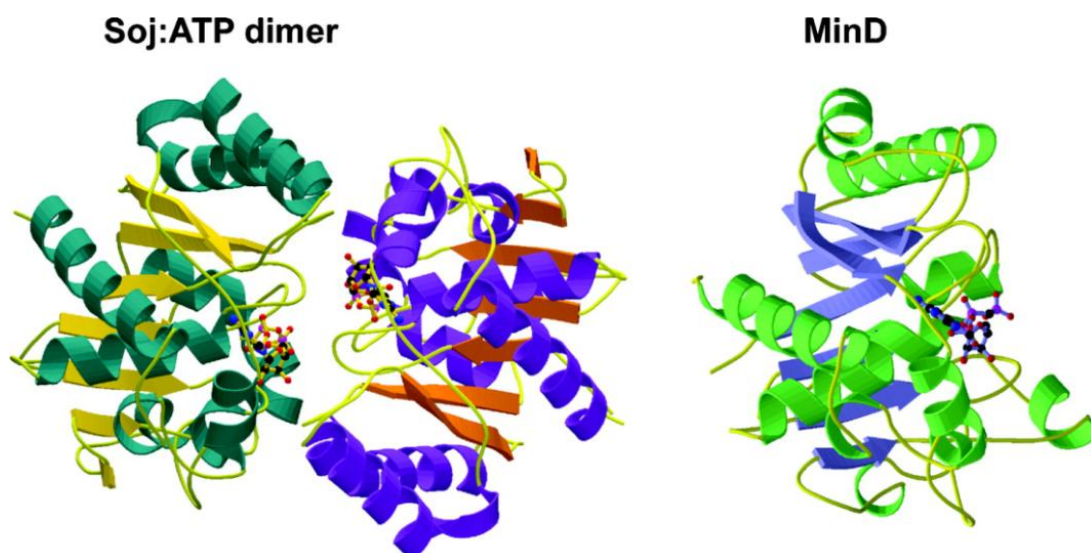


Fig.1.3 Structure of the Walker A cytoskeletal ATPase (WACA). Crystal structure of the Soj dimer (*Thermus thermophilus*) and MinD (*Pyrococcus furiosus*) (taken from [39]).

ParF is another plasmid-borne WACA. It acts in concert with **ParG**, which is related to **ParR**, the adaptor from ParMRC system [40, 41]. These permutations of similar proteins reinforce the idea that the cytoskeletal filaments use common principles. ParF also forms ATP dependent polymers [42].

Soj is a chromosomal version of ParA, present in few bacteria. Soj is known to oscillate in concentration from one side of the nucleoid to the other [43], helped by its activator **SpoOJ**. Like the rest of the WACAs, it forms an ATP dependent dimer (Fig.1.3). Soj binds unspecifically to DNA to form protein: DNA filaments [44, 45].

MipZ belongs to the growing MinD/ParA family [46, 47]. Members of this family are regulated by a nucleotide-dependent switch – in ATP form, they dimerize and bind cooperatively to the surface, DNA (ParA) or membrane (MinD). This allows these proteins to reside on the surface of the membrane until an ATPase activating protein, MinE for MinD and ParB for ParA activates them. A recent study reveals that nucleoid association by MipZ is critical for gradient formation and provides evidence that ParB regulates the ATPase activity of a member of the ParA/MinD family by promoting dimerization rather than function as an ATPase activating protein[48]. The details of this unusual ParB assisted dimerization of MipZ will require further investigations.

1.3 On the evolution of cytoskeletons

In spite of the identification of quite a few related proteins in bacteria, the invention and evolution of the eukaryotic cytoskeletons remain mysterious. An enigma about FtsZ and tubulin is that tubulin is amongst the most slowly diverging proteins in eukaryotes, yet they are as divergent from bacterial homologue FtsZ as to be practically unrecognizable [49]. FtsZ is a very ancient protein. Arginine, Lysine, Phenylalanine, Tyrosine and Histidine are rare in FtsZ sequences, and tryptophan is almost non-existent. These amino acids were the last to be added to the genetic code and probably FtsZ evolved as a functional protein before the genetic code was complete. This is plausible, as a mechanism for cell division would be needed in the earliest forms of the developing cellular life. An FtsZ based division mechanism seems quite successful as FtsZ has been retained by almost every modern species of bacteria and archaea. The missing link however, is whether there is an example of FtsZ based division in the earliest eukaryotic lines, irrespective its origin. Eukaryotes later evolved an actin-based machine for cytokinesis, and eukaryotic FtsZ underwent a drastic change to give rise to modern day tubulin. Amino acids highly conserved from FtsZ to tubulin are those involved in GTP binding and hydrolysis [50]. This puts forward one expectation from FtsZ polymers – they probably are very different in dynamics and organization from the microtubules.

A similar situation exists for MreB and actin. Bacterial MreBs are generally about 40% identical in sequence even across diverse species, similar to FtsZ. Yet MreB and actin show

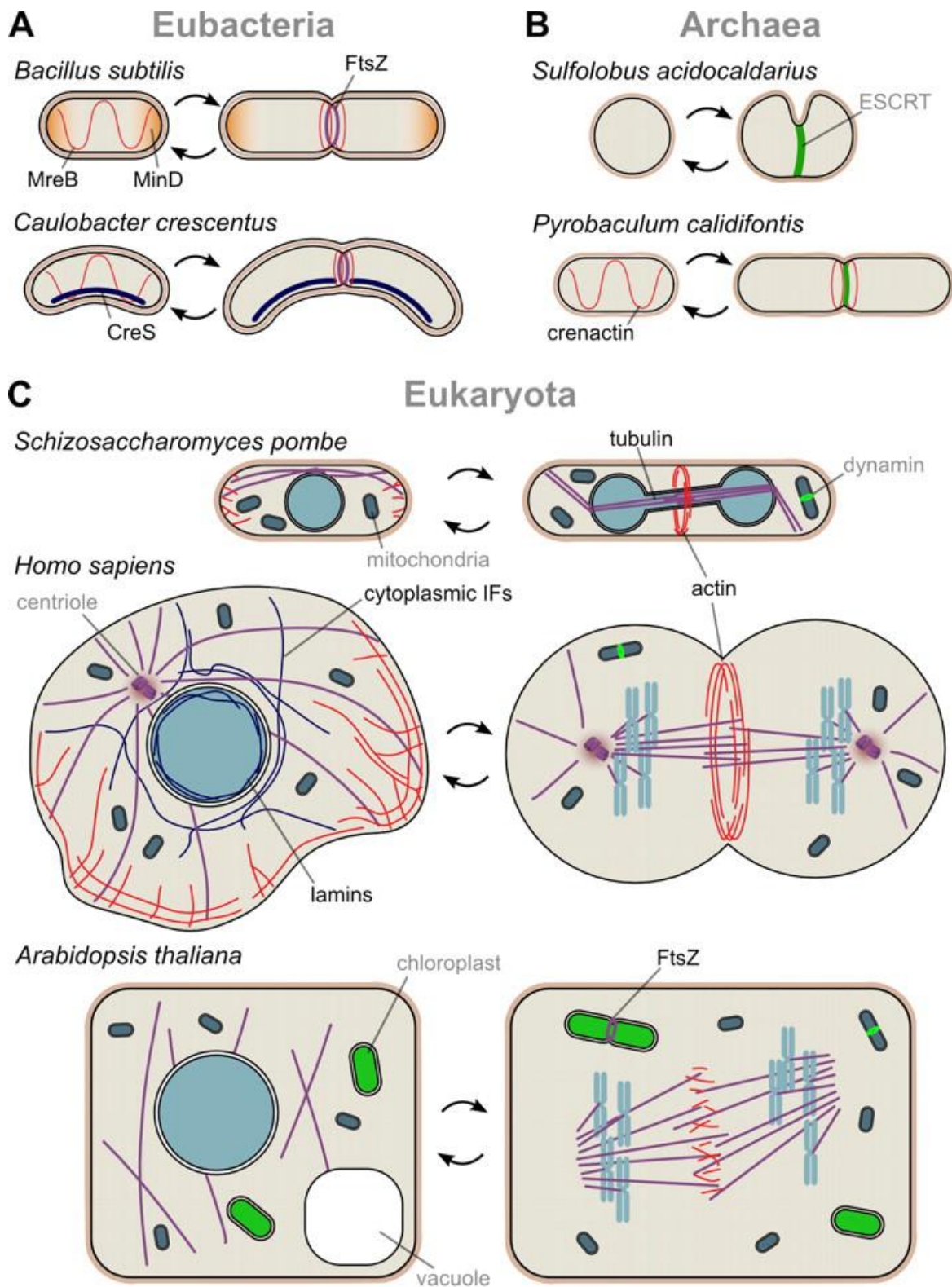


Fig. 1.4 Bacterial, archaeal and eukaryotic cytoskeletons. Schematic representations of a small number of model organisms from each of the three domains are shown, displaying the organization of the cytoskeleton in dividing and nondividing cells. Homologous filaments are coloured similarly. (taken from [16])

less than 15% sequence identity to each other, similar to FtsZ and tubulin. But, Hsp70 and sugar kinases, the other branches of the actin superfamily, show about 50% sequence identity between eukaryotic and bacterial homologs [51, 52]. In addition to MreB, distant homologs are produced by some bacterial plasmids. ParM and AlfA assemble actin-like filaments that bind a plasmid at each end and push them to opposite poles [24]. ParM and AlfA are as distantly related to each other as they are to actin, FtsA and MreB [53], It is also interesting to note that some plasmids use actin homologs whereas others use tubulin homologs for mitosis like segregation (Fig.1.4).

As with FtsZ, it has been suggested that the mechanical function of MreB was optimized early and the eukaryotic line lost its original function and acquired new ones, resulting in extensive evolution[50]. The novel functions of the highly evolved homolog eventually resulted in a contractile machine capable of carrying out cell division, various motile processes and phagocytosis. Modern actin participates in more protein-protein interactions than any other known protein. These multiple interactions would eventually constrain further divergence of actin, as also probably for tubulin, once these proteins had optimized their assembly mechanisms and their interactions with multiple motors and binding proteins.

1.4 Bacterial cell division

Most bacteria divide by binary fission, a process in which the cell grows to a particular size and then splits into two equal daughter cells. With growth, the cells replicate and segregate their chromosome, with each daughter cell receiving one copy at division. Cytokinesis in bacteria is driven by a complex ring-like structure commonly referred to as the septal ring or the divisome machinery [54]. Much of our knowledge about cytokinesis in bacteria has come from *Escherichia coli*, *Bacillus subtilis* and *Caulobacter crescentus*. As the work presented in this thesis is on the proteins of the divisome from *E.coli*, I will detail out the studies on *E.coli* but will simultaneously refer to the relevant progresses in other organisms as well.

The mature septal ring in *E.coli* contains over two dozen different protein components (Fig.1.5). Ten of these (FtsA, B, I, K, L, N, Q, W, Z and ZipA) are essential for cell constriction process, and can be considered to form the core septal complex [55, 56]. Cells lacking any of these core proteins fail to constrict and display the classical lethal division phenotype where they elongate into very long filamentous morphology.

According to the present picture of bacterial cell division, assembly of the divisome is initiated by polymerization of FtsZ into a ring-like cytoskeletal element on the inner circumference of the cell. This ring of FtsZ polymer is the first polymeric protein to localise at the future site of division[2], where it serves as a scaffold for the recruitment of the downstream components of the divisome. As a complete ring with all its components, involving membrane tethering proteins and cell wall synthesis machinery, the Z-ring then performs cell division.

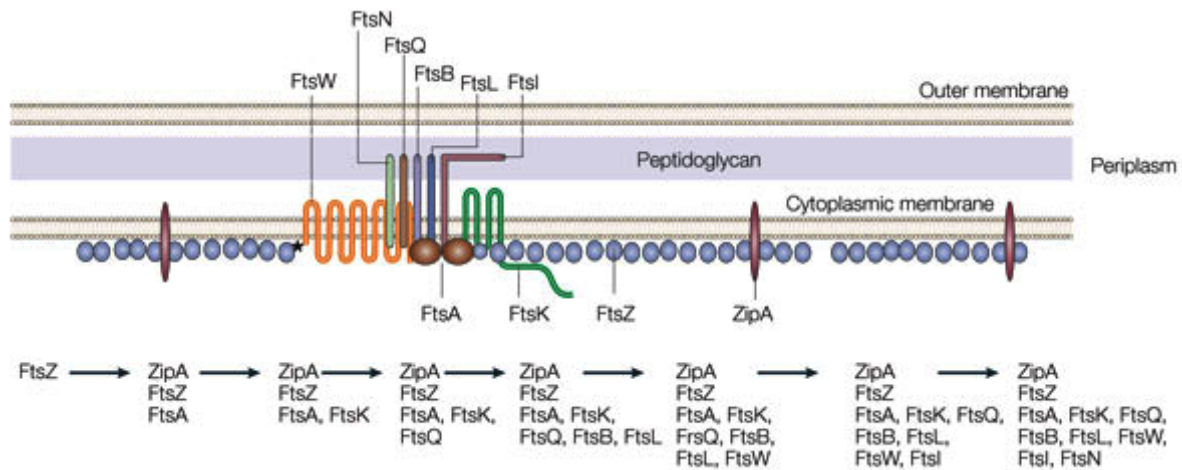


Fig.1.5 Fellowship of the ring: A model of the *Escherichia coli* Z ring and its essential protein partners is shown in cross section. FtsZ is shown as a series of single protofilaments at the membrane, although the actual structure of FtsZ in the Z ring is unknown. Both ZipA and FtsA contact FtsZ as well as the membrane in *E. coli*. However, FtsZ contacts FtsW directly in *Mycobacterium tuberculosis* (asterisk), which lacks ZipA and FtsA (taken from [56]).

1.4.1 FtsZ and the Z-ring

FtsZ was discovered by Takashi Hirota by isolating temperature sensitive mutants of *E.coli* [57]. In this genetic screen, a number of other genes involved in cytokinesis were also identified. Most of these genes were designated as *fts* because of filamenting temperature-sensitive phenotype shown by strains carrying conditional lethal mutations in the corresponding genes (FtsA, B, I, K, L, N, Q, W, Z and ZipA). Depending on the time of their recruitment at the midcell, they can be divided into two groups: The early divisome proteins – FtsZ, A and ZipA and the late divisome proteins - FtsK, Q, L, B, I and K. The late divisome proteins arrive at the cell centre after a distinct lag of about 10 min after the early divisome proteins [58]. Rod-shaped bacteria such as *E.coli* and *B. subtilis* divide symmetrically to give rise to two daughter cells of equal size. To do this, the early divisome proteins must be positioned precisely at the midcell. This is executed by Min system in *E.coli*, discussed in section 1.4.2.

FtsZ is a cytoplasmic protein that is composed of two globular domains separated by a central core helix. FtsZ, like tubulin shows GTP-dependent assembly *in vitro*. Its GTPase activity depends on polymerization as the GTPase active site is comprised of amino acids from two adjacent monomers [9, 59]. One of the notable differences between FtsZ and tubulin is the GTPase reaction kinetics. Tubulin hydrolyses GTP very quickly on polymerization, but nucleotide exchange is slow or non-existent in the polymer. Hence the microtubule polymer is mostly GDP bound, with GTP-containing subunits forming a cap at the fast growing (+)-end. This state is not thermodynamically stable and the whole polymer shows dynamic

instability - rapid shrinkage of polymers [60]. Tubulin and ftsZ form by a linear head-tail interaction and result in similar protofilaments. However, with FtsZ the lateral interactions are much weaker, and a well-defined polymer beyond a protofilament has not been experimentally observed as compared to the hollow 13-protofilament cylinder for microtubules. However, a variety of bundles structures have been observed *in vitro* depending on the experimental conditions [6, 61-63]. Structural studies have revealed that FtsZ consists of two independently folding halves – the N-terminal and the C-terminal halves (Fig.1.6) [64].

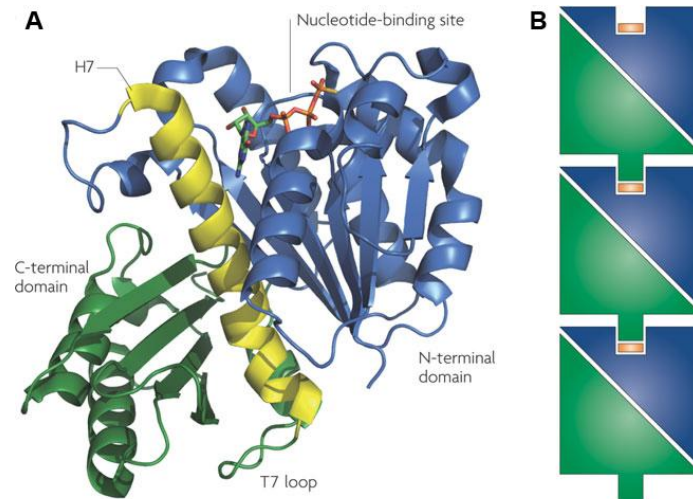


Fig.1.6 The crystal structure of a *Bacillus subtilis* FtsZ monomer bound to GTP- γ S (Protein Data Bank entry 2RH0). FtsZ is composed of two independently folding domains and a central core helix, H7. The amino-terminal domain contains the tubulin signature motif, GGGTGTG, and forms the nucleotide-binding site. At the base of the carboxy-terminal domain, following H7 is the catalytic T7 or synergy loop. The extreme C-terminal tail, which forms the binding site for several division proteins, is not visible in the crystal structure. B. FtsZ polymerises by the head-to-tail association of individual subunits, shown in blue and green, to form a single-stranded protofilament with a longitudinal subunit repeat that is similar to that of tubulin. Insertion of the T7 loop into the nucleotide-binding site (orange) of the subunit below places two highly conserved aspartate residues in the vicinity of the FtsZ γ -phosphate; these aspartate residues are thought to activate the GTPase activity of FtsZ by polarizing an attacking water molecule (taken from [64]).

Immunoelectron microscopy revealed that FtsZ forms a ring at the division septum [65]. Fluorescence microscopy studies, using *E.coli* cells expressing a fraction of their total FtsZ as FtsZ-GFP confirmed that it assembles into a ring-like structure at the division septum [66]. Throughout the cell-division, the FtsZ ring remains at the leading edge of the septum. Fluorescence Recovery After Photobleaching (FRAP) on these studies revealed that the FtsZ in the ring is highly dynamic with a half-life of about 10 s, which is consistent with the

GTPase rate observed *in vitro* [67]. This suggests that the flux of FtsZ in and out of the ring is coupled to and limited by the hydrolysis. Since the protofilaments are much shorter than the circumference of the bacterium, they must bundle up and presumably form a ring-like structure with staggered overlap between protofilaments. Support for this kind of a model comes from a study of *C. crescentus* by cryo-EM tomography [68]. The images from this study showed short protofilaments scattered around the circumference of the cell and a more refined helix-like structure when reconstructed. However, this model still does not reconcile with the fast dynamics FtsZ shows both *in vitro* as well as *in vivo*.

The FtsZ ring is tethered to the inner membrane of the bacterium by two proteins – FtsA and ZipA [69]. ZipA has a transmembrane domain and a long tether between the transmembrane domain and the FtsZ binding domain. FtsA, a homologue of actin, binds to the membrane through an amphipathic helix. Both proteins interact with FtsZ through a short conserved domain near the extreme C-terminal tail of FtsZ [70]. Z-rings can form in the absence of either of the two proteins, but not when both of them are absent [69]. Both ZipA and FtsA are required for the recruitment of the downstream divisome proteins, implying that both proteins have distinct roles in divisome assembly.

In vitro, FtsZ polymers seem to depend on the nucleotide state. In the GTP bound state, FtsZ protofilaments seem predominantly straight, while highly curved when bound to GDP [6]. Based on this and the short protofilaments observed *in vivo* by cryo EM in *C.crescentus* cells, Li *et. al.* proposed an ‘iterative pinching’ model. In this model, FtsZ is proposed to generate force by a GTP-hydrolysis dependent change in the curvature of filaments attached to the inner membrane of the cell, depolymerisation, nucleotide exchange and rebinding to the membrane in the form of GTP-bound, straight filaments [68]. However, the physical parameters of the filaments, such as stiffness and intrinsic curvature should be at the right values for such a model to work and it was argued whether the FtsZ filaments are stiff enough to be able to generate a contractile force based on this mechanism. A GTPase mutant-FtsZ D212G, which hydrolyses about 10 times slower than the wild type did not cause any difference in the duration or efficiency of cytokinesis in *E.coli* cells, questioning the importance of GTPase activity in force generation [71]. An alternative mechanism proposed is dependent on short protofilaments sliding against each other in the ring [72-75]. None of the mechanisms have been experimentally verified so far.

One problem in studying the role of FtsZ in force generation is to deal with the adaptor proteins – FtsA and ZipA, which bind FtsZ to the membrane. To circumvent this problem, Osawa *et al.* replaced the C-terminal tail of FtsZ, which is required to bind to membrane anchoring FtsA or ZipA, by the yellow fluorescent protein (YFP) and a membrane targeting sequence (MTS) resulting in FtsZ-YFP-MTS (Fig.1.7) [76]. The MTS is a short amphipathic helix sequence derived from MinD [31]. When tested *in vivo*, this artificial construct was still able to form Z-rings, suggesting that FtsA only acts as a linker between FtsZ and the

membrane. It is not required to form Z-rings *per se*, although these cells were not able to divide and showed filamentous growth,

To test if FtsZ-YFP-MTS can also assemble to Z-rings *in vitro*, Osawa *et al*, purified this protein and mixed it with liposomes. In the presence of GTP, FtsZ-YFP-MTS formed rings inside tube-like liposomes. These rings diffused along the length of the liposomes and coalesced into brighter rings. These rings appeared to generate constrictions on the liposomes, leading to the conclusion that FtsZ can alone generate force. However there are many caveats in these experiments [76]. One is that all the monomers in these experiments have MTS, an amphipathic helix. Thus, a large number of MTS in the form of a ring can produce visible distortion in the liposome just by inserting into the membrane. Secondly, the FtsZ might possess some intrinsic curvature. The experiments performed by Osawa *et al*. are on liposomes of diameter of about 10 μm , whereas the bacteria are about 1 μm in diameter. The constrictions observed could be completely due to physiologically irrelevant mechanisms.

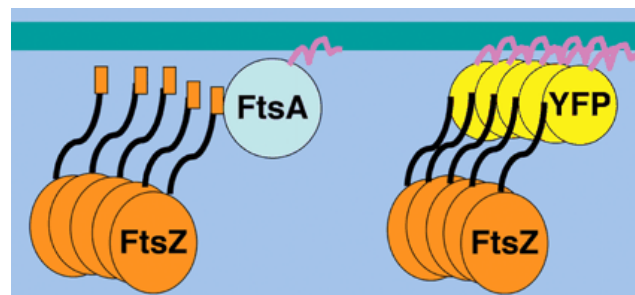


Fig.1.7 FtsZ is normally tethered to the membrane by FtsA (left). The C-terminal peptide (orange) of FtsZ binds FtsA, and FtsA binds the membrane by its amphipathic helix (purple). In FtsZ-mts (right), the FtsA-binding peptide is replaced with yellow fluorescent protein (YFP) and an amphipathic helix (taken from [76]).

In vivo, not every FtsZ molecule in the ring is directly coupled to the membrane. The cell division is in fact, very sensitive to the ratio of FtsA to FtsZ [77-79], which in the wild-type *E.coli* cells is about 1:5. This is still a mystery as to what do FtsZ and FtsA accomplish synergistically. A recent study by leaver *et al*. showed that cells lacking a cell wall do not need FtsZ for cell division, but use an alternative mechanism presumably involving dynamic instability of membranes [80]. This study also supports the Z-ring as just a scaffold directing peptidoglycan synthesis and not as an active force generator.

1.4.2 Positioning of the Z-ring – Nucleoid Occlusion and Min system

Proper fission at the mid-cell requires accurate placement of the Z-ring along the cell axes. Lateral positioning of the Z-ring is determined by two negative regulatory systems – The Min system and Nucleoid Occlusion (NO) (Fig.1.8) [30]. NO counteracts assembly of the Z-rings in the vicinity of the chromosomes and is mediated by DNA-binding proteins SlmA in *E.coli*

and Noc in *B.subtilis* [81, 82]. Noc binds to ~ 70 chromosomal sites that are conspicuously absent from the chromosomal terminus. Inserting Noc binding sites in this region delays cell division, indicating Noc helps coordinate Z-ring assembly with progression of chromosome replication. How DNA bound Noc in *B. subtilis* and SlmA in *E.coli* interacts with FtsZ and inhibits Z-ring assembly needs further clarification.

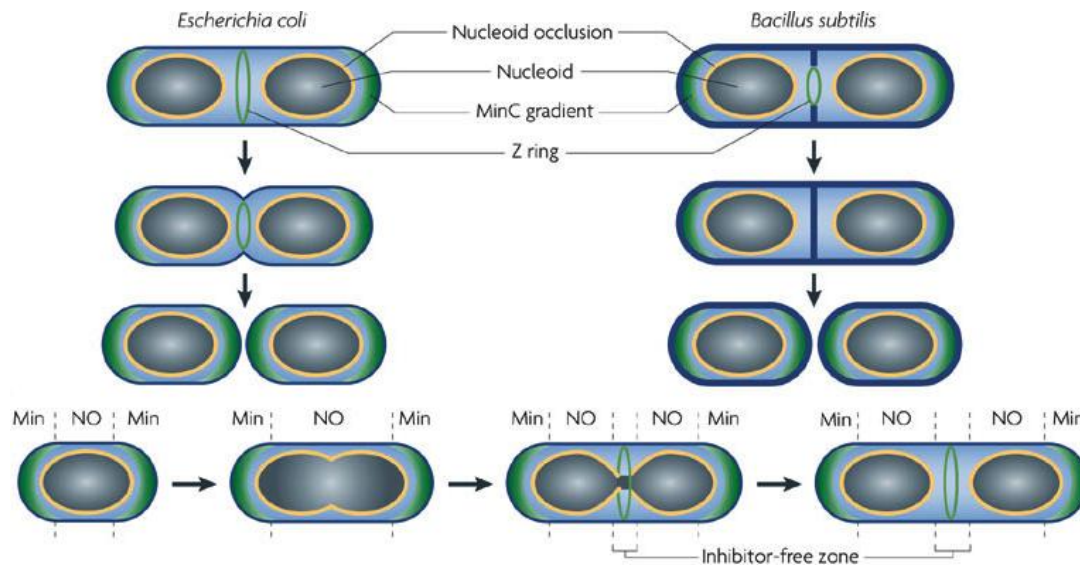


Fig.1.8 Positioning the Z-ring and two different modes of division. After chromosome replication and segregation into nucleoids the Z ring assembles at mid-cell. The ring then constricts to bring about division. Cell wall synthesis follows the ring inwards. In *Escherichia coli*, synthesis of the division septum is accompanied by constriction of the outer membrane. In *Bacillus subtilis*, a cross wall of peptidoglycan initially divides the cell before it is degraded and remodelled to form the new, hemi-spherical cell poles. Both a Min system and a Nucleoid occlusion system work to inhibit FtsZ assembly at poles. (taken from [64])

The Min system in *E.coli* is a dominant determinant of lateral positioning of the Z-ring, and its absence leads to frequent fission near a cell-pole and the consequent release of chromosome-less mini-cells (hence the name for the proteins – Min proteins) [83]. The Min protein systems consist of three oscillating proteins in the *E.coli* - MinC, MinD and MinE. Typically, MinC, MinD and a portion of MinE accumulate along the membrane at one cell end as another portion of MinE accumulates more sharply in the form of a MinE-ring that appears to cap the Min polar zone and prevent it from extending past mid-cell. The MinE ring moves pole-ward until the Min polar zone shrinks as they are released from the membrane to the cytoplasm. All the three proteins then start reassembling on the membrane on the opposite end. The Min oscillations have long been speculated to be a self-organization process [30]. The MinD protein is the energy consumer in the system. MinD possesses an interesting membrane targeting sequence (MTS) [31], which has also been used by Osawa *et al.* to bypass the requirement of FtsA or ZipA to bind FtsZ to the membrane [76]. This amphipathic

helix binds cooperatively to the membrane, binding only when more than one MTS is present, for example, by oligomerization of MinD. MinD dimerizes on binding to ATP, and this results in the dimer of MinD binding to the membrane through the double MTS [84]. MinE stimulates the ATPase activity of the membrane bound of MinD. As a result of ATP hydrolysis, MinD is monomerized, and both proteins detach from the membrane. Coupled with diffusive components of the proteins in a conserved system, the interplay of MinD and MinE gives rise to patterns of distribution of proteins on the membrane, this phenomenon has been reconstituted *in vitro* on two dimensional lipid bilayers (Fig.1.9) [34].

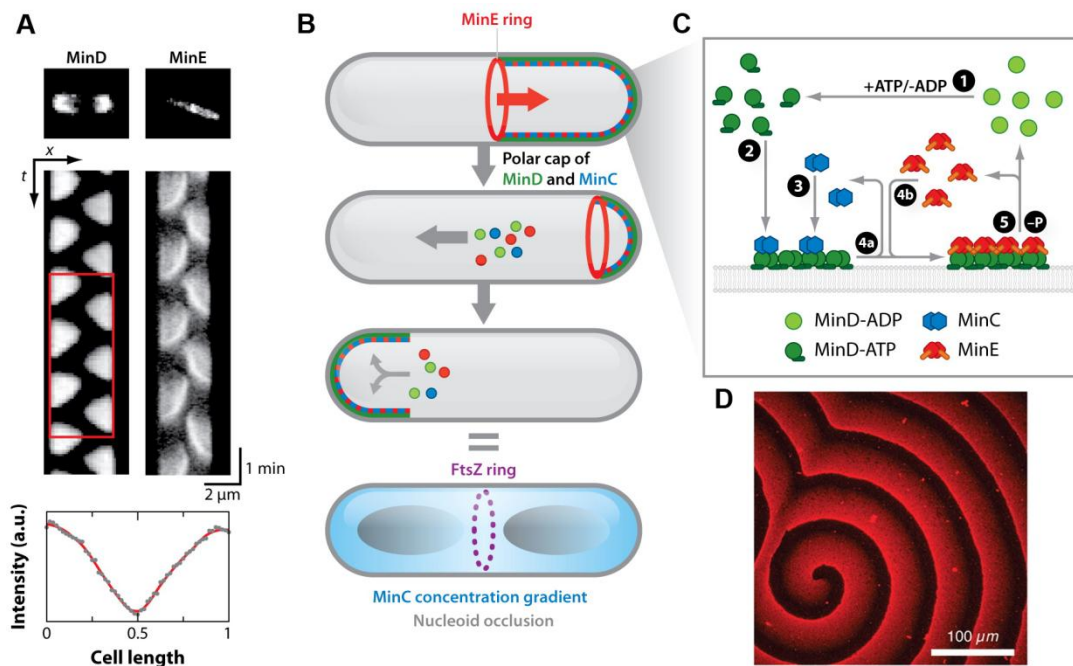


Fig.1.9 Oscillatory patterns of Min proteins in vivo. (A) Top: Micrographs of GFP-MinD and MinE-GFP in vivo. Middle: Kymograph of pole-to-pole oscillations of MinD and MinE in cells of normal length (shorter than 5 μm). Bottom: Time-averaged intensity profile along the red rectangle shown in the kymograph. (B) Illustration of Min protein dynamics in *Escherichia coli*: MinD-ATP (green) binds to the membrane and recruits MinC (blue). MinE (red) displaces MinC and then stimulates MinD ATPase activity, causing the release of proteins from the membrane. All three proteins diffuse through the cytoplasm and, after nucleotide exchange by MinD, rebound to the plasma membrane. Bottom: Illustration of the inhibitory gradient of MinC and nucleoid occlusion (gray ellipsoids), which together restrict FtsZ polymerization (purple) to the center of the cell. (C) Biochemical reactions underlying the oscillations. After binding to ATP [1], MinD binds to the membrane as dimers [2]. MinC [3] and MinE [4b] can bind to membrane-bound MinD, with MinE able to displace MinC from MinD [4a]. MinE stimulates the ATPase activity of MinD, whereupon both proteins detach from the membrane [5]. Finally, MinD exchanges its bound nucleotide [1]. (D) Reconstituted Min waves on a supported lipid bilayer. (taken from [85])

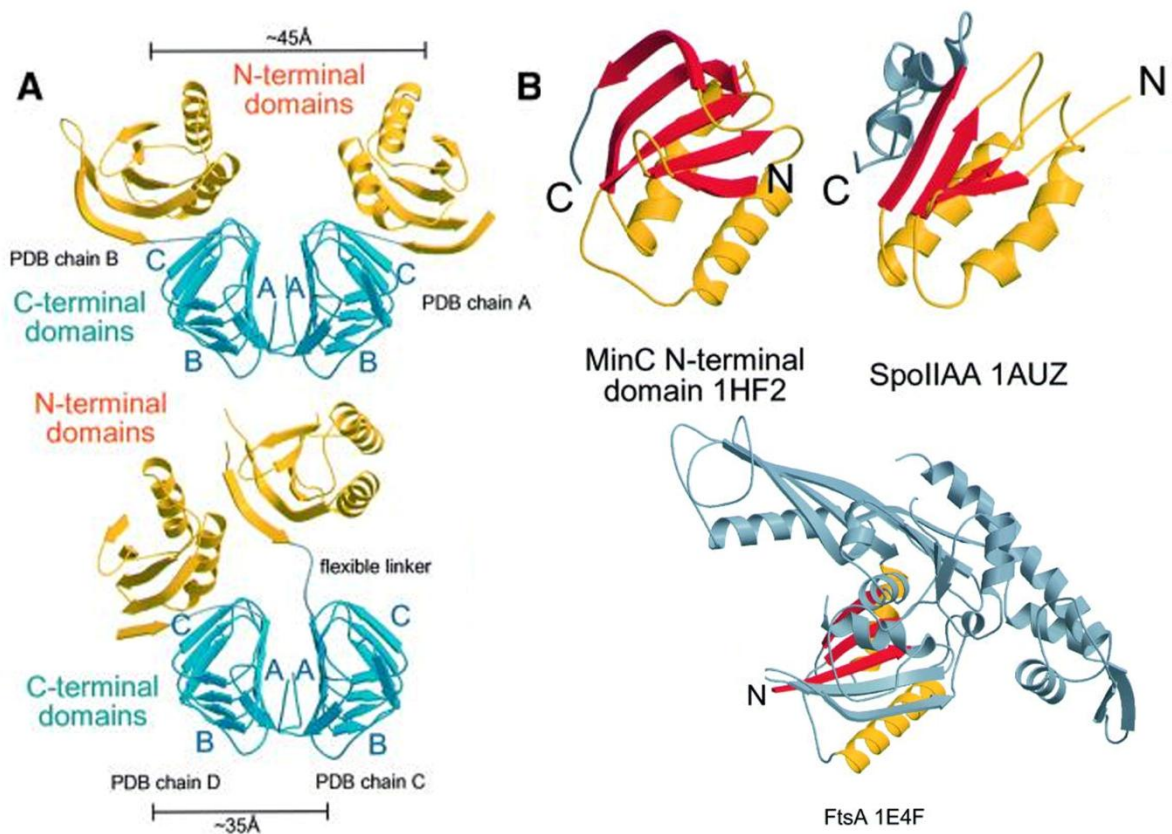


Fig.1.10 Structure of MinC (A) An asymmetric unit contains two different MinC dimers, highlighting the flexibility of the linker region (linker, grey; N-terminal domain, yellow; C-terminal domain, blue). Face ‘A’ of the triangular C-terminal domain forms the dimer interface alone in dimer AB (top). **(B)** Structural alignment of the N-terminal domain of MinC from *T.maritima*, SpoIIAA from *B.subtilis* (PDB 1AUZ; [86]) and FtsA from *T.maritima* (PDB 1E4F; [87]). FtsA shows the highest DALI score of 3.7, r.m.s.d. 3.2 Å over 74 residues. SpoIIAA has a DALI score against the N-terminal domain of MinC of 3.5, r.m.s.d. 3.6 Å over 72 almost consecutive residues. Aligned stretches are coloured, all other residues are shown in grey. (taken from [88])

MinC, the inhibitor of FtsZ is a passenger of the MinDE waves. MinC has two domains – The N-terminal domain, MinC-N, and the C-terminal domain – MinC-C. MinC-N is considered the primary inhibitory domain (Fig.1.10) [89]. MinC-N blocks the Z-ring assembly when overexpressed *in vivo*, and it inhibits FtsZ polymers *in vitro*. The MinC-C mediates the dimerization of MinC and its binding to MinD. The homodimeric nature of MinC was verified when the structure of MinC from *Thermatoga maritima* was solved. This study also suggested that the dimeric MinC may bind only polymeric FtsZ and act selectively only on FtsZ filaments. The N-terminal domain of MinC revealed a fold that is distantly related to SPOIIAA and even more distantly related to FtsA (Fig.1.10). Although the similarities are not very strong, it is believed that the structural similarities reflect a common modality of function, by binding to the same site on the FtsZ polymer [88].

In vitro analysis showed that MinC inhibited FtsZ polymers at approximately 1:1 stoichiometry [90, 91]. However the GTPase activity of FtsZ is not inhibited even by a 2.5 fold excess of MinC. MinC is also completely inactive against FtsZ polymers assembled in GMPCPP or in GDP-AIF [92, 93]. Also FtsZ-D212G, a GTPase deficient FtsZ mutant was resistant to MinC [94]. This suggests that the GTPase activity of FtsZ is necessary for MinC to act on the FtsZ polymers and disassemble them. With these characteristics, the mechanism of FtsZ disassembly by MinC is not yet completely known. The other mystery is the low stoichiometry *in vivo* relative to the observed 1:1 stoichiometry *in vitro*.

1.5 Objective of this work

To measure the properties and behaviours of individual proteins and their interactions with their relevant partners within the context of a system is a herculean task. Within the network of various proteins and their multiple interactions, it is extremely difficult to tease apart a particular phenomenon emerging from interactions between a few proteins. Additionally, the membrane plays an influencing role in many of these protein- protein interactions. In many systems, total behaviour is largely governed by physical phenomena like diffusion or membrane transformations or geometry. Teasing apart relevant interactions and mechanisms giving rise to a crucial phenomenon in a living system forms a small step towards understanding an organism. One way to deduce the properties of a particular set of proteins involved in is to reconstitute the ‘phenomenon’ using the minimal number of required components [95].

Self-assembly and self-organization are concepts that are used increasingly broadly in biology from studies of molecules to studies of animal societies [96]. Both self-assembly and self-organization refer to processes in which multiple entities become components of a functional whole. There are mainly two kinds of self-assembly – a) static self-assembly deals with equilibrium structures, and b) dynamic self-assembly, which is a non-equilibrium process in which energy is supplied to the system to maintain a steady state population of ordered structures. FtsZ and other biological cytoskeletal molecules fall into this category. Self-organization occurs when elements dynamically interact with each other to generate a system that acquires emergent properties, which cannot be directly inferred from individual characteristics of the interacting elements. The Min system is an example of self-organization by reaction-diffusion processes. Thus, in *E.coli*, cell division and division site positioning is dependent on two closely working systems – the self-assembling FtsZ and the self-organizing Min system. Both these systems work in concert to bring about cell division at precisely the mid cell of the *E.coli*.

Extensive genetic and biochemical studies have led considerable insight into the FtsZ polymers and its putative role in force generation. However, the organization, dynamics of the steady state polymers is not clearly understood. Most of the studies have reported a wide spectrum of morphologies and inconsistencies. On the basis of genetic studies, it has been

proposed that the self-organizing Min system comprising of three proteins MinC, MinD and MinE can spatially regulate the FtsZ polymers. However, there is no direct experimental evidence if these three proteins are sufficient to accomplish this. How MinC mediates interaction between the MinDE oscillations and FtsZ polymers is also not completely known. The aim of this thesis was to investigate the dynamic self-assembling properties of FtsZ *in vitro* using bottoms-up approach. Further, I also investigated how, given the properties of FtsZ polymers, might MinC interact with FtsZ and couple the FtsZ to MinDE waves. This work demonstrates the capacity of simple biochemical circuits for generating complex spatial and temporal regulation.

Chapter 2

Materials and methods

2.1 Constructs

DNA manipulations and sequencing were carried out by standard procedures. For all PCR amplifications, Native Pfu polymerase (Stratagene) was used. Digested vectors were dephosphorylated with Antarctic phosphatase (New England Biolabs). For ligations, Fast-link DNA Ligation Kit from EPICENTRE Biotechnologies. Mutagenesis was achieved by QuickChange lightning Single or multi mutagenesis kits (Agilent Technologies). New clones were evaluated by restriction digestion. Obtained clones with an insert or mutagenesis were sequenced (MPI-CBG DNA sequencing facility). Obtained sequences were compared against published sequences from NCBI, identical clones were amplified and purified (Qiagen) and stored at -20°C.

pET11b FtsZ-YFP-MTS, pET11b MTS-43aa-FtsZ-YFP and pET11b MTS-1aa-FtsZ-YFP:

These plasmids were obtained from prof. Harold Erickson at Duke University. Previously published studies describe these constructs [76, 97].

pET11b FtsZ-F268C:

Mutagenesis was carried out with AAC ATC ACG GCG GGC TGC GAC CTG CGT CTG GAT and ATC CAG ACG CAG GTC GCA GCC CGC CGT GAT GTT which changed the phenylalanine at position 268 to cysteine resulting FtsZ-F268C.

pET28a NZ:

A PCR with primers GGT CGC TAG CAT GGA ACT TAC CAA TGA CG and ATT ACG ATC GGC GAT ACC TTG CAC AGC was used to amplify N-terminal sequence of FtsZ from pET11b FtsZ-YFP-MTS corresponding to 1-196 amino acids (NZ). The fragment was incubated with NheI (restriction sites are underlined) and ligated into similarly treated pET28a to obtain a plasmid containing NZ. The resulting ORF encoded for a fusion protein

of NZ connected to the N-terminal hexahistidine tag by a short linker and the sequence for Thrombin cleavage site and a T7-tag.

pET28a MinDMinE, pET28a MinE, pET28a MinC and pET28a MinCeGFP:

These constructs were previously cloned in the lab. Previously published studies describe these constructs.

2.2 Expression and purification of proteins

2.2.1 Growth and harvest of bacteria

BL21 cells were transformed with the respective plasmid and grown in LB medium with Kanamycin (50 µg/ml LB Kan) or Ampicillin (50 µg/ml LB Amp) for 12 hours at 37⁰C. A sample of this culture was mixed with 100% glycerol at a ratio of 1:1 and stored at -80⁰C.

For the expression of Min proteins, overnight cultures in LB Kan medium were diluted 100 fold in the same medium and growth was continued at 200 rpm at 37⁰C to an optical density of 0.6 at 600 nm. To induce overexpression of the respective protein, Isopropyl-β-D-thiogalactopyranosid (IPTG) was added to 1 mM and cells were grown for 4-5 hours at 37⁰C. Cells were collected by centrifugation for 20 minutes at 4⁰C in an Avanti J20-XP centrifuge using a JLA 8.100 rotor. The cell pellet was suspended in lysis buffer (50 mM NaH₂PO₄ pH7.5, 300 mM NaCl, 20 mM imidazole, 10% glycerol, protease inhibitor (Roche biochemicals), 1 mM TCEP) and stored at -80⁰C.

For expression of FtsZ proteins, overnight cultures in LB amp with 0.1% glucose medium were diluted to 100 fold in the same medium and grown at 37⁰C to an optical density of 0.6 at 600 nm. The cells were centrifuged and re-suspended in an equivalent volume of LB Amp without glucose. To induce overexpression of the protein, IPTG was added to 1 mM and grown for 4-5 hours at 37⁰C. The cells were collected and stored as described for Min proteins but with a different lysis buffer (50 mM TRIS 50 mM pH 7.9, 1 mM EDTA, 50 mM KCl, 10% glycerol, 1mM PMSF, 1 mM TCEP, Protease inhibitor).

2.2.2 Purification of proteins

FtsZ and its mutant versions:

Cells were thawed to room temperature from -80⁰C. Cells were lysed by sonification for 10 s for ten times with a break of 30 s in between on ice. The lysed cells were centrifuged at 32K X g for 20 min. at 4⁰C. The supernatant was removed in a fresh tube. The proteins in the supernatant were precipitated by adding ammonium sulphate to 35 % saturation. The solution was then centrifuged at 22K X g for 20 min at 4⁰C. The pellet was then suspended in column buffer A (TRIS 50 mM pH 7.9, 1 mM EDTA, 100 mM KCl, 10% glycerol, 1 mM TCEP) and dialysed against the same buffer to remove the ammonium sulphate. The dialysed solution is

passed through a 0.22 μm filter and loaded on an anion exchange column (Resource Q 6 ml, Amersham Biosciences). The protein was then eluted with column buffer B, similar to column buffer A, but with 500 mM KCl. FtsZ eluted from 220-350 mM KCl. Since the absorbance of FtsZ at 280 nm is very low, sample fractions were analysed using SDS-PAGE (Fig.2.1, 2.2). The protein is stored at -80°C .

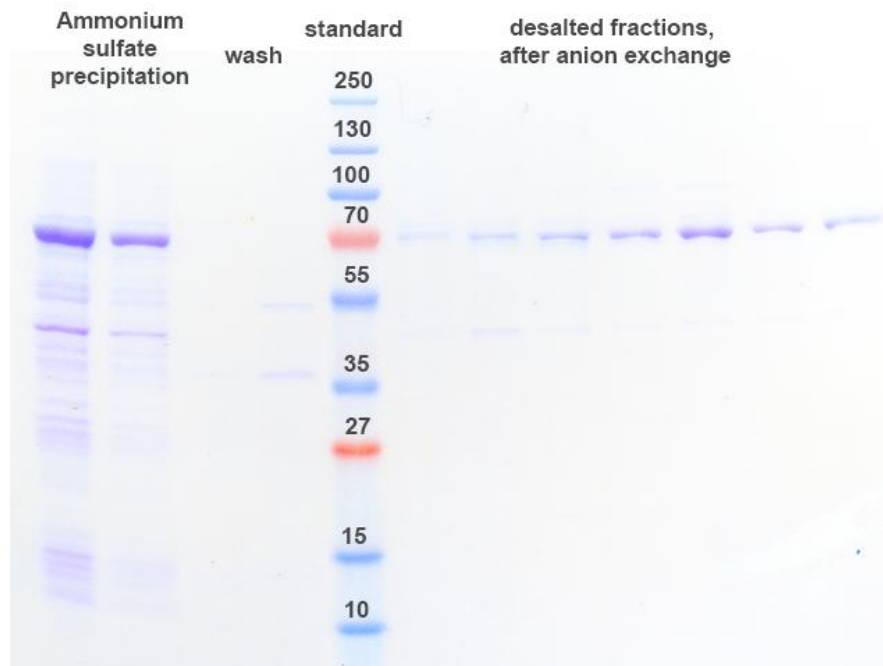


Fig.2.1 Coomassie stained polyacrylamide gel of the purification of FtsZ-YFP-MTS.

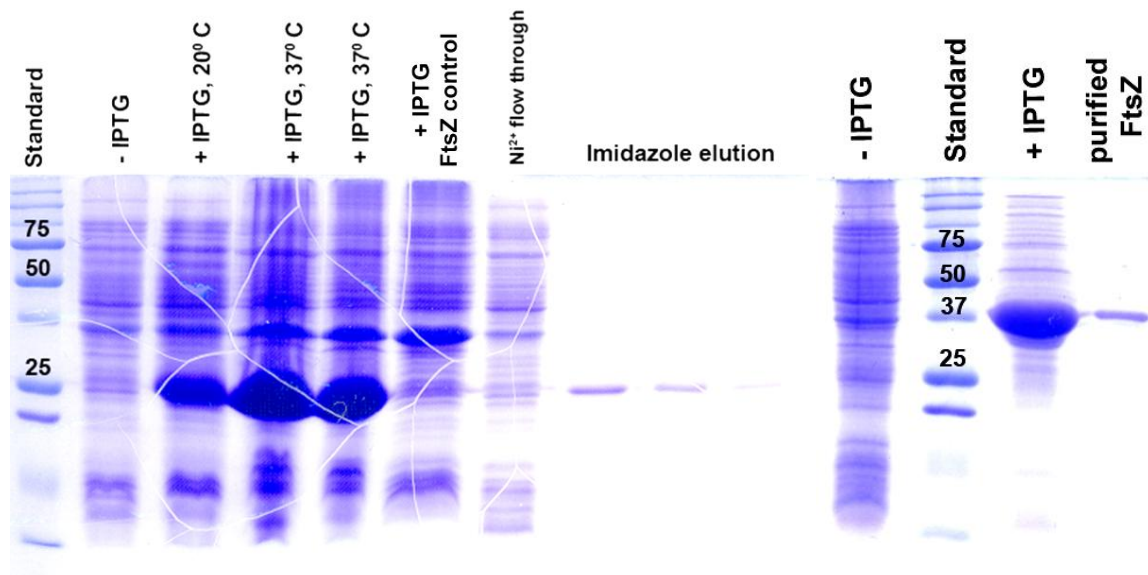


Fig.2.2 (Left) Coomassie stained polyacrylamide gel of the purification of FtsZ N-terminal half, NZ (N-terminal half of FtsZ) by Ni^{2+} affinity chromatography. (Right) Coomassie stained polyacrylamide gel of the purification of wild type FtsZ.

Min proteins and the NZ:

All the Min proteins and NZ (N-terminal half of FtsZ) are purified using Ni²⁺ affinity chromatography as they have a hexa-histidine tag. Cells were thawed and were lysed by three passages through a Emulsiflex C5 (Avestin). The crude lysate was then clarified by centrifugation at 10 000 rpm for 45 min at 4⁰C in an Avanti J20-XP centrifuge using a JLA 25.50 rotor. The supernatant was loaded onto a Ni²⁺ sepharose column (Ni-NTA superflow, Qiagen). The column was washed with lysis buffer with 20 mM imidazole. The protein was eluted with the lysis buffer with 250 mM imidazole. Peak protein fractions were pooled and the buffer was exchanged to storage buffer (50 mM HEPES pH 7.25, 150 mM KCl, 10% glycerol, 0.1 mM EDTA) using PD10 desalting columns (Biorad). Protein purity was analysed by SDS-PAGE gel stained with Coomassie Blue (Fig.2.3). Concentrations were estimated using absorption at 280 nm; Proteins were stored at -80⁰C.

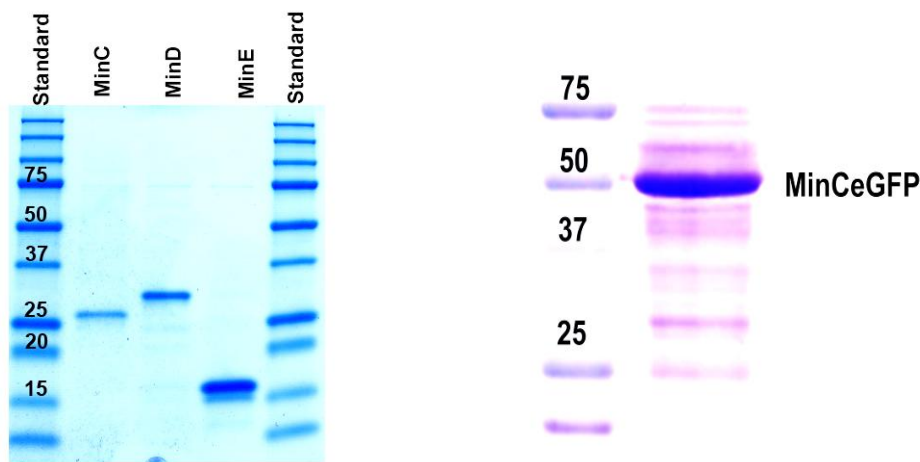


Fig.2.3 Coomassie stained polyacrylamide gel of purified Min proteins

2.2.3 Protein labelling with fluorescent dyes

The protein MinE has only one cysteine accessible for labelling with thiol-reactive probes: MinE Cys-51. FtsZ has no cysteine. To label it with dyes, we mutated the phenyl alanine at position 268 to cysteine resulting FtsZ-F268C. This mutation does not alter the wild-type activity of the protein. Labelling reactions were carried out with thiol-reactive dyes according to the protocols of the manufacturer (Alexa-647 –maleimide, Molecular probes and Cy5, GE Healthcare). The reaction was quenched with 10 mM β -mercaptoethanol and the excess dye was separated from the protein by passing the reaction mixture through a PD10 desalting column. Samples were frozen in storage buffer (50 mM HEPES pH 7.25, 150 mM KCl, 10% glycerol, 0.1 mM EDTA) at -80⁰C. Average labelling efficiencies were 80% for MinE and 99% for FtsZ. The activities of the proteins were confirmed by self-organizing assays for Min proteins and FRAP assays for FtsZ.

2.3 GTPase activity assays

The GTPase activity of FtsZ assembled on supported lipid bilayer was quantified using malachite green assay. The assay is based on a Malachite green complex which specifically binds to released phosphate ions, resulting in an increased absorbance at 650 nm. This increase is detected quantitatively using a spectrophotometer and compared against a phosphate standard.

2.4 Microscopy

2.4.1 Confocal Laser Scanning Microscopy

Confocal laser scanning microscopy was performed using a Zeiss LSM 510 microscope (Zeiss, Jena, Germany) with Zeiss C-Apochromat 40 x, NA 0.75 water immersion objective. The laser power was adjusted depending on the available signal intensity under different experimental conditions. The fluorescence signal was detected with a photon multiplier tube. Fluorescence Recovery after Photobleaching (FRAP) was also performed using this setup and the data was analysed independently using ImageJ and Origin.

2.4.2 Total Internal Reflection Fluorescence Microscopy

TIRF microscopy was carried out using a setup built around an Olympus IX-71. The 488 nm line from an Ar ion laser and 647 nm line from HeNe laser were selected using an acousto-optic tunable filter (AA optoelectronic). The 488 nm and 633 nm beams were coupled into a single optical fibre and delivered into the TIRF module. The beam from the fibre was collimated and expanded using a combination of lenses. The collimated beam was then passed through a combination of a polarizer and a quarter wave plate. The beam was then focussed at the back focal plane of a Olympus Apo 100 x 1.45 oil objective using a lens. Fluorescence was separated from excitation laser lines using a FF 497/661 dichroic filter (Semrock) and split into two channels using a W-View beam splitter (Hamamatsu) equipped with 560 DCSP, 560 DCXP, HQ 525/50 and HQ700/75 filter (AHF). This separates the green fluorescence from the red fluorescence and projects the images side by side on an Andor iXon EM-CCD camera. The camera spatial sampling was at 156 nm/pixel. The laser power was adjusted depending on the available signal intensity under different experimental conditions.

Photobleaching of the dye was reduced by adding an oxygen scavenging system according to [98]; Glucose oxidase (165 U/ml), catalase (2170 U/ml), β -D-glucose (0.4% wt/wt) and trolox (2 mM) (All from Sigma chemicals) was added to 100 μ l of reaction mixture.

Single particle analysis and localization was done using QuickPALm plugin with ImageJ (<http://code.google.com/p/quickpalm/>). The program first identifies peaks in the pixel intensity values above threshold brightness for a single frame of the movie. By fitting the

intensity around the peak to a two-dimensional Gaussian the position is determined to sub-pixel resolution.

Residence times of the proteins is estimated by plotting a histogram of the track lengths (i.e. the number of frames the particle is detected) and fitted to a single exponential. The observed exponential decay has a time constant of τ , which represents the average residence time of a particle. This observed time is a combination of the real residence time of the protein and the bleaching of fluorophores. The time constants of these two processes are related by:

$$\frac{1}{\tau_{obs}} = \frac{1}{\tau_{bleach}} + \frac{1}{\tau_{res}}$$

Where τ_{bleach} is the time constant of bleaching and τ_{res} is the the constant of protein residing on the filament [99].

2.5 Fluorescence Correlation Spectroscopy

Fluorescence correlation spectroscopy and cross-correlation spectroscopy (FCS and FCCS) were performed on a commercial Zeiss LSM 780. Correlation and cross-correlation curves were fitted appropriately by model equations for three-dimensional free Brownian diffusion according to published literature. Alexa 488 was used as a standard probe of known diffusion constant.

For probing interactions of FtsZ-YFP-MTS with MinCeGFP or NZ on the solution above bilayer, the focus was parked above the filament network and fluorescence fluctuation was recorded. Coorelation curves were fitted with appropriate FCS model equation for three-dimensional free Brownian diffusion according to published literature [100].

2.6 Fluorescence Intensity Distribution Analysis

FIDA is based on the collection of photon counting numbers, n , recorded in time intervals of fixed duration and uses this information to assemble a count number histogram $P(n)$. The statistics are obtained using FCS module in Zeiss LSM 780. This distribution $P(n)$ is fit assuming a certain number of fluorescent species, and estimate unknown concentration and specific brightness values. The particle brightness is compared against a standard fluorescent particle, which is known to be a monomer. Equations used for fitting were according to published studies [101]. To investigate MinC dimerization, we used eGFP tagged MinC and compared the brightness against monomeric eGFP.

Silanisation according to ref. [24] was done to prevent protein binding to the glass surface. The coverslips were extensively cleaned and covalently derivatized with dichloro-diethyl silane by sonication in silanization solution (95% isopropanol, 5% H₂O pH 5). The inhibited protein binding was checked using confocal microscopy. Silanisation resulted in almost no fluorescence at the glass surface.

2.7 Lipid membrane systems

2.7.1 Supported lipid bilayer as model membranes

Lipid bilayers on solid supports as a model system for biological membranes were developed about two decades ago [102]. The key feature of lipid membranes, lateral and rotational mobility of individual lipids is well preserved. This is because the bilayer is not in direct contact with its support; a thin layer of water (in the order of 1 to 2 nm) acts as a lubricant and allows for the rapid diffusion of the lipids in both membrane leaflets [103, 104].

Supported lipid bilayers (SLBs) offer a range of advantages compared to free standing membranes. A membrane confined to the surface of a glass coverslip is much easier to image using fluorescence techniques like TIRF microscopy. TIRF microscopy allows imaging at faster time scales and at single-molecule resolution [105].

2.7.2 Supported lipid bilayer formation

Preparation of small unilamellar vesicles (SUVs):

E.coli polar lipids dissolved in chloroform were transferred into a glass vial and the solvent was evaporated under a gentle stream of nitrogen. Any residual solvent was further removed by drying the lipid film in a vacuum for 1 hour. The lipids were rehydrated in respective reaction buffer to a lipid concentration of 4 mg/ml and incubated at 37⁰C for 30 minutes. The lipid film was then completely resuspended by vortexing rigorously resulting in multilamellar liposomal mixture. This mixture was then placed in a bath sonicator where shear forces help to reduce the size of the vesicles giving rise to small unilamellar vesicles. The SUV solution was stored at -20⁰C as 20 µl aliquots.

Formation of supported lipid bilayer:

The reaction chamber for bilayers was prepared by attaching a plastic ring on a cleaned glass cover slip with a mica sheet on top using UV glue (Norland optical adhesive 88). The mica is attached to the cover glass using UV glue for confocal imaging or the objective oil for TIRF imaging. For supported bilayer formation, the SUV dispersion was diluted in reaction buffer to 0.5 mg/ml of which 75 µl were added to the reaction chamber. Adding CaCl₂ to a final concentration of 5 mM induced fusion of the vesicles and the formation of a lipid bilayer on the mica surface. After incubating for 30 minutes at 37⁰C, the sample was rinsed with 2 ml pre-warmed reaction buffer (Fig.2.4).

2.7.3 Curved support substrate preparation

Concave curvature substrates:

Curved substrates were made by electron beam lithography. The glass surface was coated with a 70 nm thick Tantalum mask, which acts as a resist. A 100 nm thick layer of photoresist

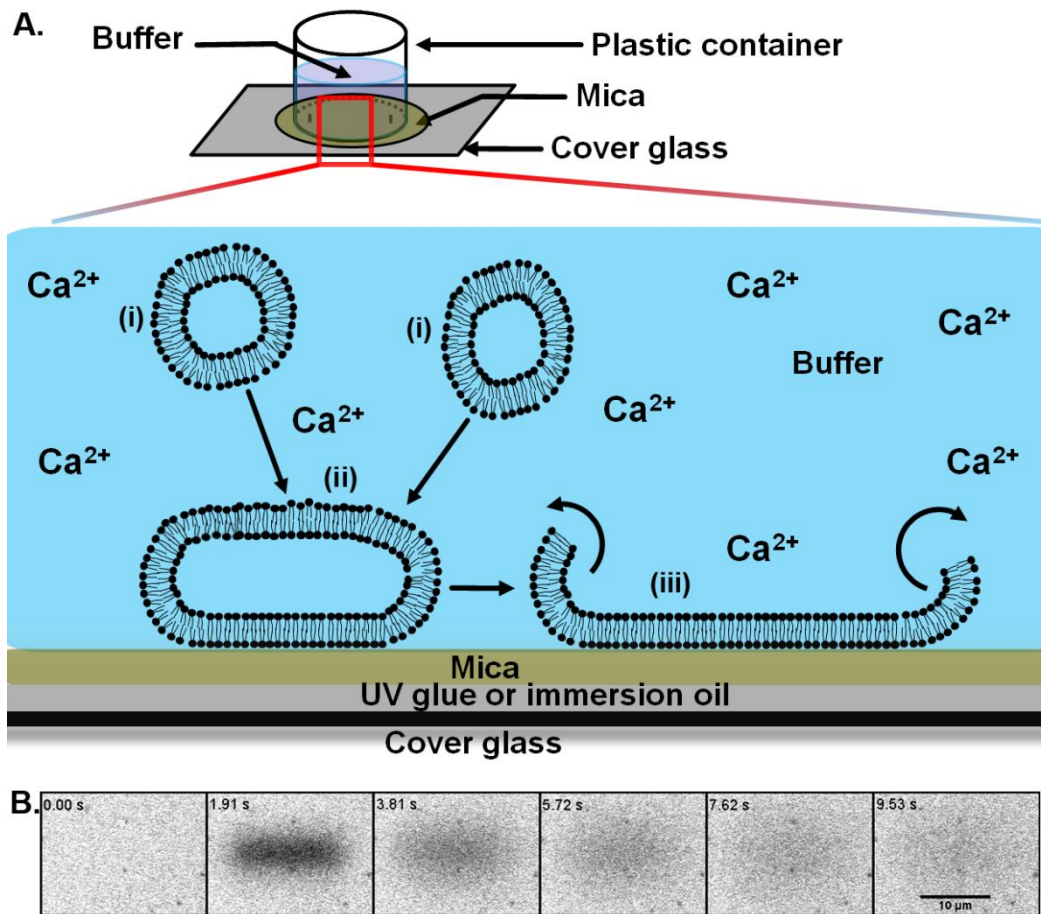


Fig.2.4 (A) Formation of supported lipid bilayers on a Mica support on a cover glass. Small unilamellar vesicles (SUVs) (i) are adsorbed on the support (ii) and spontaneously rupture in the presence of Ca²⁺. (B) Proper formation of bilayers is probed by fluorescence recovery after photo bleaching (FRAP).

- AR N 7520.18 was deposited on this layer by spin coating at 8000 min⁻¹ for 35 s and then dried at 85 ° C for 3 min. Electron beam lithography was done on the substrates mapping the pattern required using a scanning electron microscope (Hitachi S4500, Hitachi High-Technologies Corporation, Tokyo, Japan). This was followed with ion beam etching to remove the Tantalum coating. The photoresist was then removed and the second etching was done which creates channel owing to differential etching rates on places with and without Tantalum. The desired surface curvature was obtained by carrying out a multilevel etching process in an ion beam etching system (IonSys500, Roth&Rau, Wüstenbrand, Germany).

Convex curvature substrates:

Capillary fibres are extracted from Whatman glass microfiber filters (GF/A), cleaned in alcohol, sonicated and dried on a cover glass. The diameter ranged from 100 nm to 2000 nm. The capillaries were then extracted in a tube by flowing buffer on the dried capillaries on the

cover glass. The suspension was again sonicated and incubated with SUV solution in the presence of 0.1 mM Calcium Chloride. This resulted in the capillaries coated with bilayers.

2.7.4 Giant Unilamellar Vesicles

GUVs were prepared by electroformation. 5 μ l of *E.coli* lipid extract at 1 mg ml⁻¹ in chloroform was spread on two Platinum wire electrodes. The electrodes with the lipid films were immersed in a chamber containing 300 mM sucrose solution and were connected to a power generator. Electroformation was performed at 2 V and 10 Hz for 1 h at 37°. The GUVs were released from the electrodes by changing the frequency to 2 Hz for 30 min. The GUVs were then transferred into a chamber having equi-osmolar polymerisation buffer. To change the osmolarity, a 0.5 M glucose solution was added to the chamber.

2.8 AFM imaging and data processing

AFM measurements were performed using NanoWizard I system (JPK Instruments, Berlin, Germany) combined with LSM 510 Meta optical system (Zeiss, Jena, Germany). Gold sputtered samples were imaged in air, in contact (constant-deflection) mode using non-coated silicon cantilevers (DP15/HiRes-W/AIBS, MikroMasch, Spain) with typical spring constant 40 N/m (only vertical deflection images are shown where noise was reduced by Gaussian filter size set to 2px). Fixed samples based on the curved substrate were imaged in liquid (5mM HEPES, 75mM NaCl, pH 7.4) using silicon nitride cantilevers (MLCT/cantilever A, Veeco, CA) with typical spring constant 0.05 N/m. All images were taken with scan rate set to 1-2Hz and scan size to 1024x1024 pixel squared. Analysis of data was performed using Gwyddion 2.10 software (www.gwyddion.net).

Chapter 3

Results I: The FtsZ filaments are a disordered dynamic bundle with constant turnover throughout the length

3.1 Preface

FtsZ, a homologue of tubulin is a GTPase protein that is found in most eubacteria and archaea. In bacteria, FtsZ is the first protein to localise to the midcell as a part of the cytokinesis machinery [2]. *In vivo* imaging of FtsZ shows it as a ring structure (the Z-ring) contracting as the septum constricts [66]. FtsZ also displays dynamic turnover *in vivo* where it exchanges between the Z-ring and the cytoplasmic pool at a timescale of seconds [67, 106].

FtsZ has been implicated in generating force to construct the septum by a variety of proposed mechanisms [68, 73, 75]. However the limited understanding of the structure and organisation of the FtsZ polymers *in vivo* has prevented a definitive model so far. Various attempts have been made to understand the FtsZ polymer structures. Electron microscopy studies have shown a wide range of morphologies of FtsZ filaments owing to variations in buffer and substrate conditions [7, 59, 107-110]. Atomic Force Microscopy (AFM) studies have shown that FtsZ filaments continuously rearrange, break and anneal [63]. At low concentrations, FtsZ assembles into single stranded tubulin-like protofilaments. It has also shown that at higher concentrations, the protofilaments become crowded and display lateral interactions which organise them into sheets or bundles [7]. They can also form nucleotide-dependent straight or curved mini-rings, resembling alpha/beta/gamma tubulin [6].

The FtsZ monomer comprises of two independently folding subdomains. FtsZ assembles in an orientation similar to that of tubulin, such that the GTP molecule binds between the N-terminal of one monomer and the C-terminal of the other [8]. The nucleotide binding pocket

between the two monomers is partially exposed, raising a possibility of nucleotide exchange without subunit turnover [8]. This phenomenon could well affect the dynamics of FtsZ. An emerging question is whether FtsZ filaments have a mechanism leading to dynamic instability as found in homologous microtubules?

A key but untested hypothesis is about how the protofilaments are organised in the FtsZ bundle. One idea is that the short protofilaments – about 100 nm in length, overlap in a staggered manner by lateral interactions and form longer discontinuous bundles. Another possibility is that the protofilaments undergo extensive annealing and result in a bundle of a few, long annealed protofilaments [56, 111]. To test these models and to elucidate the exact nature of the dynamic FtsZ bundles, we used a membrane binding FtsZ – FtsZ-YFP-MTS assembled on supported lipid bilayers.

3.2 The Z-ring *in vivo* – Assembly and Dynamics

We performed STED microscopy on cells expressing wild type FtsZ from a normal locus and FtsZ GFP from a separate chromosomal locus. Single cells could not be imaged in a time-lapse manner owing to photo bleaching of GFP. Therefore, we imaged different cells representing different stages of assembly of the Z-ring. The Z-ring starts as a bright nucleus and seems to grow into a complete ring (Fig.3.1.A). A complete ring appears to assemble by annealing of growing filaments (Fig.3.1.B-D).

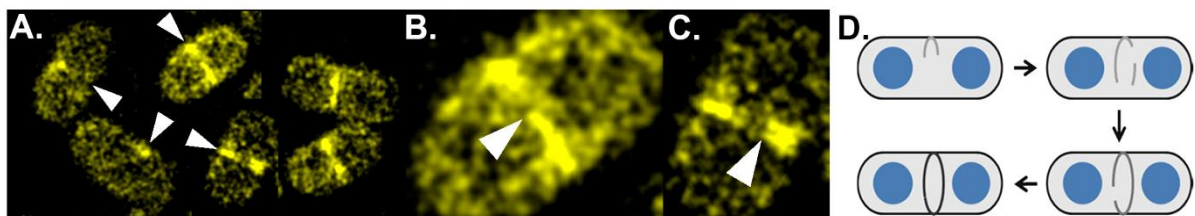


Fig.3.1 In vivo assembly of the Z-ring – STED microscopy of *E. coli* expressing FtsZ-GFP. (A-C) Z-ring assembles by growth and annealing. (D) Schematic representation of how the Z-ring might assemble.

The Z-ring constriction proceeds at a linear rate on an average. It binds many proteins that regulate the FtsZ polymers by bundling or disassembling. During the active stage of constriction, whether these proteins are active to an extent to influence the dynamics of FtsZ is an important consideration in the mechanism of constriction. With many bundling proteins known, whether the turnover activity is affected during the process of constriction is an important clue towards the mechanism of constriction. FRAP on the Z-ring during constriction stages recover with a half-time of about 10 s (Fig.3.2). They do not show any variation in the turnover behaviour at the various stages of constriction suggesting that the structure, organisation and dynamics of the filaments are always the same irrespective of the process of constriction.

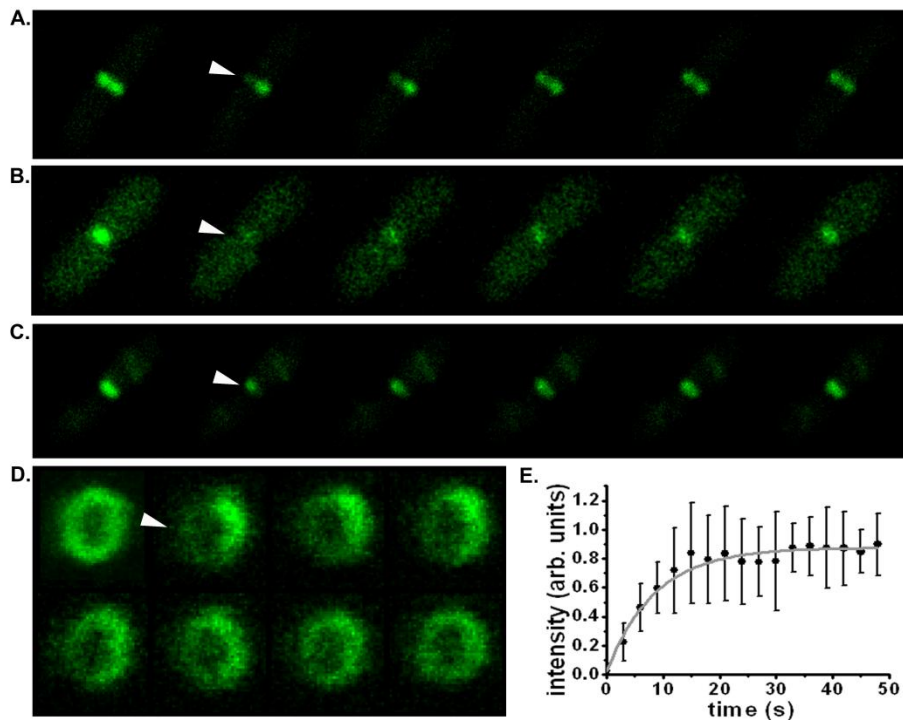


Fig.3.2 FtsZ in the Z-ring shows dynamic turnover throughout all stages of cell division. Photobleached regions recover (white arrows) (A-D). Recovery occurs with a turnover of about 10s in dividing cells.

3.3 Filaments assemble on the membrane by annealing/ disassemble by fragmentation

To visualise FtsZ polymerisation in real-time, we used a modified version of FtsZ, FtsZ-YFP-MTS, where MTS is the membrane targeting sequence from *E.coli* MinD. Since the YFP-MTS is in the C- terminus of the protein, it does not affect any other known interacting sites required for polymerisation or lateral interactions. We observed the assembly of 1:1 FtsZ-YFP-MTS and WT-FtsZ on an *E. coli* polar extract lipid bilayer using TIRF microscopy. Fig.3.3.A shows images of FtsZ polymerisation at every 10 seconds. Since a single MTS of the *E.Coli* MinD shows poor affinity for the membrane, the filaments are attached to the membrane only when the FtsZ-YFP-MTS begins to polymerise in the presence of GTP. A ratio lower than 1:1 of FtsZ-YFP-MTS to WT-FtsZ does not result in consistent polymers probably because the polymers are unable to bind to the membrane efficiently. Very high concentrations ($> 0.4 \mu\text{M}$) of total FtsZ leads to a very dense network, which was nearly irresolvable by fluorescence. At an optimum concentration of about $0.05 - 0.4 \mu\text{M}$, the assembly of the filaments and growth into a network could be imaged. The presence of the membrane substrate supports lower critical concentrations of FtsZ-YFP-MTS for polymerisation. The polymerisation events can be explained in the following way: as the monomers begin to polymerise into protofilaments, they are recruited to the membrane due to multiple MTS binding simultaneously. The protofilaments diffuse around and increase in length and width by annealing with other protofilaments. We cannot be sure about the lengths

of individual protofilaments owing to the optical resolution limit. However, earlier studies have reported an average size of around 80 - 150 nm for single stranded FtsZ filaments. These short protofilaments overlap, form lateral bonds, and assemble into longer filaments. If the concentration of the filaments is too low, the probability to form lateral bonds that make multi-subunit thick filaments and to grow into longer filaments is low, owing to fewer collisions. Consequently, no higher order stable network is formed, but individual short stable filaments exist on the membrane. At sufficiently high concentrations ($> 0.1 \mu\text{M}$), the protofilaments settle into a stable network. With increasing concentrations of FtsZ, the amount of polymers or the total length of polymers in the network increases proportionally. Once the network has been formed, there are almost no filament ends and the network remains stable in the presence of GTP. We observe smaller protofilaments overlapping to form longer filaments (Fig.3.3.C) and longer filaments annealing and breaking (Fig.3.3.E) while settling into a higher order network (Fig.3.3.D). We analysed the movies using an ImageJ based plugin which thresholds and skeletonizes the filaments, and then analyses for total length, branches, junctions and end points of the filaments with time (Fig.3.4.A-G). The growth rate constant of filaments (i.e. bundles of ‘protofilaments’) constituting the network is $18.56 \mu\text{m s}^{-1} \mu\text{M}^{-1}$ (Fig.3.4.H, I). Assuming that a filament is 6 subunits thick, the assembly rate constant for the network is about $750 \text{ subunits s}^{-1} \mu\text{M}^{-1}$. However, this is not very high if

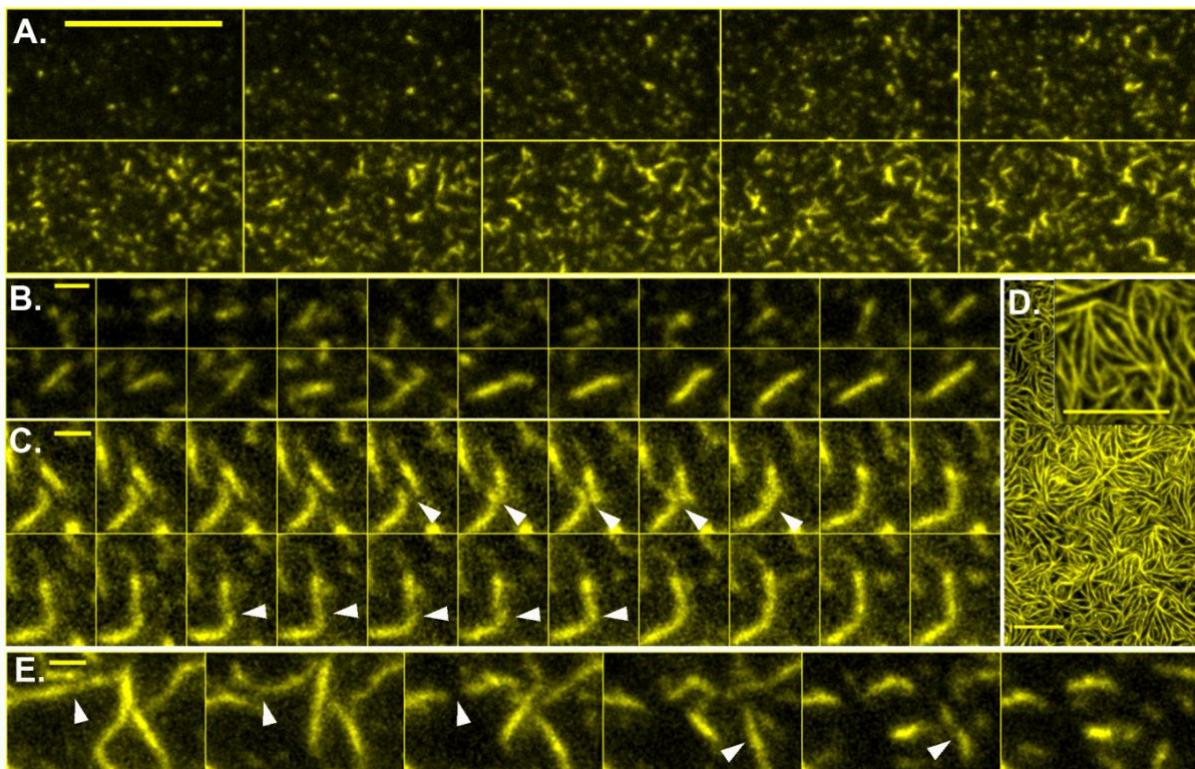


Fig.3.3 Assembly and disassembly of FtsZ network. (A) Assembly of FtsZ on supported lipid bilayer. Each frame: 5s. (B, C) The filaments display annealing and fragmentation events in the course of assembly into a network. (D) A stable FtsZ network. (E) Disassembly of FtsZ filaments. Scale bar: A: $10 \mu\text{m}$ B-E: $2 \mu\text{m}$ D: $5 \mu\text{m}$.

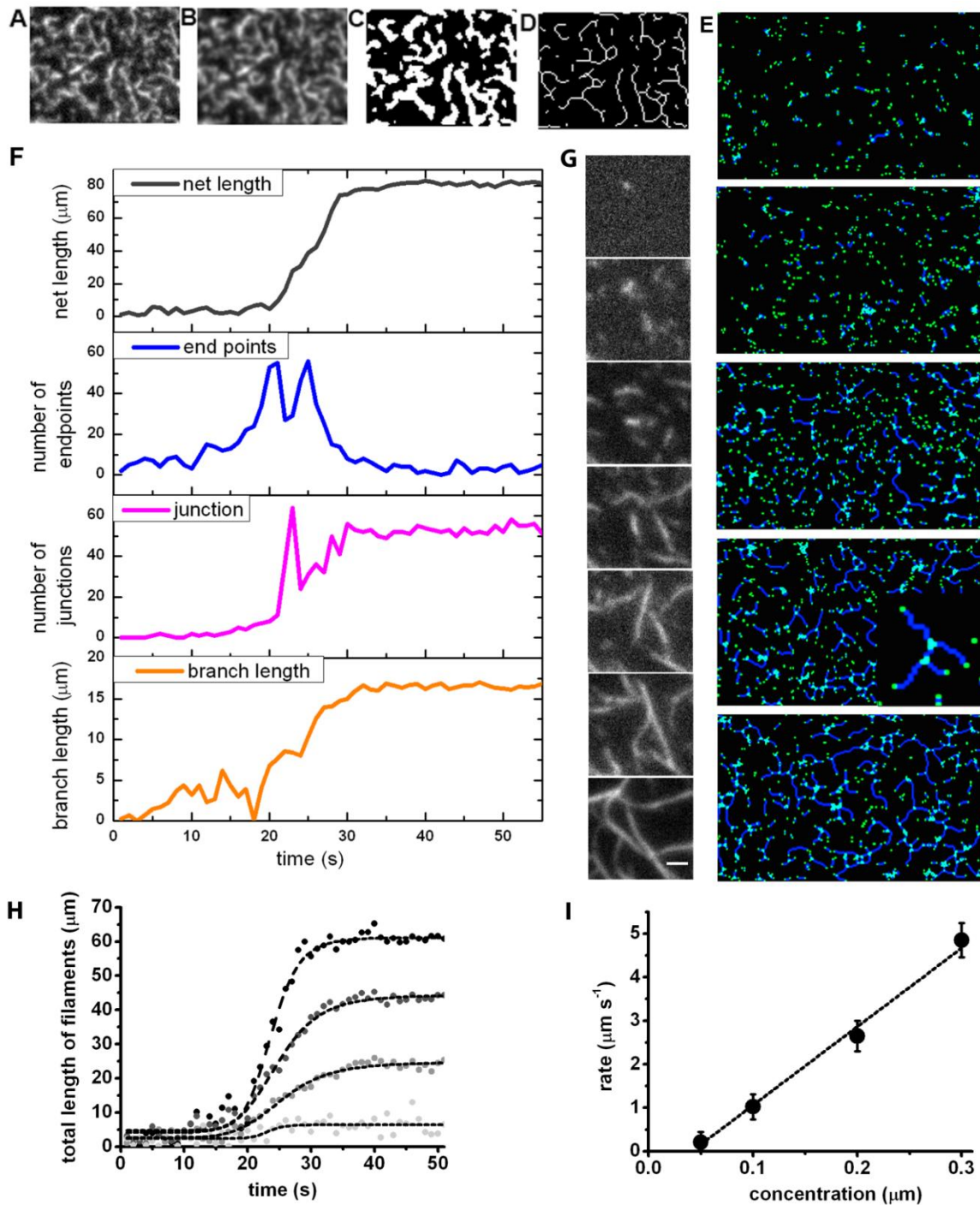


Fig.3.4 Analysis of FtsZ network assembly. (A-D): Example images of process of skeletonizing the time frames. (E) Example of analysis of skeletonised network assembly movies. (F) Graphical representation of evolution of various parameters of network assembly, junctions are in cyan, branches are in blue and end points and nucleations are in green. (G) Example montage of FtsZ network assembly showing nucleation, growth, branching and annealing of ends. (H) Growth characteristics of FtsZ network. Increased concentration of FtsZ results in longer net length of filaments in the network. (I) Growth rate of FtsZ network.

the number of nucleation sites, and the number of annealing events are considered. It is very difficult to take these into account as they are constantly changing during the process of assembly. As an approximation, dividing by the number of nucleation sites measured at the initial time points of the polymerization events, the rate constant lies between 7.5 to $10 \text{ s}^{-1} \mu\text{M}^{-1}$. At limiting concentrations of GTP, the filament disassembles, which is similar to the disassembly and dispersal of the Z-ring reported previously. The disassembly is the reverse phenomenon of the assembly, with the larger protofilaments breaking into smaller protofilaments (Fig.3.3.E). The network disassembly occurred at a lower rate of 5 subunits/second. Our observations demonstrate how the FtsZ filament is assembled out of small overlapping protofilaments. However, once the filaments assemble, the protofilaments lose their identity and are just the part of a dynamic filament. This is also shown effectively in the fluorescence recovery after photobleaching (FRAP) and the single molecule experiments described below. The end to end annealing of multiple filaments forming a single filament argues that the ends of the filaments are indistinguishable from the middle of the filament, ruling out the possibility of any specialised structure at the filament ends.

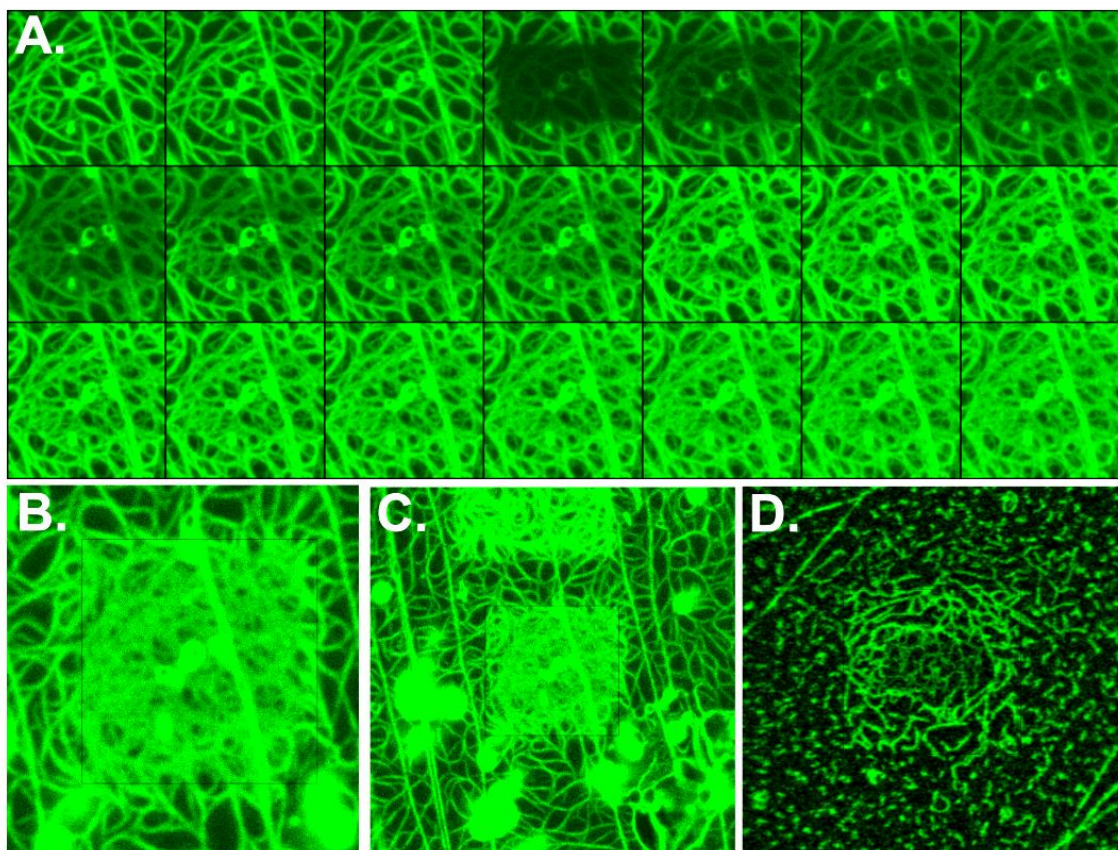


Fig.3.5 Photo-induced effects on the FtsZ-YFP-MTS polymers. (A) Montage of time series of FtsZ network with no oxygen scavenging system in the solution. (B) A zoomed out view of the region in A. (C) Distinct bundled regions in the network due prolonged exposure to laser. (D) FtsZ polymers are depolymerised by MinC (Chapter 4), however, bundled polymer due to photo-induced effects are resistant to MinC.

We also observed that exposing the filaments to laser light resulted in increased bundling and formation of static network with low turnover *in vitro* (Fig.3.5). This effect could be avoided by the use of oxygen scavenging system as described in materials and methods [98]. However, such photo-induced effects should be carefully considered as they can skew interpretations. All our experiments were performed in a buffer with an oxygen scavenging system.

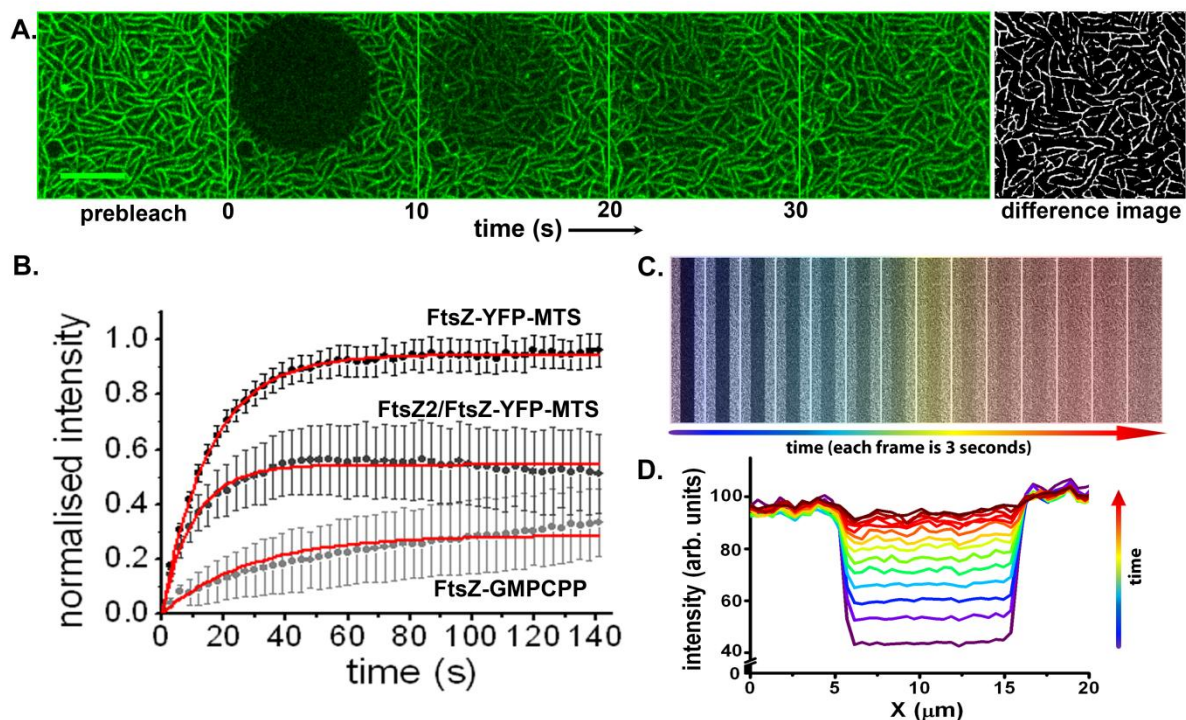


Fig.3.6 Dynamics of FtsZ filaments *in vitro*. (A) Fluorescence recovery of FtsZ after photobleaching. The spatial pattern remains same before and after fluorescence recovery. (B) Fluorescence recovery curves after photobleaching of only FtsZ-YFP-MTS, copolymers of FtsZ2/FtsZ-YFP-MTS and FtsZ assembled with GMPCPP. (C) The recovery in the filament network is a reaction dominant system. (D) Evolution of the profile of bleached region in (C) with time showing sharp boundary retained.

3.4 The FtsZ filaments are an irresolute bundle devoid of dynamic instability

We performed FRAP on the FtsZ assembly on the bilayer to study its dynamics. Fig.3.6.A shows the recovery of fluorescence in a stationary FtsZ filament network after photo bleaching. It is a reaction dominant recovery (Fig.3.6.C,D) with exchange occurring between the filament bundle and solution. The stationary filaments recover all along the length of the pre-existing filaments. The putative mechanism for this process is shown in Fig.3.7.E. We purified FtsZ-D212G, a previously studied hydrolysis deficient mutant implicated in dynamic instability in FtsZ filaments [71]. FtsZ-D212G copolymerises with FtsZ-YFP-MTS and WT-FtsZ (Fig.3.7.D). FRAP on the copolymer network shows partial recovery though with the same half time, showing that the WT-FtsZ/FtsZ-YFP-MTS show the same behaviour despite

the presence of hydrolysis deficient mutant. Additionally, a fraction is completely stagnant, probably due to the stronger lateral bonding in the presence of hydrolysis deficient mutant. We performed Malachite green on similarly assembled polymer network on bilayers to assay the GTP hydrolysis rate in our system (Fig.3.7.B). We compared it with the FRAP turnover times (Fig.3.6.B) and single molecule residence times of FtsZ-Cy5 in FtsZ-YFP-MTS/WT-FtsZ copolymer network (Fig.3.7.A). The values are summarised in Fig.3.7.C. The measured rates are very similar, suggesting that a monomer in the filament bundle of a copolymer of WT-FtsZ and FtsZ-F268C leaves similar to that in the absence of FtsZ-F268C.

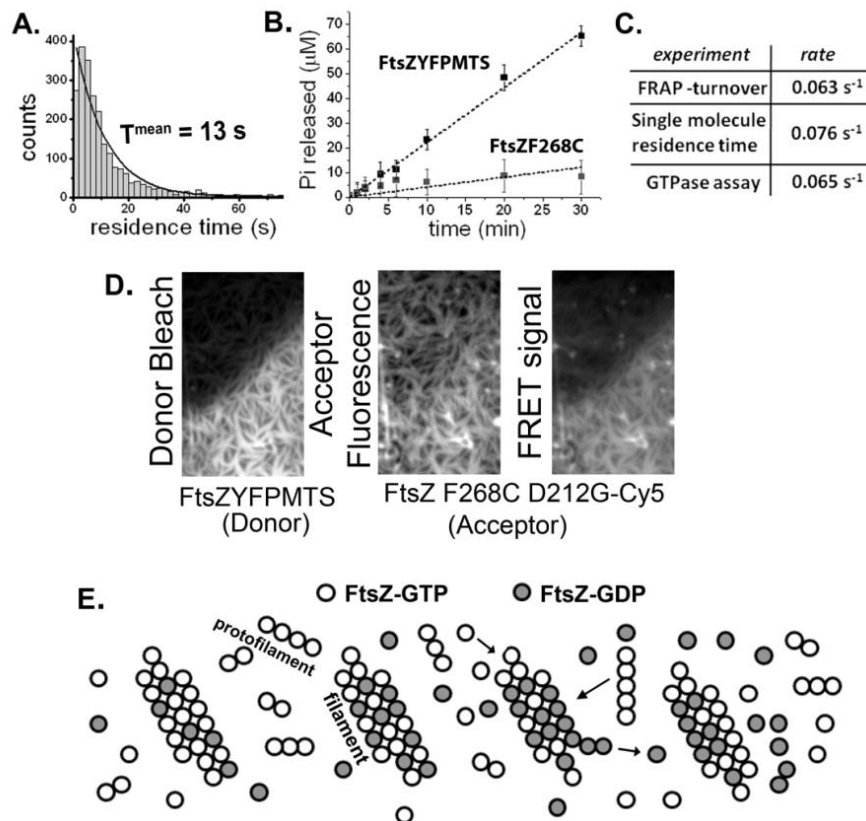


Fig. 3.7 Single molecule dynamics and hydrolysis in FtsZ. (A) Single molecule residence time distribution of FtsZ in the filament. (B) GTPase activity of FtsZ-YFP-MTS and a hydrolysis mutant FtsZF268C assembled on bilayer. (C) Table summarising rates of subunit turnover and phosphate release. (D) FtsZ2 and FtsZ-YFP-MTS copolymerise uniformly as supported by donor photobleaching and show no special regions of ‘cap’ like structure. (E) Schematic explaining the recover characteristics in the filament.

3.5 Exchange of nucleotides in FtsZ bundles

The FtsZ nucleotide binding pocket is partially exposed to solution as observed from structural studies. This raises the possibility of nucleotide exchange in the polymers without any subunit exchange [8]. Nucleotide exchange will allow filaments to be more stable and may have implications on its dynamic properties [39]. To assess whether nucleotides

exchange into the assembly of FtsZ on the membrane and also to determine the rate of such an exchange, we tried using GTP- γ -Cy5. We imaged to determine if it exchanged into FtsZ filaments assembled in GMPCPP. However, since the FtsZ did not polymerise well with GTP- γ -Cy5, we did not pursue imaging single molecule hydrolysis events. In addition, the rates of incorporation obtained by imaging GTP- γ -Cy5 would have been unreliable. Nevertheless, GTP- γ -Cy5 clearly exchanged into GMPCPP assembled filaments after they were soaked in GTP- γ -Cy5 for about 20 minutes (Fig.3.8.A). To estimate the rate of nucleotide exchange, we soaked the GMPCPP assembled filaments in 0.5 mM GTP. As GTP was exchanged into the filaments, hydrolysis was initiated, which resulted in turnover (Fig. 3.8.B). The turnover of FtsZ in the filaments can be assayed using FRAP. The mobile fraction in the turnover should be directly proportional to the amount of GTP exchanged into the filaments. With consecutive FRAP events, the mobile fraction increased, as more GTP exchanged with GMPCPP in the filaments (Fig.3.8.C,D). The turnover reaches a complete mobile fraction in about 10 minutes in an excess of GTP.

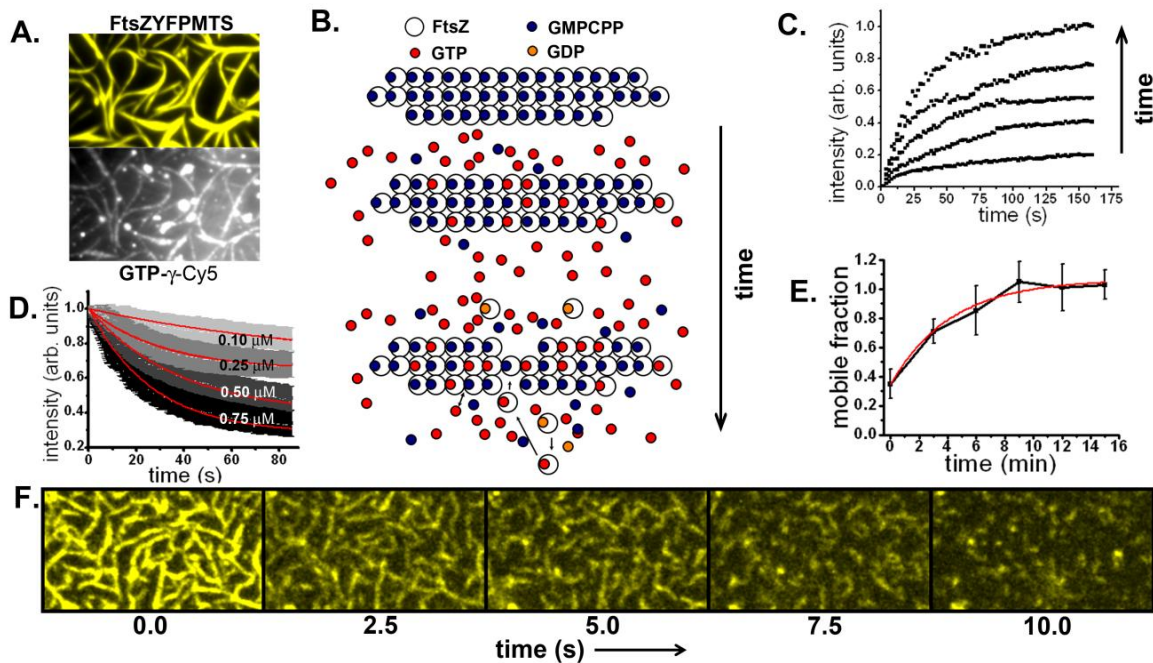


Fig.3.8 Exchange of nucleotides in FtsZ bundles. (A) GTP- γ -Cy5 exchanged into the FtsZ-YFP-MTS filament assembled in GMPCPP. (B) Schematic of the FRAP assay for nucleotide dependent subunit turnover. FtsZ network assembled with GMPCPP is soaked in GTP and FRAPped every 2.5 minutes. (C) Example FRAP curve of GMPCPP-FtsZ assembly soaked in GTP every 2.5 minutes. (D) Depolymerisation induced by soaking GMPCPP-FtsZ assembly in GDP. The red curve shows the fit to a single exponential decay. (E) Mobile fraction of subunits in the FtsZ bundle with time from FRAP curves. The red curve shows fit to a single exponential growth. (F) A montage of depolymerisation of FtsZ assembly by addition of GDP.

On the other hand, soaking GMPCPP assembled FtsZ filaments with GDP disassemble the filaments as GDP filaments are unstable (Fig.3.8.F). This is in agreement with various previous studies where it has been shown that hydrolysis or presence of GDP induces disassembly [112, 113]. GDP induces disassembly of GMPCPP-FtsZ filaments in a concentration dependent manner (Fig.3.8.D). Therefore the disassembly is clearly due to the exchange of GDP into the filaments. The rate of depolymerisation is an indication of the rate of GDP exchange. The filaments depolymerise with a half-time of about 15- 100 seconds depending on the concentration of GDP added.

Nucleotide exchange into filaments without subunit exchange has also been reported by other studies and our results are in good agreement with these studies [114-116]. However, the rate of exchange seems to depend on the nucleotide used and hence parallels cannot be drawn between them.

3.6 NZ binds to the FtsZ filaments, disassembles by sequestration of monomers

Crystal structure studies have shown previously that the FtsZ monomer consists of two independently folding domains - the N-terminal domain and the C-terminal domain (Fig. 3.9.A). The N-terminal is expected to act as an end-capping unit for protofilaments as well as sequestering units in the solution. The NZ can only bind at the C-terminal ends of a protofilament. Since the NZ does not have the C-terminal half to enable it to polymerise further, it is essentially an end capping unit for the FtsZ protofilaments. We probed the interaction of NZ with FtsZ network. We find that NZ binds throughout the length of the protofilament (Fig.3.9.B). The FtsZ filament lattice constantly generates ends as a result of monomers moving out of the lattice due to GTP hydrolysis.

Adding NZ in excess causes disassembly of the FtsZ network (Fig.3.9.C). We confirmed that this was predominantly due to sequestration of monomeric FtsZ by fluorescence cross correlation spectroscopy at a focus point above the FtsZ filament network assembly (Fig.3.9.F, H). The FCCS was done at lower concentration of NZ as correlation studies require that the number of particles be low in order to sense the fluctuations. The depolymerisation characteristics of the filament network are similar to that of a GTP-limited one. The filament loses subunits throughout its length, as indicated by the loss of fluorescence along the filament. The network subsequently breaks up and numerous fragmentation events take place along with lateral depolymerisation (Fig.3.9.C). The disassembly is hydrolysis limited as NZ does not influence the GTPase activity of FtsZ in any manner. The NZ is therefore used as a control for hydrolysis limited disassembly of FtsZ filaments in experiments described later. The disassembly activity of NZ by sequestering monomers is perhaps similar to the action of SulA, which is expressed during the SOS response to DNA damage [117-120]. This however, needs experimental confirmation. SulA also needs the turnover of FtsZ for its activity to disassemble FtsZ polymers and NZ may offer a comparable control to elucidate the mechanism of SulA.

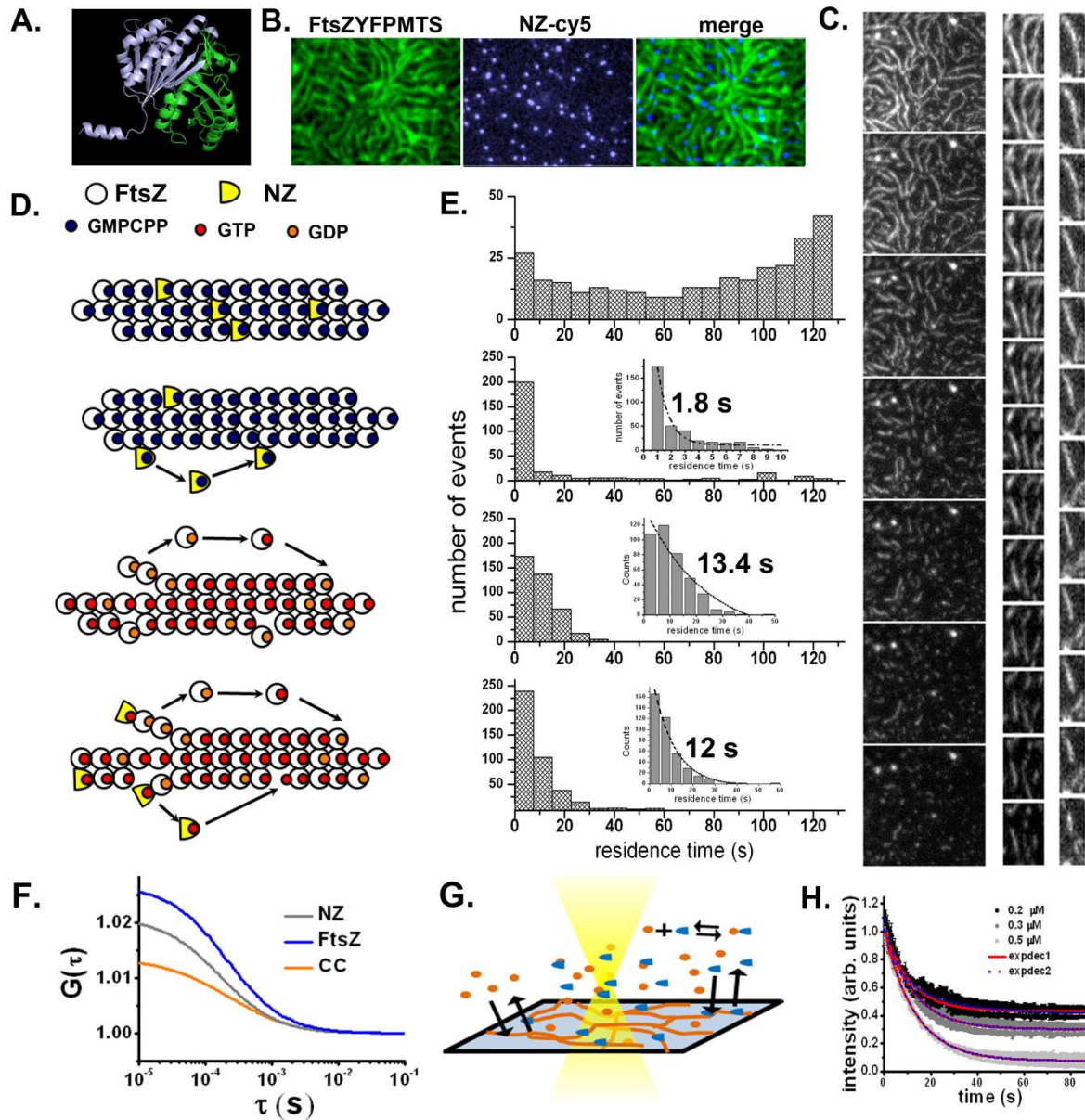


Fig.3.9 NZ depolymerises FtsZ by sequestering monomers. (A) Crystal structure of FtsZ with the N-terminal in Blue and C-terminal in yellow. (B) Single molecules of NZ-Cy5 interact with FtsZ-YFP-MTS network. (C) Montage showing depolymerisation of FtsZ filaments on addition of NZ, The characteristics are similar to that of MinC induced disassembly – overall decrease in filament intensity as well as breakage of the filaments. (D) Schematic representations of NZ single molecule residence times measured in different conditions. (E) Single molecule residence times of NZ on FtsZ filaments in different conditions. (F) FCCS curves of NZ interaction with FtsZ in the solution above the FtsZ network. (G) Schematic of the FCCS experiments. (H) NZ depolymerises FtsZ in a single exponential fashion in a concentration dependent manner reflecting sequestration of FtsZ monomers by NZ units.

3.7 Conclusions

Visualisation of FtsZ assembly on lipid membrane allowed us to observe its assembly characteristics. In particular, using the end capping NZ fragment of FtsZ, we were able to establish the following: (i) FtsZ filaments form by nucleating at multiple sites and elongate by end to end joining/annealing of these filaments. (ii) The exchange of subunits occurs throughout the filaments and each subunit space in the filament is an exchangeable site. (iii) There is exchange of nucleotides in the filaments, although at a much slower rate compared to subunit exchange from filaments. (iv) The filament assembly bundles further at higher divalent ion concentrations. This bundled filament shows different morphology and dynamics. They also show a switch from steady state turnover to disassembly. (v) All disassembly events, induced by GTP exhaustion, NZ or in bundles are phenomenological opposite events of assembly.

Can we correlate all the observations with the known features of FtsZ assembly, its structural similarity to tubulin and to dynamic instability? The Z-ring is thought to contain 6 to 7 protofilaments [39, 111, 121]. The amino acids on the lateral surfaces of the FtsZ are different from those of tubulin. However, FtsZ and tubulin are homologous in their longitudinal contacts and form similar protofilaments [122]. Microtubules and FtsZ polymerise in completely different ways. Microtubules polymerise by nucleation and then grow or shorten at their ends by addition or loss of $\alpha\beta$ -tubulin subunits from the protofilament ends. The cylindrical architecture of the microtubules is a result of combination of lateral and longitudinal interactions between the subunits [60]. On the other hand, the FtsZ first polymerises into single stranded protofilaments and subsequently interacts laterally to settle in to a bundle. The exchange of subunits is not only from the ends as for microtubules, but also from the middle of the filament. This argues for the following details concerning the dynamics of FtsZ filaments: the filament ends are no different from the middle and there is no specialised stabilising structure equivalent to a GTP cap. This partially rules out any kind of tread milling at the ends and dynamic instability. These filaments are closer to intermediate filaments in their dynamics and organisation.

The only factor suggesting a possibility of dynamic instability in FtsZ is the prohibited nucleotide exchange in filaments. Many studies have suggested that the filaments contain mostly GTP [114, 123]. We looked at nucleotide exchange in the filaments. Our experiments show that exchange of GTP into GMPCPP filaments can occur but it is extremely slow compared to subunit turnover time. Substituting GDP in the solution resulted in depolymerisation in a concentration dependent manner. This suggests that GDP also can exchange into the filaments and destabilise them, resulting in their disassembly. The basic structure of FtsZ filaments needs to be revised to a filament lattice where exchange occurs throughout and there is no real 'protofilament' once a filament has been assembled. The FtsZ filament is a partially disordered lattice of subunits in length and in breadth of about 5-7

subunits. Nucleotide exchange into the subunits stabilises the filament to some extent. This needs to be considered in mechanisms involving interaction of other regulatory proteins with FtsZ.

To summarize, we propose that it is the all-subunit equivalent and exchangeable, partially disordered architecture of the FtsZ filament, which is inadequate for a dynamic instability like mechanism. Other factors like nucleotide exchange need to be considered carefully while setting a criterion for dynamic instability. Our approach also provides a way of studying other interacting partners of FtsZ and their effect on FtsZ assembly and dynamics. With a better understanding of FtsZ filament organisation, force generation and modulation of FtsZ assembly can perhaps be more clearly elucidated.

Chapter 4

Results II: Dimeric MinC disassembles FtsZ

4.1 Preface

MinC, which directly interacts with FtsZ is thought to couple MinDE waves to FtsZ and regulate the localisation of FtsZ [30]. The exact mechanism of action of MinC on FtsZ is unclear. MinC does not affect FtsZ GTPase activity, and does not actively depolymerise FtsZ. MinC disassembles FtsZ polymers only when FtsZ undergoes hydrolysis induced turnover. How this cycling of subunits in FtsZ is linked to MinC activity is not known [92]. MinC has two functional domains - MinC N-terminal (1-115), and MinC C-terminal (116-231), henceforth referred to as MinCN and MinCC. MinCN has been shown to prevent sedimentation of FtsZ in vitro and block cell division upon over-expression [89, 93]. The MinCC interacts with MinD, mediates homo-dimerization of MinC itself and can block cell division when over-expressed along with MinD. Mutations in FtsZ rendering it resistant to depolymerisation by MinCN are on the H10 helix of FtsZ, accessible only at protofilament ends. A previous model assumes this helix to be accessible only upon GTP hydrolysis. This model assumes that the filament is mostly GDP-bound with a bend between subunits that makes the H10 accessible [90]. However, this has been refuted by many studies that demonstrate FtsZ to be mostly GTP-bound. Another study reported that MinC controls the scaffolding function of FtsZ by antagonizing the mechanical integrity of FtsZ structures. Why does the mechanical integrity decrease? By what mechanism does MinC execute this is still not clear [92].

These conflicting data raise the possibility that the turnover of FtsZ is itself responsible for the activity of MinC, with MinC binding to the protofilament ends in a polymer. A clear understanding of FtsZ organisation and its hydrolysis induced turnover are critical for elucidating how it is regulated by MinC, or any other interacting protein. Using the dynamic

FtsZ filaments assembled on bilayers, we observed the kinetics and characteristics of their disassembly by MinC. Comparing the dynamics against disassembly by a control protein fragment – NZ (chapter 3) allows us to elucidate the mechanism of MinC action more accurately.

4.2 MinC-GFP is a strong dimer

MinC and MinC-eGFP were purified as dimers by gel extraction chromatography. Since MinC has been previously reported to be a dimer [88], we determined whether MinC-eGFP was also a dimer by gel extraction (Fig.4.1.A). To measure the dissociation constant, we performed fluorescence intensity distribution analysis on MinC-eGFP with monomeric eGFP as a control. Even at very low concentrations, MinC-eGFP showed particle brightness that correspond two eGFP molecules (Fig.4.1.B). This was also confirmed by single molecule imaging where the intensity distribution of MinC molecules corresponded to double that of monomeric eGFP (Fig.4.1.C). Further, 90 percent of the molecules immobilised on a cover glass showed two-step photobleaching (Fig.4.1.D), indicating that even at nanomolar concentrations, MinC exists as a dimer.

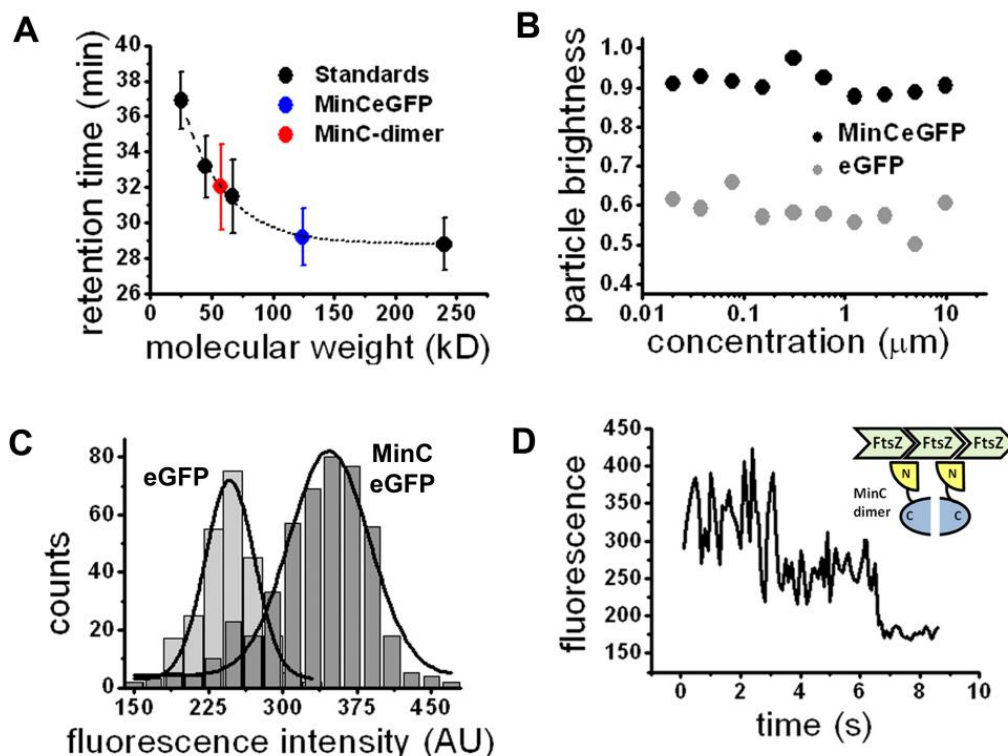


Fig.4.1 Dimeric MinC depolymerises FtsZ. (A) Purified MinC and MinC-eGFP exist as dimers. (B) MinC-eGFP is a strong dimer even at very low concentrations. (C) Fluorescence intensity distribution of eGFP and MinC-eGFP. (D) Example of two step bleaching observed with TIRF, inset: redrawn model of dimeric FtsZ selective for polymeric FtsZ.

4.3 Dimeric MinC depolymerises FtsZ filaments by occupying binding sites

Next, we explored the activity of MinC on FtsZ polymers assembled on lipid bilayers. MinC disassembled the FtsZ filament network on bilayers (Fig.4.2.A). The process of disassembly shows two main characteristics: overall decrease of the filament intensity (Fig.4.2.B) and breaking of filaments over the course of disassembly (Fig.4.2.C). The MinC dimers depolymerise FtsZ in a concentration dependent manner with complete disassembly observed with an FtsZ to MinC ratio of about 1:1. The time course of depolymerisation resembles an exponential decay. At higher concentrations of MinC, the depolymerisation curve could be more precisely described as a sum of two exponentials (Fig.4.2.D). At lower concentrations, MinC does not completely depolymerise FtsZ, but subsequent addition of MinC results in increased disassembly (Fig. Fig.4.2.E). MinC recruitment to the membrane by MinD results in more efficient FtsZ depolymerization (Fig.4.2.F). This is presumably due to increased concentration of MinC on the membrane bilayers.

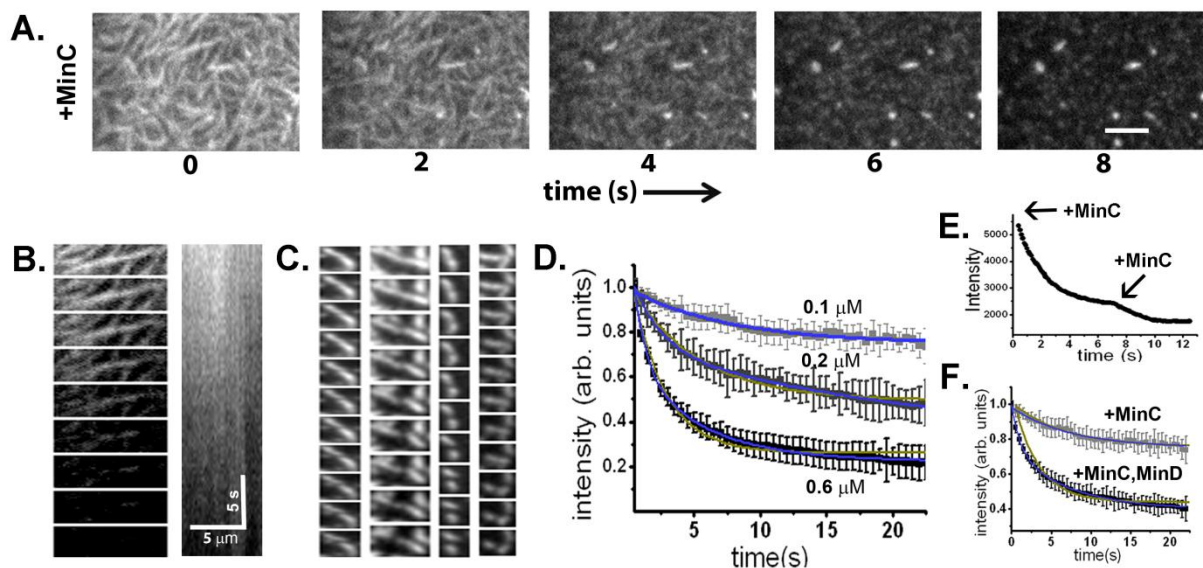


Fig.4.2 MinC disassembles FtsZ network. (A) Disassembly of FtsZ polymers on addition of MinC. (B) Montage (left) and kymograph (right) of a depolymerising FtsZ filament. (C) filaments showing breakage events while disassembly by MinC. (D) FtsZ disassembly is MinC concentration dependent. (E) Polymer FtsZ can be depolymerised further by addition of more MinC. (F) MinD enhances the efficiency of disassembly of FtsZ by MinC. Scale bar: (A,B): 5 μm.

Based on the ratio of FtsZ to MinC, a phase diagram of FtsZ vs. MinC concentration ratio was generated (Fig.4.3.A). Depending on the relative concentrations of MinC to FtsZ, there are three different regimes of depolymerisation dynamics. At lower MinC to FtsZ ratio, the filaments are stable, but, they are decreased in their intensity representing a new steady state. Photo bleaching shows turnover in the filaments suggesting that the monomeric FtsZ still rebinds to the pre-existing filaments. At almost equal concentrations of MinC and FtsZ, the

filaments are present, but they are completely disassembled and reassembled, resulting in a constant turnover of the filaments themselves rather than the monomers on existing filaments. At higher ratios of MinC to FtsZ, the MinC completely disassembles the polymers, and new filaments do not form. Fig.4.3.B shows the behaviour of FtsZ filaments in two different regimes – one at the lower concentration of MinC, where the filaments remain stationary, but with a lower intensity. This shows the usual turnover activity of the FtsZ filaments. The other regime is when the amount of FtsZ and MinC are almost equal. At these ratios, the filaments completely disassemble, but reassemble at the same time on other exposed membrane parts, resulting in new filaments that are not stationary (Fig.4.3.B).

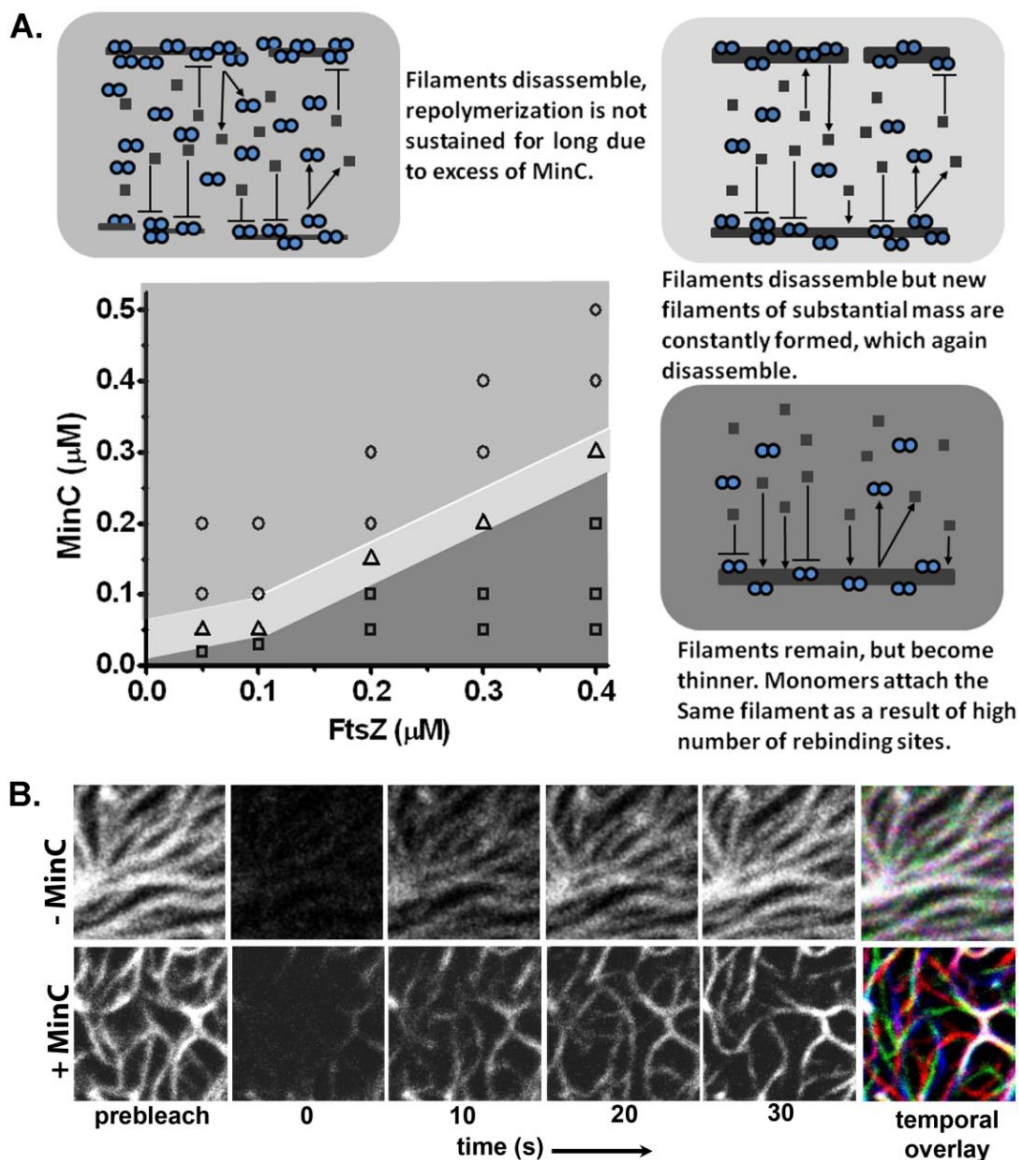


Fig. 4.3 (A) Phase diagram of MinC action on FtsZ. (B) Filament dynamics and FRAP recovery with and without MinC. Right: Temporal overlay of the sample with 5 s interval.

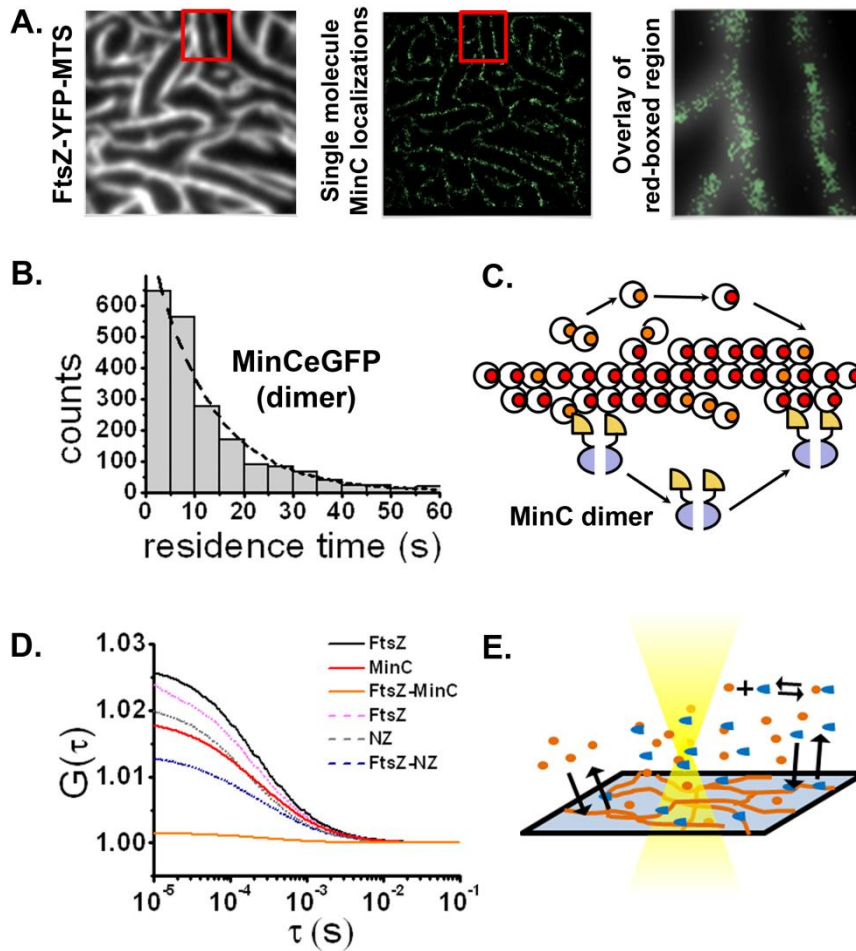


Fig. 4.4 (A) 20 nm resolution localisation of MinC-eGFP on FtsZ network. (B) Single molecule residence time distributions of MinC dimers on FtsZ filaments. (C) Schematic representation of interactions of MinC-eGFP dimers with FtsZ. (D) FCCS studies showing MinC and NZ interaction with FtsZ in the solution above the FtsZ network. (E) Schematic of the FCCS experiments.

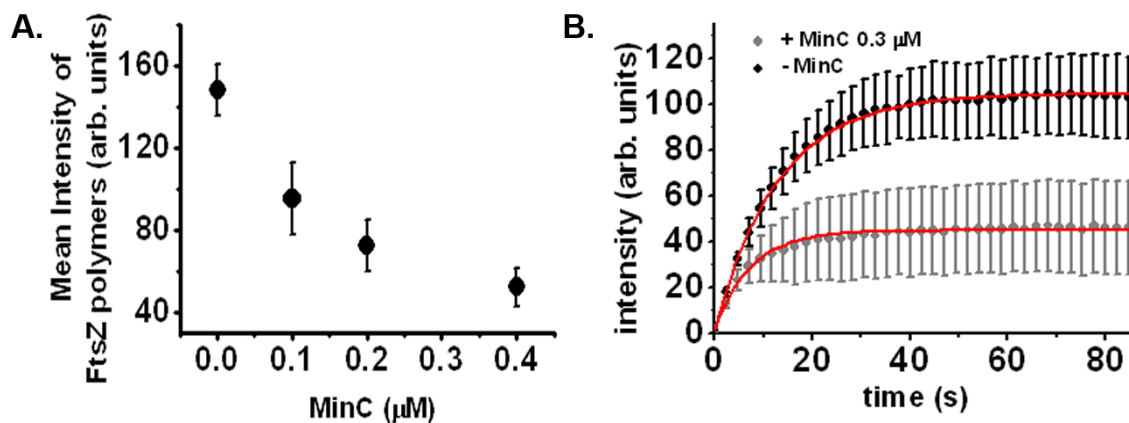


Fig. 4.5 (A) MinC reduces the polymeric FtsZ in a concentration dependent manner. (B) FtsZ shows a faster turnover in the presence of MinC.

Single molecule tracking and localization of MinC-eGFP dimers on a network FtsZ did not show any movement along the FtsZ filament. MinC-eGFP binds uniformly with the same affinity throughout the filament showing no preferential binding at any particular region (Fig.4.4.A). The MinC dimers were stably bound to a spot within their residence time. The residence time of the MinC-eGFP dimers were very similar to that of FtsZ, about 11.5 s (Fig.4.4.B,C). From this, we infer that MinC dimers bind to FtsZ polymers, and leave the filament along with the FtsZ, the rate of which is determined by the GTP hydrolysis. We infer this as MinC occupying FtsZ turnover sites, resulting in a decrease of binding of FtsZ in the filament. This inhibition in turnover at sites occupied by MinC results in fragmentation and increased release of FtsZ subunits (Fig.4.7.D). How and where MinC binds on the FtsZ has been described in earlier studies [90-92] and described further in this chapter.

To probe such a passive mechanism of depolymerisation using the turnover of FtsZ, we used N-terminal of the FtsZ - NZ. Chapter 3 describes the activity of the NZ protein on the FtsZ filaments. Briefly, it acts as an end capping protein and sequesters monomers in solution. We used this fragment to compare it with MinC as an FtsZ-hydrolysis limited depolymerase.

Two colour Fluorescence cross correlation spectroscopy revealed that NZ and FtsZ interact in solution, whereas MinC-eGFP and monomeric FtsZ do not show such an interaction (Fig.4.4.D, E), as has been suggested by previous experiments. We can therefore, rule out a model where MinC depolymerises FtsZ by sequestering monomers in the solution. MinC has also been previously reported to not influence the GTPase activity of FtsZ. The maximum rate of depolymerisation of FtsZ should be then hydrolysis limited in both the MinC and NZ mediated disassembly of the FtsZ network. However, we find that MinC depolymerises FtsZ at a faster rate at higher MinC concentrations.

A plot of initial rates of depolymerisation vs. concentration of NZ or MinC shows this clearly (Fig.4.6.A). At low concentrations, depolymerisation is limited by the concentration of NZ or MinC. If the depolymerisation kinetics is determined purely by hydrolysis, the rates should saturate at the GTP-hydrolysis rate of FtsZ and the concentration of NZ and MinC should be irrelevant. However, although NZ disassembles at a rate limited by GTP hydrolysis of FtsZ, MinC or MinC + MinD depolymerises at a faster rate in a concentration dependent manner. Our hypothesis is that the steady state of FtsZ is shifts as MinC is added to the system. This is supported by the observation of steady state polymers after addition of MinC (Fig.4.5.A). In agreement with the establishment of a new steady state, the turnover should be taking place even in the presence of MinC. FRAP on FtsZ network in the presence of MinC reveals that the turnover is faster (Fig.4.5.B). This suggests that MinC speeds up the cycling of FtsZ in the polymer network. This puts forward an important contention. How can MinC induce faster turnover of FtsZ, and cause depolymerisation faster than the rate expected to be saturated by GTP-hydrolysis, without affecting the GTPase rate?

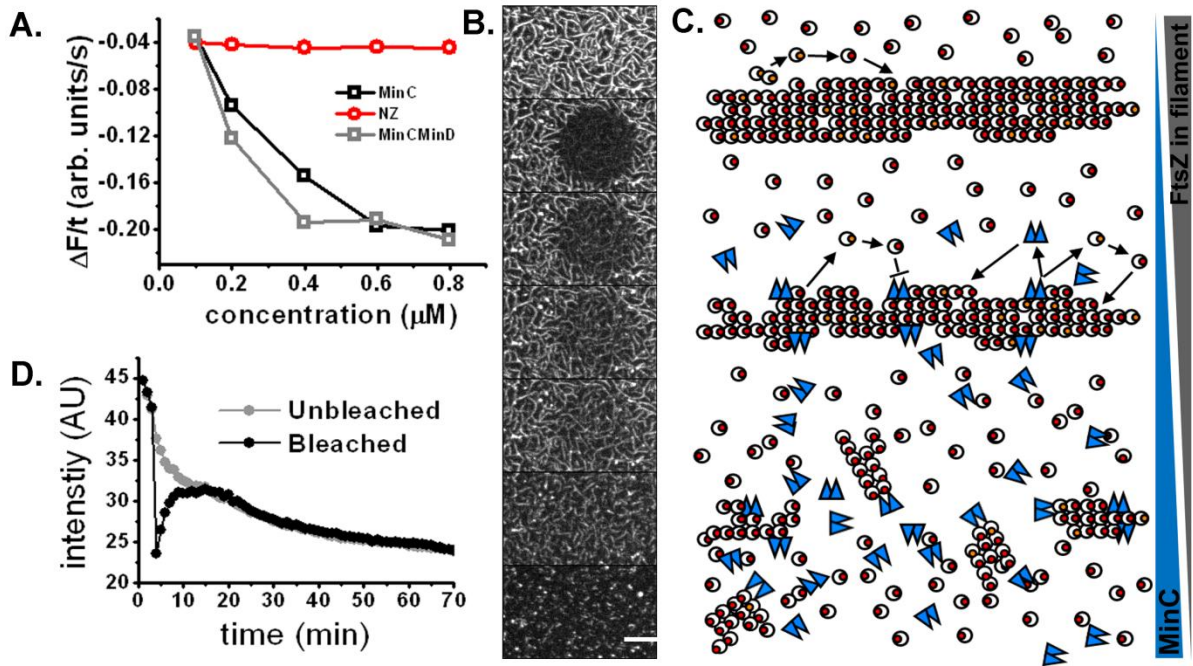


Fig. 4.6 The maximum rate of disassembly is different for NZ and MinC. (A) The initial rates of depolymerisation of FtsZ with MinC, NZ and MinD+MinC are similar, but at different concentrations, MinC shows increased rate of depolymerization. (B) FtsZ shows turnover while it is undergoing disassembly. (C) Model explaining the mechanism of disassembly by MinC. More MinC drives the filament towards a steady state with less monomer in the filament and more in the solution, while GDP bound subunits leave more readily. (D) Intensity vs. time graph of a FRAP on a disassembling FtsZ network.

Our finding that MinC depolymerises FtsZ with a higher rate than that expected by just hydrolysis suggests that MinC antagonizes FtsZ by a more complex mechanism. A model can be hypothesised based on our observations and the observations from previous studies listed below:

- Shorter FtsZ filaments are observed in the presence of MinCN and MinCN potentially interacts with the ‘minus’ end of the filament [92].
- MinCC interacts with the C-terminal domain of FtsZ and has been shown to inhibit lateral interactions. MinCN terminal interactis with H10 helix of the FtsZ subunits [90, 91].
- GTPase activity of FtsZ is necessary for the action of MinC on the polymers. Reduction in or absence of GTPase activity of FtsZ renders the filaments resistant to disassembly by MinC [92].

- d. FtsZ turnover activity generates constant ends of protofilament along the length of a bundle of FtsZ protofilaments. FtsZ polymers contain substantial amount of subunits in the GDP form [124].
- e. MinC is a strong dimer [88]. It interacts uniformly through the length of the FtsZ filament and is coupled with the turnover of FtsZ as observed by single molecule studies of MinC on FtsZ filaments.
- f. At higher concentrations, it disassembles the network at a higher rate than that expected by a simple hydrolysis dependent mechanism, exemplified by NZ induced disassembly.
- g. MinC itself lacks any hydrolysis activity. Any mechanism linked to it should be then using the hydrolysis of FtsZ.

Our observations together with the previously established facts bring out a new model, concurrent with all the mentioned facts. A concern with the MinCN weakening longitudinal model proposed by Shen *et al.* was that the H-10 helix between FtsZ dimers is not normally solvent exposed, therefore preventing MinCN interaction. However, owing to constant hydrolysis and turnover in the filament bundle, which results in monomers leaving the filament lattice, the H-10 helix is exposed at the minus-ends in the filament uniformly. We propose that MinC dimers can bind to the exposed H-10 helices through the MinC N-terminal. This also implies that the GTPase activity is critical for the action of MinC. Once bound to the minus-end, it can only be released when the terminal FtsZ subunit leaves the filament. This is supported by our observations that MinC shows very similar residence times to that of FtsZ.

However, the observation that MinC depolymerises the FtsZ assembly faster than the rate expected if limited by GTP-hydrolysis was puzzling. Since the GTPase activity is not affected at all, we hypothesised that trapped GDP-bound subunits may effectively be released from the filaments upon MinC binding to the filament and inhibiting lateral interactions as has been suggested previously. Therefore, we modelled the depolymerisation kinetics with a model where we assume a substantial amount of GDP-bound subunits in the filament or in other words, there is a lag time between GTP-hydrolysis by an FtsZ subunit and its release from the filament. This lag also results in GDP-GTP nucleotide exchange into the filaments.

4.4 Trapped FtsZ-GDP with binding site occupation by MinC model

We assume a simple model of the dynamics of FtsZ filaments, incorporating these processes:

- Binding of an FtsZ monomer to the filament on the membrane. The rate of this process is k_a (attachment), and it is dependent on the FtsZ concentration in the surrounding medium.

- Hydrolysis of GTP by a filament-bound FtsZ (GTP to GDP). The hydrolysis rate is denoted by k_h , its inverse, $1/k_h$ is the hydrolysis time τ_h (the average time of an FtsZ monomer within the filament before it hydrolyses GTP).
- Detachment of FtsZ-GDP from the filament. The rate of this process is k_d (detachment), its inverse $1/k_d$ is the ‘detachment time’ τ_d (the average time between hydrolysis and detachment).

In this model, it is assumed that FtsZ-GTP does not leave the filament. This model assumes that there are two populations of FtsZ molecules in the filaments: FtsZ-GTP (concentration C_T) and FtsZ-GDP (concentration C_D). The following differential equations describe the evolution of the concentrations of FtsZ bound to both GTP and GDP:

$$\frac{dC_T}{dx} = k_a - k_h C_T$$

$$\frac{dC_D}{dx} = k_h C_T - k_d C_D$$

The solution to these equations is:

$$C_T(t) = \left(C_{T_0} - \frac{k_a}{k_h} \right) e^{-k_h t} + \frac{k_a}{k_h}$$

$$C_D(t) = \left(C_{T_0} - \frac{k_a}{k_h} \right) \frac{k_h}{k_d - k_h} e^{-k_h t} + \left(C_{D_0} - \frac{k_a}{k_d} - \left(C_{T_0} - \frac{k_a}{k_h} \right) \frac{k_h}{k_d - k_h} \right) e^{-k_d t} + \frac{k_a}{k_h}$$

where C_{T_0} and C_{D_0} are the initial FtsZ concentrations bound to GTP and GDP respectively.

The total FtsZ concentration evolves as:

$$C_T(t) + C_D(t) = \left(C_{T_0} - \frac{k_a}{k_h} \right) \frac{k_d}{k_d - k_h} e^{-k_h t} + \left(C_{D_0} - \frac{k_a}{k_d} - \left(C_{T_0} - \frac{k_a}{k_h} \right) \frac{k_h}{k_d - k_h} \right) e^{-k_d t} + \frac{k_a}{k_h} + \frac{k_a}{k_d}$$

The kinetics are generally two-exponential, but depending on the actual values of k_h , k_d and the pre-exponential factors, the experimentally data may be well approximated by one exponential. The rates do not dependent on the attachment rate k_a . However the steady states $C_T(t \rightarrow \infty) = \frac{k_a}{k_h}$ and $C_D(t \rightarrow \infty) = \frac{k_a}{k_d}$ depend on k_a .

We fitted the data to the model with the following constraints: the values of C_{T_0} , C_{D_0} and k_h were equal for all the curves (the FtsZ meshwork is always in the same state before addition of MinC); k_a and k_d varied with the concentration of MinC.

The ‘Trapped FtsZ-GDP model’ in which the filaments have FtsZ-GDP subunits trapped in the lattice seems to agree with the depolymerization kinetics observed in the presence of MinC. The FtsZ filaments have been previously shown to have bound GDP up to 50 % of the subunits [124]. The action of MinC on the FtsZ polymers results in concentration dependent

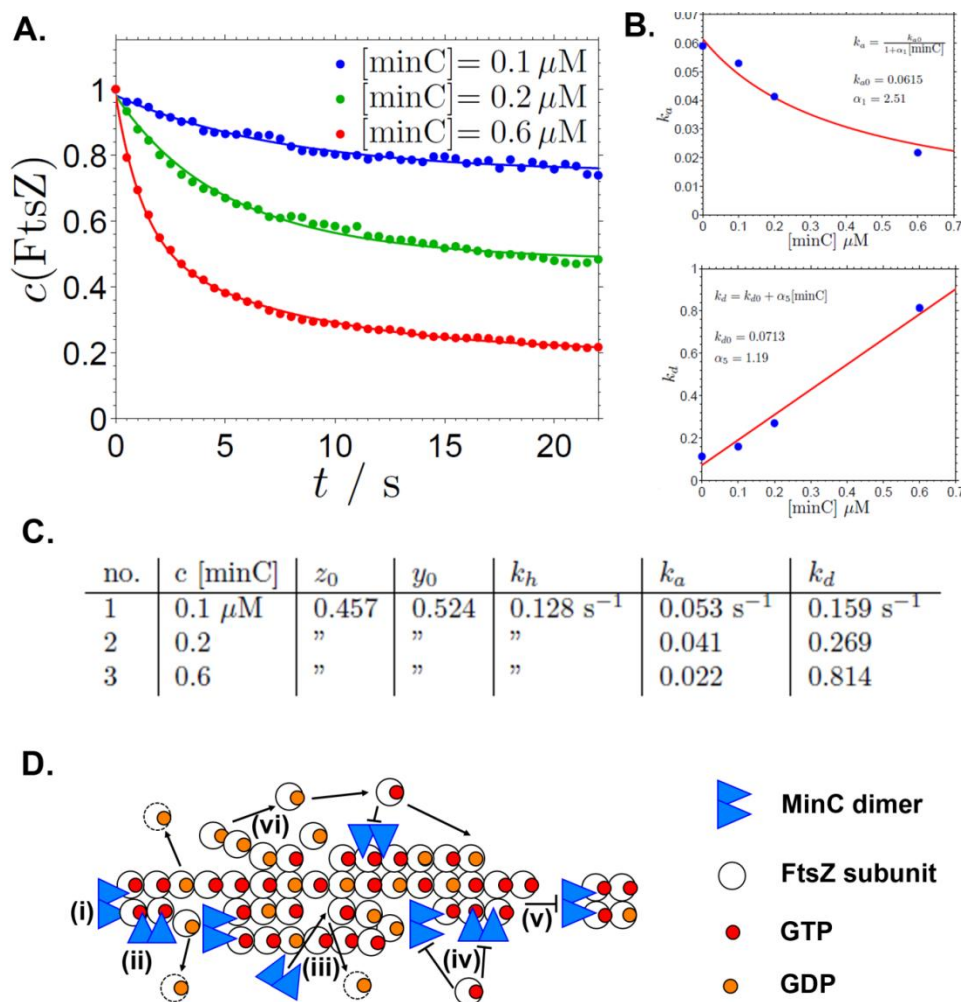


Fig. 4.7 FtsZ equilibration curves in the presence of MinC fits to the model. (A) Trapped FtsZ-GDP model fit to the depolymerisation data. (B) The experimental dependence of the rates k_a and k_d on MinC concentration. (C) Values of k_a and k_d from the fits. (D) Model of mechanism of MinC depolymerizing FtsZ filaments – (i) MinC can bind to the – end of the FtsZ filaments through the N-terminal. (ii) MinC also interacts with the C-terminal of FtsZ through the C-terminal. (iii) MinC can bind to exposed – ends in the filaments caused by a leaving FtsZ subunit. (iv) Once bound to FtsZ, MinC remains bound until the subunit leaves, blocking any incoming FtsZ subunits. (v) By inhibiting local turnover, MinC causes fragmentation of the FtsZ filaments, as well as blocks any annealing events. (vi) The net action of MinC also results in a release of FtsZ-GDP subunits trapped in the filament lattice, resulting in a concentration dependent increase in the rate of disassembly.

disassembly of FtsZ polymers. The disassembly rate increases with the concentration of MinC substantially more than just the hydrolysis limited rate of disassembly as exemplified by NZ.

The extent of coupling between hydrolysis and depolymerisation has been difficult to study experimentally. A recent study shows that hydrolysis events within a filament are random and independent of each other [125]. Ruptures also account for loss of FtsZ-GTP subunits from the end as well as within the filaments. Another important result from this study is that regardless of GTP or GDP, the filaments maintain an equivalent curved configuration. The study also emphasises that nucleotide exchange is an important factor in determining depolymerisation dynamics [59, 125], suggesting that FtsZ-GDP at the interface of a second FtsZ must be maintaining its contacts and that FtsZ-GDP resides in the lattice for a substantial time. The model also suggests that the MinC probably breaks lateral interaction leading to release of GDP-bound subunits, in contrast to NZ, which does not seem to affect the GDP-bound subunits, as indicated by the depolymerization kinetics.

Comparing the hydrolysis in bulk and subunit exchange in the filament lacks the refinement to compare the independent processes precisely. The exact associations of these events are, therefore, ambiguous. Filament rupture at GTP interface has also been predicted from various studies. MinC binding to H-10 helix can also happen at such rupture points in addition to hydrolysis regions, facilitating fragmentation. MinC, being a dimer, can also be attached to more than one FtsZ subunit at a time and therefore, result in a faster disassembly by pulling out more than one subunit with each hydrolysis event. However FCCS probing interaction between FtsZ and MinC does not show any cross correlation, suggesting minimal interaction of MinC and FtsZ in the solution. An ambiguity remains on how GTP hydrolysis is coupled to disassembly. Moreover, nucleotide exchange also plays a role in stabilising the filaments against disassembly. Resolving this issue needs a clearer understanding of these processes.

4.5 MinCDE waves spatially regulate FtsZ polymers

The concentration of MinC in the *E.coli* cell is about 400 molecules per cell compared to FtsZ which is about 15000 molecules per cell. In our *in vitro* experiments, complete disassembly occurred at a ratio of about 0.8 to 1.2 of MinC to FtsZ. The lower stoichiometry of MinC *in vivo* with respect to the FtsZ needs to be explained. We argue that since MinC works in concert with the MinDE waves, a local high concentration of MinC should be sufficient to disassemble FtsZ polymers locally. The localization of MinC is dependent on MinDE waves. To check this, we reconstituted the MinDE wavmain es with FtsZ and MinC (Fig. 4.8.A). At MinC to FtsZ ratios of 1:10, FtsZ filaments are localised complementary to the MinDE proteins comprising the waves. This is dependent on the presence of MinC. The schematic (Fig.4.8.B) shows how localised FtsZ disassembly results from the presence of the MinDE waves, whereas, absence of the MinDE proteins results in a more uniform disassembly of the FtsZ network.

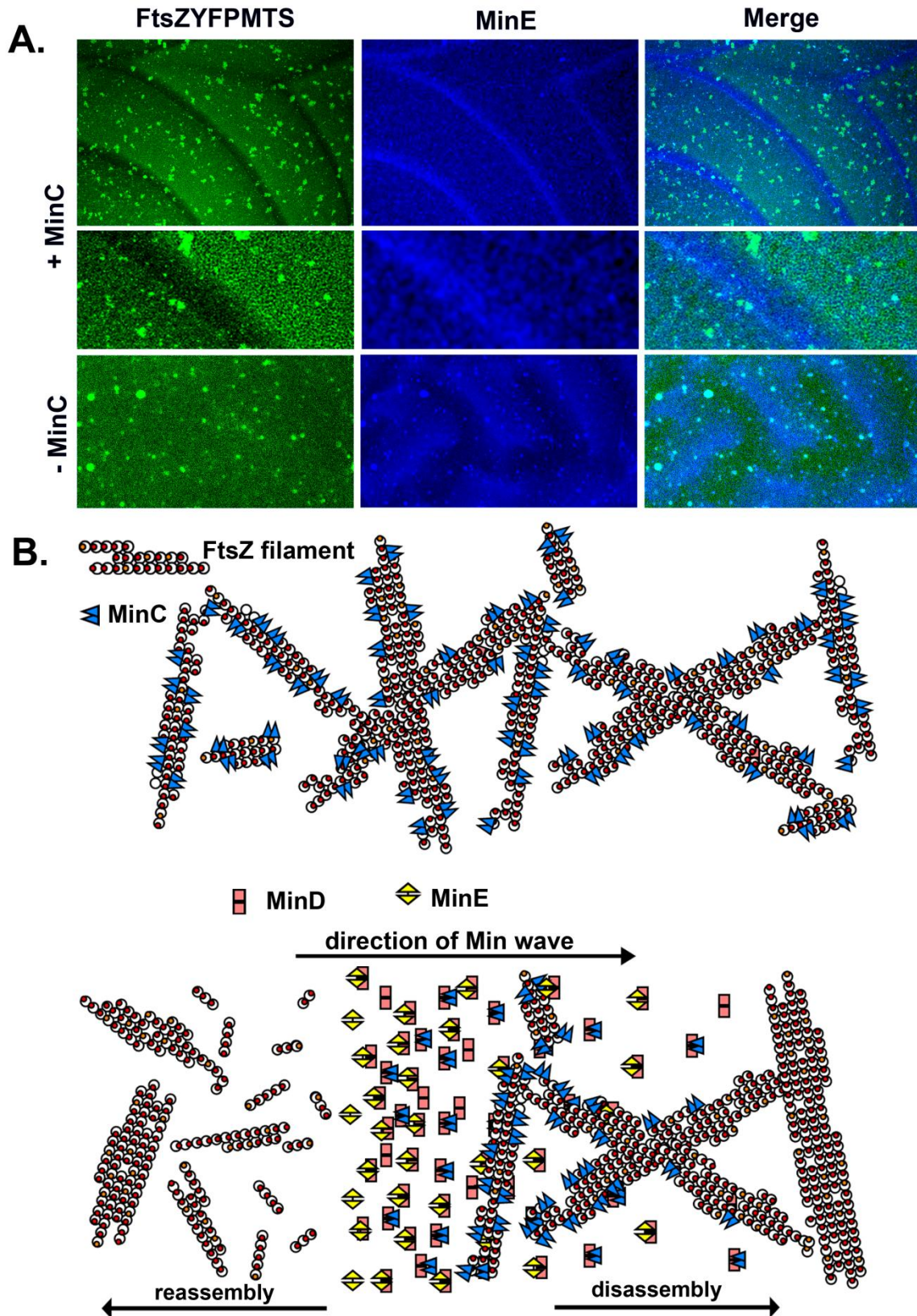


Fig. 4.8 Spatial regulation of FtsZ by MinCDE waves. (A) FtsZ is depolymerised by MinC, which localises to the waves. (B) Schematic representing the localization of MinC by MinD-MinE, resulting in localised depolymerisation of FtsZ.

4.6 Conclusions

Disassembly of FtsZ by MinC is somewhat enigmatic. It requires the GTPase activity of FtsZ, and the turnover resulting from GTP hydrolysis, but MinC does not directly modulate the GTPase activity in any way [126]. Previous studies have suggested that MinC inhibits the scaffolding function of FtsZ [92]. MinCC was suggested to bind to the filaments and prevent lateral interactions and MinCN was reported to lower the rigidity of the polymers. These studies describe the effect of MinC in terms of loss of elasticity of the FtsZ network, but not at a mechanistic level on how exactly MinC causes these effects [92].

Since FtsZ is a dynamic filament with subunit exchange throughout its length, we examined the effect of MinC on FtsZ to understand the mechanistic effects of MinC activity. First we explored if MinC was a monomer or dimer as reported previously. We found using FIDA [101], a very sensitive method to measure the brightness of a particle, that the MinC-eGFP is a very strong dimer, even at nano-molar concentrations. We then used MinC-eGFP to investigate single molecule residence times of MinC on FtsZ. Surprisingly; we found that it is very similar to that of FtsZ, suggesting that the MinC turnover on the filament is coupled to FtsZ turnover. Binding of MinC dimers to FtsZ filament sites block monomeric FtsZ rebinding, only as long as the particular set of monomers MinC is bound to reside in the filament, rendering the extent of steady state shift dependent on concentration of MinC. More MinC, results in more re-binding sites occupied, though with a turnover coupled to FtsZ, reducing the number of 'lattice sites' in the polymers and the monomeric FtsZ to new steady state equilibrium. This results in thinner filaments. This is supported by the fact that fluorescence is lost uniformly throughout the filament bundle during the process of establishment of a new steady state. The consequence of this has been observed in previous studies as loss of stiffness in FtsZ networks. We speculate that the increase in depolymerisation rates with increasing concentrations of MinC is a result of release of FtsZ-GDP trapped in the filament lattice. This assumption that FtsZ-GDP is trapped in the filament has also been hinted at by many other studies [124]. MinC facilitates the release of the FtsZ-GDP initially, resulting in the increased disassembly rate; however, it achieves a steady state again with a new lower polymer mass. The molecular details of how MinC interacts with the FtsZ filament, what regions of the structure are involved, need more structural studies of a complex of FtsZ and MinC.

How is the filament binding more pragmatic for the Min system compared to sequestration of monomers? Since the FtsZ polymers are recruited on the inner membrane surface assisted by membrane recruiting FtsA or ZipA, MinC binding to the filaments while on the membrane through MinD is a may be a more effective mode of action. As reported in the crystal structure of *T. maritima* MinC [88], the flexible linker between the N- and C- terminal domains of MinC would allow the N-terminal domains to be rotated by about 180°. This would allow both the N-terminal domains, which have been shown previously to bind to

FtsZ, to FtsZ polymers with one N-terminal rotated [88]. As has been suggested previously, dimeric MinC would be then selective for FtsZ polymer instead of monomer [88]. Intuitively, MinD binds to the C-terminal of MinC, recruiting MinC to the membrane, while the MinC N-terminal extends to interact with FtsZ on the membrane. Therefore, being localised on the membrane, MinC can more efficiently interact with polymers rather than monomers. Additionally, the dimeric nature of MinC may add to the efficient interaction with dimeric MinD on the membrane. In total, the Min system and the FtsZ filament dynamics could have evolved synergistically, to give rise to interdependence between components so as to collectively have an emergent property. The synergistic activities of independent components are - hydrolysis induced turnover of FtsZ, stable dimeric MinC able to sense polymeric FtsZ, ability of MinC to use the activity of FtsZ to disassemble, and an ensuing MinD-MinE oscillating involving ATP hydrolysis by MinD and its catalysis by MinE system on a membrane substrate, resulting in localizing MinC.

The *E.coli* FtsZ and Min proteins exemplify a self-organised system in which energy is consumed in two forms by two different components: The MinD-MinE system in which MinD hydrolyses ATP, and the FtsZ system where it uses GTP [85]. MinC links the two by virtue of its binding to MinD and its activity on FtsZ polymers. The *in vitro* experiment combining all the four components – MinCDE and FtsZ proves that the Min proteins are able to spatially regulate FtsZ polymers, as has been suggested on the basis of genetic experiments.

Chapter 5

Results III: Z-ring forming FtsZ filaments are intrinsically curved with a twist

5.1 Preface

In spite of their small size, bacteria display highly organised cytoskeletal structures like coils, helices or rings. Cytoskeletal proteins localise to distinct regions in the cells by various mechanisms. These mechanisms may involve adaptor proteins or spontaneous structural features of the proteins or their oligomers. Several of these proteins are known to polymerise and form coils, helices or rings at the inner cell membranes [56, 127]. Extensive mechanical modelling has been done to explain the occurrence of such specific structures within the small volume of bacterial cells [128-131].

During cell division in many rod-shaped bacteria, one of these cytoskeletal structures, the Z-ring, composed of tubulin homologue FtsZ, is assembled into ring like structures at the division plane. How exactly the polymerised FtsZ settles into these specific ring-like structures, and whether this ring is able to actively contribute to the division process, is not known, although various mechanical models have been proposed. The placement of the Z-ring structures in the middle, i.e., at the later division plane, is supposedly guided by the action of inhibitors localised at the cell poles or oscillating from pole to pole, and by nucleoid occlusion [121]. However, these mechanisms are only involved in the placement of the cytokinesis machinery and not in the organisation of their structural features. Knocking down proteins involved in nucleoid occlusion or oscillations still result in misplaced, but intact ring-like structures [132]. In recent studies with high resolution imaging [133] and also with cryo-electron microscopy [68], the 'Z-ring' has been generally described as a helical structure. Purified FtsZ has been studied extensively by electron microscopy and atomic force microscopy [61-63]. The FtsZ filaments show nucleotide dependent curvature [6]. The GTP

bound FtsZ filaments have a straight conformation, whereas the GDP bound filaments formed rings of about 25 nm diameter.

Lately, the idea that the FtsZ filaments in cells may possess spontaneous curvature with functional relevance has resulted from observations across various studies [63, 74, 115, 134, 135]. Consistently, many AFM or EM images from these studies show curved filaments. The role of the suggested intermediate curvature is not very clear. An *in vitro* cryo-EM study on FtsZ filaments contradicts the presence of any local spontaneous curvature [136]. However, in a recent study, Osawa et al. showed the ability of FtsZ filaments with an artificially introduced membrane targeting sequence (MTS) to bend membranes, and the influence of the MTS placement in FtsZ on the bending direction of membrane. They used an MTS from MinD at the C-terminus of FtsZ to mimic the recruitment of FtsZ to the membrane by adaptor proteins ZipA or FtsA. On shifting the MTS to the N-terminus, they show that the filaments now bend the membrane in the opposite direction. They interpret this as the action of a constriction force produced by partial Z-rings [97]. A dividing bacterial cell initially has about $2 \mu\text{m}^{-1}$ curvature, but proceeds towards much higher curvatures as the cell progresses through division. It is far from evident whether a bacterial membrane, fortified by many structural proteins, osmotic pressure, and a cell wall, would be as easily deformed. In a more conservative view, the spontaneous structure of FtsZ filaments may enable them to organise into highly curved supra structures by sensing the inner cell membrane curvature. This kind of sensing has been speculated for other families of proteins which are curvature dependent in their interaction with membranes, such as BAR domain proteins, although at completely different length scales.

Here, we studied how FtsZ filaments respond to curvature values found at various stages of bacterial division. We present evidence of FtsZ filaments displaying intrinsic curvature as well as a spontaneous twist and therefore forming a structure along the division plane simply by geometrical confinement and conformational preferences. First, we show that on free standing membranes, the protein filaments bend the membrane to their own curvature, confirming previous studies [97]. We show that FtsZ-YFP-MTS as well as MTS-FtsZ-YFP, the two constructs used by Osawa et al. [97], form ring-like filaments that interact with curved membranes and display a preference for radii of curvatures resembling a bacterial cell. Using sub-micron diameter capillaries, we test the assumption of highly curved ($10 \mu\text{m}^{-1}$) FtsZ polymers. We find it necessary to consider spontaneous twist along with curvature to explain the observed behaviour. Our findings thus suggest a mechanism for how membrane curvature and intrinsic curvature of filaments are exploited in a simple mechanical way to organise cytoskeletal elements of the divisome. Moreover, the established technique may also be used for investigation of other filaments with intrinsic curvature and effect of other interacting proteins on the curvature.

5.2 FtsZ bends the membrane towards its own intrinsic curvature

Previous studies showed that in multilamellar liposomes, the membrane-targeted FtsZ produced curved distortions on the membrane. Depending on whether the MTS was on the C-terminus or the N-terminus, the distortions were either concave or convex. On the basis of these observations, it has been concluded that partial Z-rings produce constriction forces similar to the complete Z-ring. We believe the distortions are simply caused by a bundle of curved filaments bending the flexible membrane towards their own curvature. We repeated the experiments and quantitatively evaluated the radii of curvature induced to the membranes.

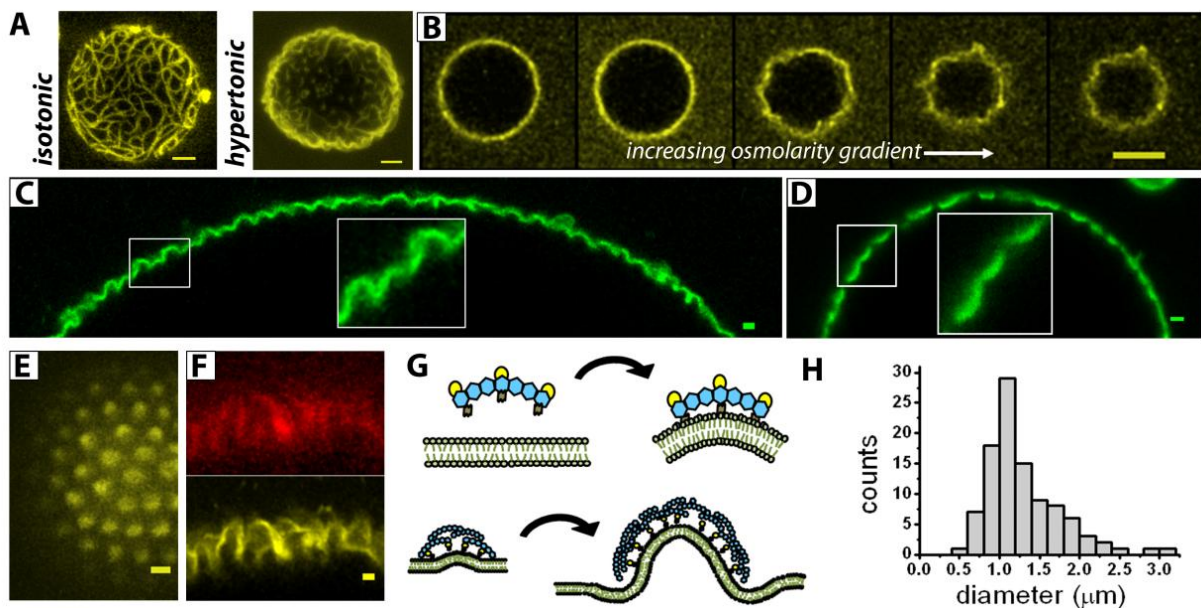


Fig.5.1 Assembly of FtsZ on GUVs. (A) FtsZ assembled on a vesicle in isotonic condition shows networks similar to planar supported bilayers, whereas in hypertonic conditions, vesicle shows curved filaments. (B) Vesicle deflating with increasing osmolarity difference. (C) MTS-FtsZ-YFP assembled on a GUV. (D) FtsZ-YFP-MTS assembled on a GUV. (E) Patches of MTS-FtsZ-YFP on the pole of the GUVs. (F) Deformed membrane (upper) and MTS-FtsZ-YFP (lower). (G) Schematic of the process of deformation of the membrane by FtsZ filaments. (H) Histogram of the radii of curvatures observed on assembling the FtsZ-YFP-MTS on GUVs. Scale bars: A: 10 μm B: 5 μm C-E: 1 μm.

We observed that the filaments do not induce curved profiles when the unilamellar vesicles are isotonic, or there is no osmolarity gradient across the membrane. They show filament networks similar to those on planar supported bilayers (Fig.5.1.A). Changing the osmotic gradient across the membranes by adding 10 mM glucose decreases intravesicular pressure and relaxes the membrane surface tension. This results in a curved topology of the membrane as well as the filaments (Fig.5.1.A,B,F). We interpret that FtsZ filaments are very elastic. Only when the membrane tension is low under hypertonic conditions, the filaments can exert

their spontaneous curvature on the membrane. Fig.5.1.C and 5.1.D show equatorial cross sections of GUVs with MTS-FtsZ-YFP or FtsZ-YFP-MTS producing spherical protrusions outwards or inwards respectively. The mean diameter measured is about 1-1.25 μm (Fig. 5.1.H). We reasoned that spontaneously curved filaments should align on similarly curved supported membranes. The behaviour of filaments at various curvatures should provide insight about the intrinsic structure of the FtsZ filaments.

5.3 FtsZ filaments respond to the curvature of supported bilayers

To test the hypothesis that FtsZ protofilaments have spontaneous curvature, we assemble the filaments on bilayers formed on curved substrates. The curved substrates are produced using e-beam lithography; their profile can be checked using AFM (Chapter 2). A pre-curved filament should align along the direction of curvature, such that the bending energy of the polymer is minimized. Fig.5.2.A and 5.2.B show the differential alignment of copolymerised FtsZ and FtsZ-YFP-MTS filaments between planar crests and curved troughs by fluorescence imaging and by atomic force microscopy, respectively. With increasing diameter of grooves above 1 μm , the preferential alignment of the filaments is lost (Fig.5.2.C).

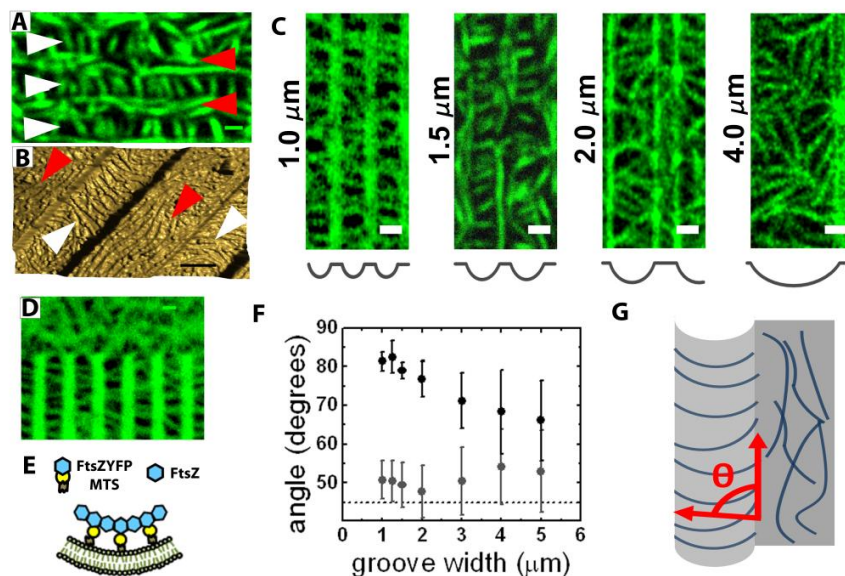


Fig.5.2 Interaction of FtsZ with curved membranes. (A) FtsZ-YFP-MTS assembly on a membrane supported by a substrate with curved troughs (white arrows) and plane crests (red arrows). (B) AFM image of the filaments assembled on the same substrate as (A). (C) FtsZ-YFP-MTS assembled on supported membranes with different radii of curvature. (D) Alignment on grooves compared to a plane substrate. (E) Schematic of the FtsZ-YFP-MTS with spontaneous curvature binding to the membrane. (F) Observed angles for FtsZ-YFP-MTS assembled on supported membranes with different radii of curvature. (G) Schematic showing the measured filament orientation angle. Scale bars: (A, B): 1.5 μm . (C,E): 1 μm .

Fig.5.2.D shows arrangement of the filaments on a substrate having both planar (top) and curved regions (bottom). Fig.5.2.E shows schematically the FtsZ and FtsZ-YFP-MTS in polymerised form with an intrinsic curvature matching the membrane curvature. We tested the precision of alignment at different radii of curvatures. We measured the angle formed by the filament with respect to the long axis of the grooves (Fig.5.2.F,G). We find that the near perpendicular alignment is most predominant at radii of curvatures $1.25 \mu\text{m}^{-1}$. Experiments above these curvatures (grooves with smaller radii) were not feasible, owing to optical resolution limits and the inability of AFM tips to scan the troughs. Therefore, we resorted to glass capillaries which show positive curvature, and used MTS-FtsZ-YFP instead of FtsZ-YFP-MTS, which should bind the membrane from the opposite side while preserving its spontaneous curvature, in agreement with the free standing membrane bending.

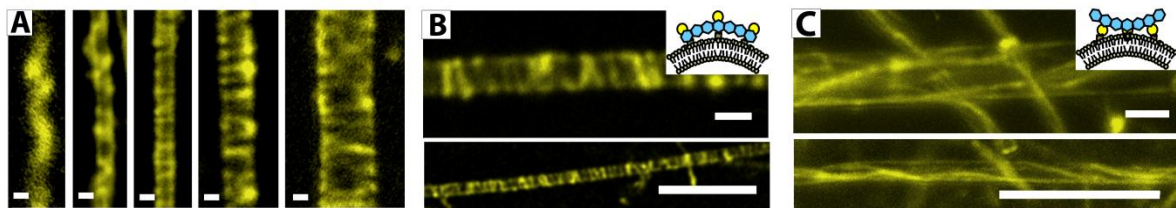


Fig.5.3 (A) MTS-FtsZ-YFP on glass capillaries of increasing sizes. (B) MTS-FtsZ-YFP on glass capillaries. (C) FtsZ-YFP-MTS on glass capillaries. Insets (B) and (C): representations of filament curvature with respect to the membrane curvature dependent on the position of MTS. Scale bars: (A): $1 \mu\text{m}$, (B,C): top: $1 \mu\text{m}$, bottom: $10 \mu\text{m}$.

5.4 FtsZ polymers on membrane curvatures higher than $1 \mu\text{m}^{-1}$

In order to probe the behaviour of FtsZ filaments on curvatures higher than $1 \mu\text{m}^{-1}$, we coated glass capillaries with bilayers and assembled MTS-FtsZ-YFP, a version of FtsZ with the MTS on the N-terminal. This results in the MTS on the opposite face of FtsZ [97]. In such a case, spontaneously curved FtsZ filaments which were aligning on grooves through MTS at C-terminal, should bind and align on capillaries through the MTS on N-terminal. Consistent with the direction of spontaneous curvatures, MTS-FtsZ-YFP could also align on glass rods of different sizes coated by lipid bilayers (Fig.5.3.A). Fig. 5.3.B and 5.3.C shows the difference in the orientation of the polymers depending on whether MTS-FtsZ-YFP or FtsZ-YFP-MTS are used. The filaments show constant turnover as is expected from an active filament resembling *in vivo* structure (Fig.5.4, 5.5). In contrast to grooves, capillaries also allow for longer filaments to complete the circumference and assemble complete rings or helices. For a capillary size range of 0.5 to $1 \mu\text{m}$, the MTS-FtsZ-YFP filaments align almost perpendicularly to the longitudinal axis of the glass rod ($75^\circ \pm 16^\circ$). Occasionally, 2-4 complete turns were also observed. The FtsZ-YFP-MTS filaments, on the contrary, bind along the longitudinal axis of the rod ($23^\circ \pm 12^\circ$).

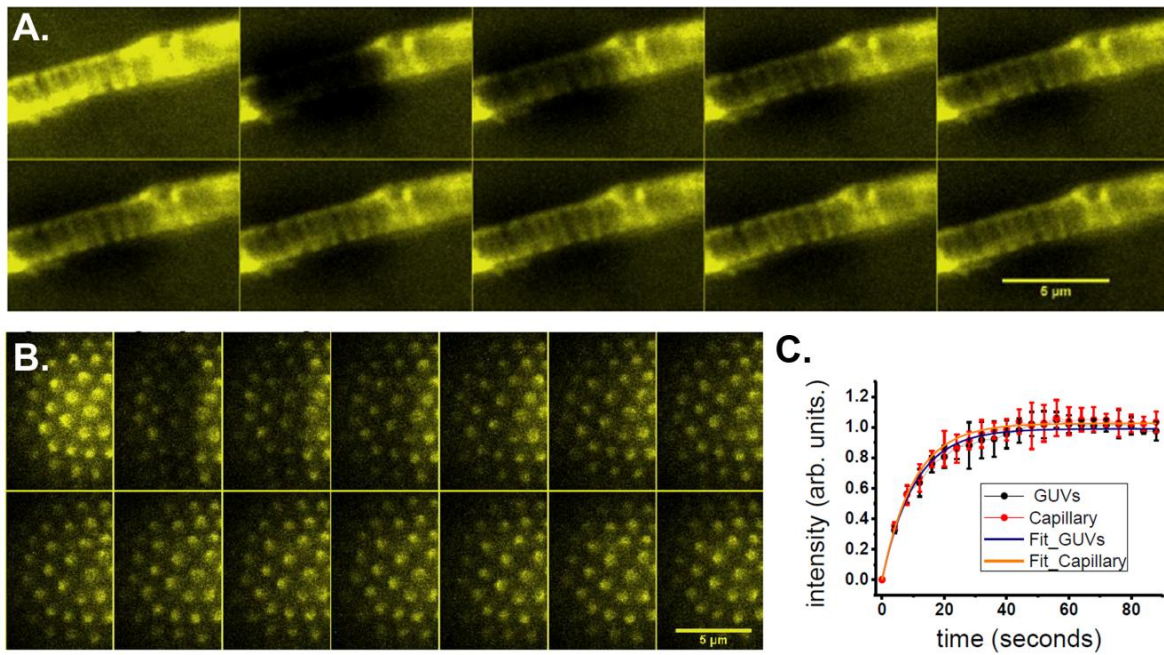


Fig.5.4. (A) montage of FRAP on the ring-like structures on the capillary. (B) Montage of FRAP on protrusion formed by MTSFtsZYFP on Giant Unilamellar vesicles. (C) FRAP recovery plot comparing filaments on capillaries and freestanding membranes.

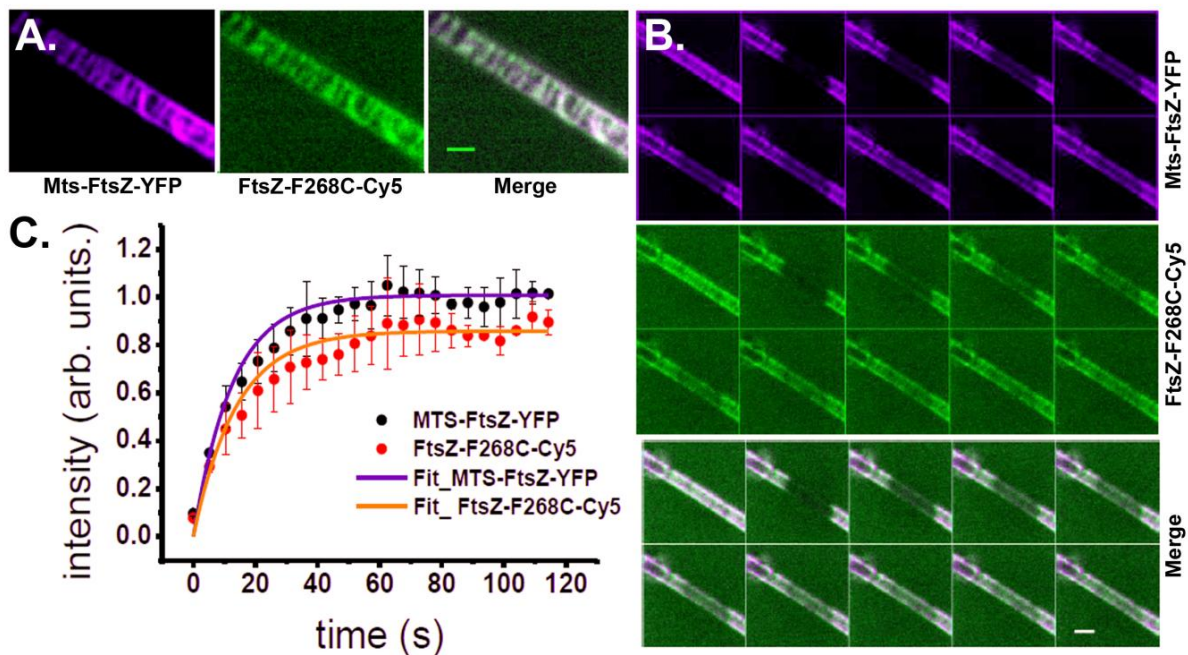


Fig. 5.5. Directly membrane bound FtsZ (MTS-FtsZ-YFP) and FtsZ-F268C-Cy5 copolymerise and show turnover. (A) MTS-FtsZ-YFP and FtsZ-F268C-Cy5 copolymerise. (B) Both MTS-FtsZ-YFP and FtsZ-F268C-Cy5 show recovery on photobleaching. (C) Plot comparing the recovery of MTS-FtsZ-YFP and FtsZ-F268C-Cy5. Scale Bar: 1 μ m.

The filaments assembled on the capillary are active and show characteristic turnover activity. Fig.5.4.A shows rings assembled on membrane coated capillary showing recovery after photobleaching. The capillary support does not have an effect on the recovery times as filaments on free standing membranes also recover with the same dynamics. (Fig.5.4.B,C). To test whether the MTS has an effect on the alignment of the polymers on the capillary, The MTS-FtsZ-YFP was copolymerised with a non-MTS version of FtsZ labelled with Cy5 (Fig.5.5.A). The ring-like structures formed have both the FtsZ uniformly incorporated and show normal recovery activity, while the alignment is preserved well (Fig.5.5.B,C). Therefore, any contribution from the MTS can be ruled out and the curvature sensing comes from the intrinsic structure of the filament.

If spontaneous curvature and flexural rigidity of the FtsZ polymer accounts for the FtsZ alignment, then alignment should be close to 90 degrees as long as the spontaneous curvature matches the capillary curvature. Further, using smaller capillary sizes, it should be possible to test the assumed high curvature of the FtsZ polymers of $10 \mu\text{m}^{-1}$. Owing to the optical resolution limit, it was not possible to estimate capillary sizes or filament orientations accurately for capillaries below a micron in diameter (Fig.5.3.A). Therefore, we performed scanning electron microscopy (SEM) on these samples and quantified the behaviour of filaments on the capillaries (Fig.5.6.B-C). Fig.5.6.A shows a plot of θ , the angle with respect to the long axis of the capillary, for different radii of capillaries. The mean width of the filaments were about 25 nm, about 4-7 subunits thick laterally (Fig.5.6.A, inset). Fig. 5.6.C shows the assembly of filaments on two differently sized capillaries of 500 nm (top) and 100 nm (bottom).

A simple model of a filament of smaller curvature attaching to a capillary of higher curvature aligning at an angle so as to match the spontaneous curvature of the filament with the directional curvature did not fully reconcile with our experimental observations (Fig.5.8.A). This was highlighted by the fact that the mean curvature of filaments did not stay constant for

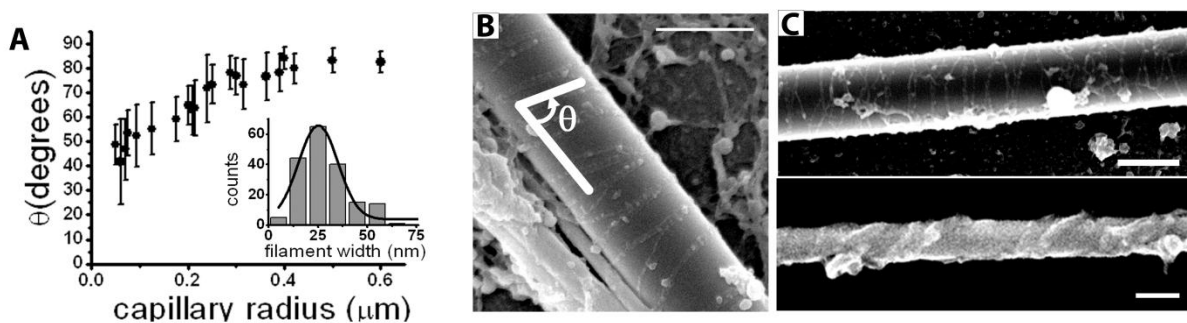


Fig. 5.6. (A) Alignment of filaments with respect to the long axis of the capillary vs. radii of capillaries. Inset: distribution of widths of measured filaments. (B) Example SEM images of filaments on a capillary showing the measured angle. (C) Filament arrangement on capillary of diameters 500 nm (top) and 100 nm (bottom). Scale bars: (A): 1 μm , F (top): 500 nm, (bottom): 100 nm.

different capillary radii but increased towards lower radii (Fig.5.8.D). However, one needs to take into account that FtsZ helices winding around a cylindrical capillary are not characterised only by their curvature but also a non-vanishing twist if their pitch is not zero. To better investigate the spontaneous shape of the FtsZ helices outside of a confining geometry, we explored the morphology of the polymers on a planar bilayer.

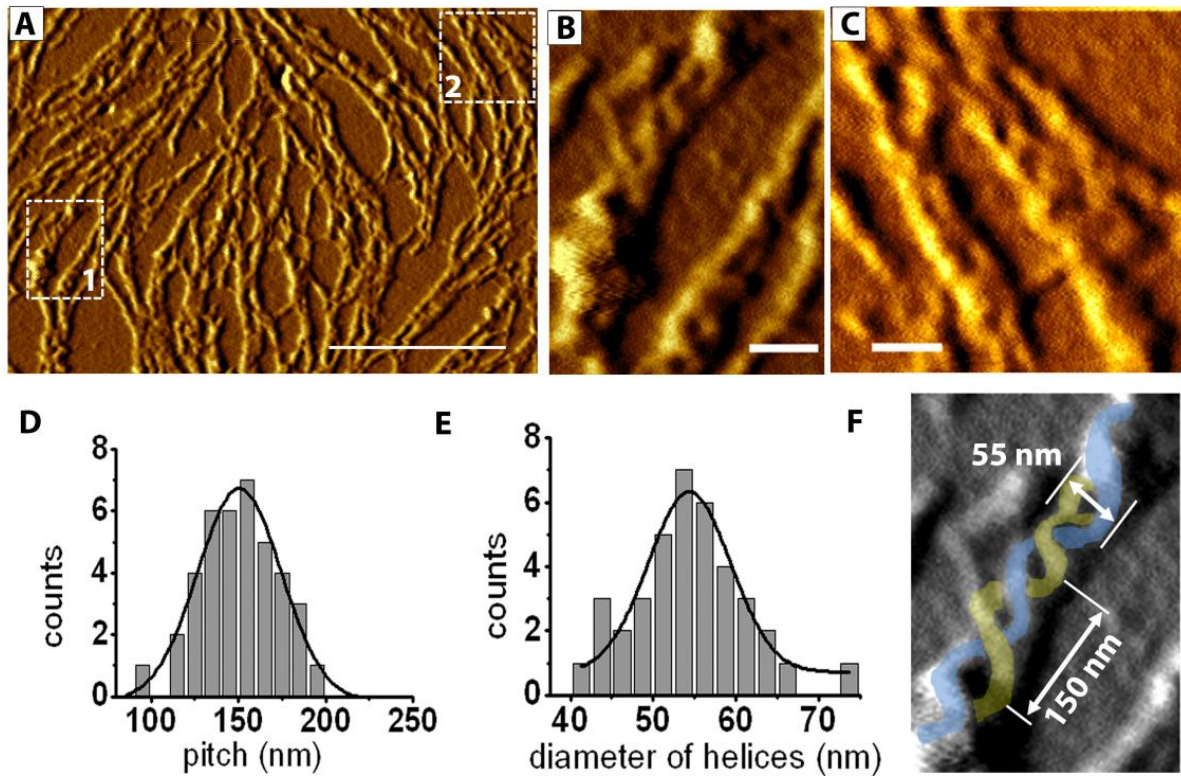


Fig. 5.7 FtsZ polymers on planar bilayers. (A) AFM image of FtsZ filaments assembled on planar supported *E.coli* lipid extract membrane. (B,C): Zoomed image of boxed regions- 1 and 2 in Fig.(A). (D) Histogram of the pitch distribution. (E) Histogram of the distribution of the helix diameters. (F) False coloured helices are shown with average values of pitch and diameter measured. Scale bar: (A): 1 μm (B,C): 100 nm.

5.5 Spontaneous curvature and twist in FtsZ filaments

The FtsZ filaments on capillaries do not reflect the intrinsic structures of FtsZ filaments, as the binding energy to fixed curved structures always accounts for some deformation. We explored the FtsZ assembly on a flat bilayer, where they are not confined by any given curved geometry, and therefore, they should settle close to their spontaneous geometrical configuration. Since fluorescence microscopy cannot resolve these structures due to the optical resolution limit, we performed Atomic Force Microscopy (AFM) on the assembly to probe for any specific structures. AFM indeed revealed the presence of abundant helical structures along with some filaments (Fig.5.7.A). The twisted filaments are woven into two filament helices as seen in the height image (Fig.5.7.B,C). They show a pitch of about 150

nm and a diameter of about 55 nm (Fig.5.7.D-F). These structures seem to confirm the presence of a finite twist along with a spontaneous curvature (Fig.5.7.B). We assume that the helical structures assembled on bilayers represent the inherent structure of the FtsZ filaments. The values of the preferred curvature and the twist of the FtsZ helices on a capillary could then be approximated from the measured values of pitch and diameters of the free-standing helices. We identified the curvature and the torsion of the free-standing helices on planar bilayers with the preferred curvature and twist of FtsZ helices on the cylindrical capillaries.

We model the behaviour of helical filament on a cylindrical surface, with the membrane targeting sequence facing inwards to the centre of the cylinder as in case of MTS-FtsZ-YFP or equivalently, outward as in case of grooves with FtsZ-YFP-MTS (Fig.5.8.A,B). The FtsZ helix will take the measured values of spontaneous curvature and twist if the filaments are under no geometrical constraints. The conformational energy of the helix will be minimal at these values. In the presence of a geometrical confinement as in the cases of capillary or grooves, the filaments will take a conformation which minimizes the energy under the given geometrical constraints. The more the capillary diameter deviates from the native helix diameter (≈ 55 nm), the more the filament's curvature and twist will deviate from its spontaneous values (Fig.5.8.D). Using the measured values of spontaneous curvature and twist, and energy minimisation (Appendix), we could fit the plot of angle vs. radius (Fig.5.8.C), in contrast to a model only considering spontaneous curvature, which did not fit the data.

5.6 Conclusions

A large plethora of different shapes of non-membrane attached FtsZ filaments have been observed in various studies mainly using EM and AFM [7, 62, 63, 107, 108, 110, 113, 137]. Almost all of these studies use electron microscopy grids, carbon grids or mica as support to observe the filaments. They also seem to depend on buffer conditions, sample preparation methods and substrates. Surface interactions may play a role in collapsing the filament away from its spontaneous structure. The filaments in the GTP state should show turnover, an important property of the filaments observed *in vivo*. Our experiments are performed with filaments assembled on membranes which show normal turnover activity, and can be considered closer to the filament *in vivo*. Moreover, on the membrane, they are closer to the spontaneous state, and the membrane allows the filament to slide and diffuse into the energy minimised state. We believe our *in vitro* system recapitulates the essential FtsZ tethered to the membrane system as is expected *in vivo*.

The behaviour of filaments on capillaries of different radii agrees very well with a model of intrinsic filament curvature and spontaneous twist, rather than a previously suggested model that considered only spontaneous curvature [97, 111]. Therefore, our data strongly suggests that the *E. coli* FtsZ filaments have spontaneous curvature and twist.

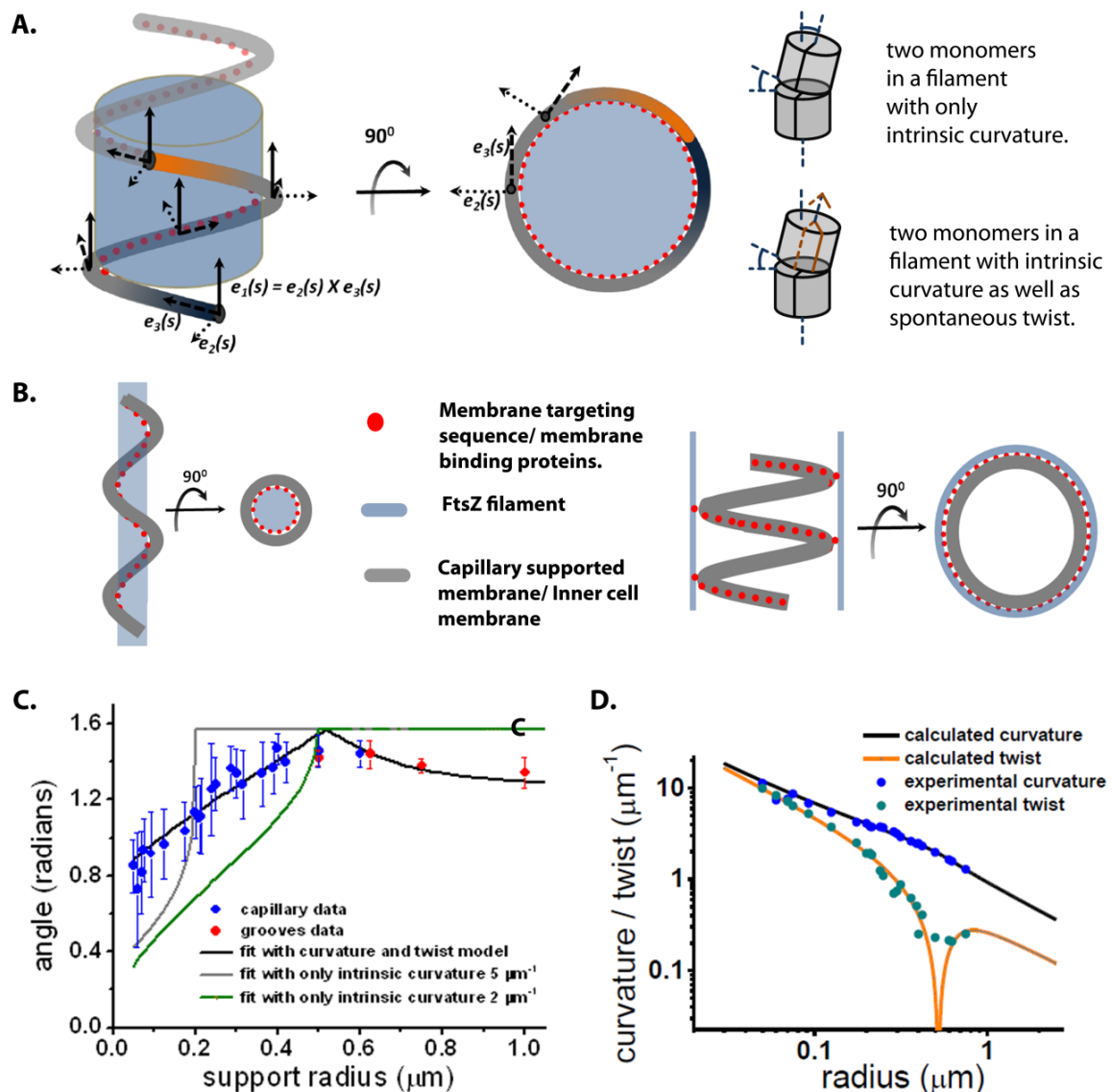


Fig.5.8 Curvature and twist in FtsZ filaments. (A) The difference between a model with only spontaneous curvature and a model with spontaneous curvature and spontaneous twist. (B) Schematic shows filament with MTS-FtsZ-YFP on capillaries with MTS facing inwards or FtsZ-YFP-MTS with MTS always facing outwards. (C) Plot of angle vs. curved support radius showing a fit with a curvature and twist (black). The expected trend with only spontaneous curvature of $5 \mu\text{m}^{-1}$ (grey) and $2.5 \mu\text{m}^{-1}$ (green) is also shown. The blue dots correspond to data from capillary, the red from the grooves. (D) Curvature and twist experimentally observed and calculated.

Photo-activated localisation microscopy (PALM) studies in *E.coli* reveal helical FtsZ at the centre rather than a complete ring [133]. Our model suggests a peak alignment around the bacterial diameter, though the curvature and twist may be far from the spontaneous values (Appendix). With adaptor proteins attaching the FtsZ filaments to the membrane in vivo, a

similar behaviour can be envisaged. The twist will be close to zero for radii around 0.5 μm , making it appear like a ring with normal fluorescence microscopy. Interestingly, 3D reconstructions from Cryo-EM done on *C.crescentus* also show helical arrangement rather than a closed ring [68]. If FtsZ would generate active constriction force, the alignment should be close to 90 degrees at all substrate curvatures as the filaments would continuously strive to achieve highest curvature possible. This is clearly not the case in our observations.

The ability of the FtsZ filament to align at such a range of radii in our experiments without assembling to its native conformation of helical structures suggests a substantial elasticity in the FtsZ filament. Most estimations of bending modulus are based on two dimensional analysis of filaments adsorbed on surfaces. We believe that this strongly affects the interpretations when surface interactions play a role. Our estimations of constrictive force from the model with curvature and twist yields a maximum force in the order of 0.06 pN (Appendix). If only spontaneous curvature would be dominant, then the constrictive force would be around 3 pN. This is lower than the previously estimated values. With a highly flexible filament, models that rely mainly on FtsZ filament bending to generate constriction forces have to be reconsidered.

In summary, our experimental results indicate that FtsZ filaments have an intrinsic curvature and a spontaneous twist that allows them to assemble into a Z-ring at the equatorial region of the cell prior to division. Apart from nuclear occlusion and Min waves as localisation cues, minimization of the FtsZ polymer conformational energy by spontaneous curvature and twist may thus be an important additional cue assembling and organizing the Z-ring as the platform for downstream processes of cytokinesis. Evolution of self-assembly in biological systems has led to generation of several highly functional molecules performing specific functions, in this case, a polymer with an intrinsic helical structure. Filament forming proteins are interesting from the aspect of understanding as well as designing self-assembling units. We believe that our approach of investigating the mechanics of curved polymers on curved membrane surfaces provides an attractive assay to quantitatively study mechanical cues such as membrane curvature and for protein recruitment and regulation in similar systems.

Chapter 6

Outlook: Towards a 3-dimensional reconstitution of bacterial cell division

The oscillations of Min proteins *in vivo* are confined to an enclosed volume of highly defined dimensions of a rod-shaped *E. coli* cell. Mutants which exhibit aberrant shapes, and therefore exhibit more than two cell axes, show Min oscillations along the longest axis. The cell division occurred at the centre of the long axis of aberrant cells. This suggested that the Min system functions as a geometry sensing system in these cells.

The Min waves on the supported lipid bilayers *in vitro* differ from the *in vivo* situation. The oscillations are transformed into waves on 2-dimensional lipid surface. The supported lipid bilayers on a cover glass provide unrestricted access to space and are not enclosed considering the volume of buffer above the bilayer and geometry. Reconstituting waves on patterned surfaces of a variety of geometry coated with lipid bilayers revealed that the Min waves travel along the longest axis of the membrane patches. These initial results demonstrate that the Min protein waves adapt according to the available geometry and space.

An intriguing question is why the *in vitro* waves are much larger compared to the *in vivo* situation. One of the theoretically predicted reasons for this is the mean diffusion length of a protein coupled with reaction rate (ATPase rate) in an enclosed geometry. To experimentally verify any theoretical models, an experimental system which allows protein enclosure with *in vivo* like geometry and with lipid bilayer is needed. Glass capillaries are an attractive substrate to mimic *in vivo* like situations as they can be manipulated efficiently. Glass capillaries can be coated with lipid bilayers using similar procedures as established for planar substrates.

Glass capillaries can be manipulated by capillary pullers to result in accurate diameters. Using a microinjection pump, solutions can be easily exchanged in these capillaries. As a proof of principle, we demonstrate reconstitution of Min waves inside capillaries (Fig. 6.1.A).

The initial results demonstrate that the Min waves are able to self-organise along the long axis of the cylindrical geometry (Fig.6.1.B,C).

The glass micro capillary system can be used to investigate the effect of volume, geometrical parameters like diameter and length effect the self-organisation of Min waves under confined geometry. A further extension of this experimental system would be to study how Min waves spatially regulate FtsZ rings - a more complete reconstitution of the Min system *in vitro*.

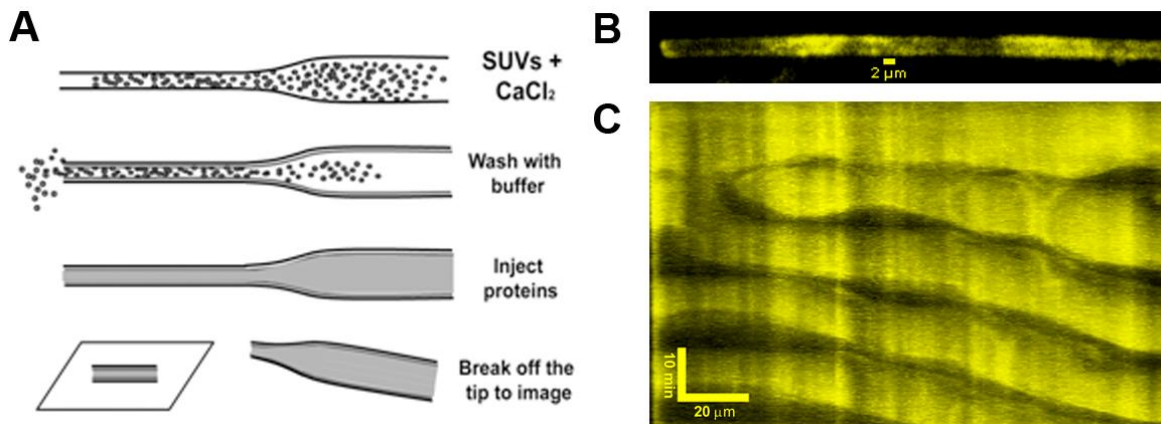


Fig. 6.1 (A) Methodology of coating insides of capillaries with bilayers and injecting proteins. (B) Min proteins inside a capillary. (C) Kymograph of the Min waves along the long axis of the capillaries.

Chapter 7

Concluding remarks and additional directions

Despite their small size, bacteria must organise cellular events in time and space. In the well-studied bacteria *E.coli* and *B.subtilis*, this regulation is achieved by the combination of two negative regulatory systems: Min, which prevents Z-ring assembly near the poles, and the nucleoid occlusion (NO), which prevents Z-ring assembly over the nucleoid. How exactly the Z-ring is regulated by the proteins which mediate the interactions between MinDE waves or Nucleoid and FtsZ is not well understood. A hindrance in understanding these interactions are because the dynamics and organization of the FtsZ filaments are not well understood.

In chapter 3 of this thesis, we demonstrate the ability of FtsZ to polymerise and assemble into two dimensional networks. With single molecule imaging and FRAP, we show that (a) The filament is an irresolute bundle structure with constant turnover and almost equivalent at the middle and centre, (b) The subunit leaves the filament as soon as it hydrolyses GTP and (c) In such an arrangement, a stabilising structure like a ‘GTP cap’ is very improbable and therefore the classical dynamic instability may not be present.

This new understanding of FtsZ polymers enabled us to investigate how MinC disassembles FtsZ. In Chapter 4 of this thesis we describe how stable MinC dimers disassemble FtsZ polymers by occupying binding sites, thereby inhibiting turnover. Our results reveal why GTP hydrolysis is necessary for MinC activity. A model where the filament has a substantial amount of GDP-bound subunits fits with the depolymerization kinetics observed. This fact challenges the hypothesis that GTP hydrolysis by FtsZ is mainly responsible for force generation. The *E.coli* FtsZ and Min system exemplify a self-organization system in which energy is consumed in two forms by two different components: The MinDE system in which MinD hydrolyses ATP, and the FtsZ system where it uses GTP. MinC links the two by virtue of its binding to MinD and its activity on FtsZ polymers. The *in vitro* experiment combining

all the four components – MinCDE and FtsZ proves that the Min proteins are able to spatially regulate FtsZ polymers, as has been suggested on the basis of genetic experiments.

One important aspect of the Z-ring assembly is its specific organization into ring-like structures. Intrinsic curvature has been proposed since a long time. However, experimental evidences confirming this has been elusive. In chapter 5 of this thesis, our experimental results show that FtsZ filaments have an intrinsic curvature and a spontaneous twist that allows them to assemble into a Z-ring at the equatorial region of the cell prior to division. Apart from nuclear occlusion and Min waves as localisation cues, minimization of the FtsZ polymer conformational energy by spontaneous curvature and twist may thus be an important additional cue for assembling and organizing the Z-ring as the platform for downstream processes of cytokinesis.

To conclude, the experiments reveal that GTP hydrolysis is mainly used by MinC to disassemble FtsZ. MinCDE are enough to spatially localise FtsZ polymers. FtsZ polymers have an intrinsic curvature which is a geometric cue to assemble FtsZ into a ring-like structure. Together, the primitive cytoskeleton, and its regulators have evolved to give rise to interdependent processes. Despite the progress we made in understanding the FtsZ and Min system, many questions remain unanswered:

1) What roles do other interacting proteins play in the Z-ring?

Filamentous temperature sensitive A (FtsA) is a bacterial actin homolog involved in FtsZ-ring assembly and cytokinesis in a wide range of bacteria [138]. The ratio of FtsA to FtsZ is very important for a proper cell division to be carried out. *T. maritima* FtsA-FtsZ complex has been reconstituted confirming that FtsA tethers FtsZ to the membrane [88]. FtsA has been also shown to assemble into filaments. How does the A-ring assist in the putative constriction is unclear. What is the role of ZipA, which is thought to tether as well as bundle FtsZ filaments? An increasing number of proteins are being discovered which seem to affect the FtsZ bundle structure. One of the most striking to have an effect on the FtsZ curvature is FzIA, discovered in *Caulobacter crescentus*. FzIA is thought to activate ring constriction by inducing highly curved helical bundles of FtsZ filaments [139].

2) Is intrinsic curvature a common theme in FtsZ across all species of bacteria?

We have described the intrinsic curvature and twist in the *E. coli* FtsZ filaments. Round bacterial cells also exhibited intact Z-rings. In giant bacterial cells like *Metabacterium polyspora* and *Epulopiscium spp.*, which grow up to about 10 μm in size, the FtsZ interestingly form 1 μm sized endospores, which does not need larger than 1 μm FtsZ rings [140, 141]. This suggests one possible fact about the FtsZ: The FtsZ filament has evolved to function at diameters around 1 μm . What is the structure

to function relationship in a filament with intrinsic curvature? Where does such a filament stand in the evolution of other tubulin homologs?

3) Can FtsZ generate force?

To date, there has been no clear demonstration of FtsZ as a force generator. A single study of reconstituted chimeric FtsZ-YFP-MTS rings in multilamellar liposomes reports weak constrictions. However, the effect of MTS is not clear in this study. Also, as shown in Chapter 3, exposure to laser leads to excessive bundling and loss of turnover activity. Such effects should be more carefully considered in such experiments. There have been many models proposed regarding the mechanism of force generation with solely FtsZ. One of them is how the intrinsic curvature is able to bend the membrane from a lower curvature to a higher ‘preferred’ filament curvature. We explored the nature of intrinsic curvature in FtsZ filaments and found that the FtsZ prefers curvature about $1 \mu\text{m}^{-1}$. Our observations also suggested that the FtsZ filaments are not very stiff and may be incapable of generating any active force. Recently, the L-form (wall-less derivatives of common bacteria) of *Bacillus subtilis* was found to propagate independently of FtsZ [80]. Almost all the species of bacteria that possess FtsZ also have FtsA [138]. Therefore, it is acceptable to assume that they have a coordinated role in cell division.

Isolated chloroplasts are able to show constrictions [142]. However, chloroplasts machinery is more complex with FtsZ and Dynamin involved together [143]. What seems to be a conserved theme is FtsZ and peptidoglycan synthesis going hand in hand as has been discovered for some algae chloroplasts [144, 145]. It is still unclear whether this conservation extends across to bacteria too. FtsZ could be a filament which can adapt to changing geometries while guiding the peptidoglycan synthesis machinery to which the Z-ring is connected.

The mycoplasmas lack a cell wall, but they divide by binary fission. They have been shown to possess the *ftsZ* gene [146, 147]. However, more studies are required to establish FtsZ as a part of minimal division machinery generating force in these organisms.

If FtsZ generates force, more complex experimental designs are needed to elucidate quantitatively the force generation and its mechanism. However, one should be careful with the experimental models to distinguish the force generated by intrinsically curved filaments going towards its native curvature and the distinct physiologically relevant force generated by FtsZ to go from $1 \mu\text{m}^{-1}$ towards higher curvature.

Appendix:

A1. Fluorescence Recovery after photobleaching experiments.

The raw FRAP curves were normalised using the following equation:

$$C(t) = \frac{A_0}{A(t)} \times B(t) \quad (\text{Equation 1})$$

Where A_0 is prebleach intensity of the an area distant from the bleach area, $A(t)$, the intensity with time during the experiment and $B(t)$ the intensity with time at the area of bleaching. Then the normalised curve is given by:

$$N(t) = \frac{C(t) - C_1}{B_0 - C_1} \quad (\text{Equation 2})$$

Where B_0 is intensity at the area of bleaching before the bleaching, and C_1 the first point after bleaching from equation 1.

Binding model:

We use a reaction dominant model for the Fluorescence recovery as diffusion is much faster than the timescales of FtsZ turnover in the filaments. Equation 11 from Sprague *et al* [148] was used to fit the recovery curves. The binding model can be applied for the FtsZ assembly:

The photobleaching experiments are done after the FtsZ filament network is stable and has reached equilibrium. Consider 'v' as the concentration of vacant binding sites. These are the part of the filament and are largely immobile within timescales of the experiment. 'f' is the concentration of unbound FtsZ, which is in the form of small protofilaments as well as monomers. There exists equilibrium within the free unbound population owing to nucleotide hydrolysis in protofilament and protofilament breaking. However, since the rate of turnover within this free population is limited by the rate of hydrolysis, we can assume it to be comparable to total turnover in our assembly. Since there will be a large number of vacant sites available throughout, the free unbound protofilaments will be mostly bound to the filament by diffusion and capture.

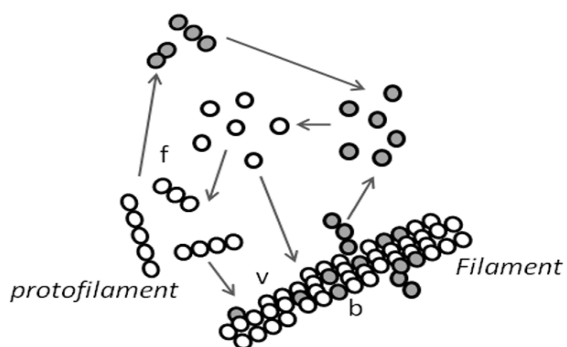


Fig A1: FtsZ subunits- f, unbound protein binding to vacant sites v and form bound species of concentration b.

At equilibrium, $f = F_{eq}$, $v = V_{eq}$ and $b = B_{eq}$.

In a reaction dominant case, where diffusion is rapid, we can assume $f = F_{eq}$, a constant since molecules will almost instantly equilibrate.

$$\text{Hence, } \frac{db}{dt} = K_{on}^* F_{eq} - K_{off} b \quad (\text{Equation 3})$$

K_{on}^* is a pseudo-first order rate constant given by $K_{on}^* = K_{on} V_{eq}$. This is because the bleaching will decrease the number of fluorescent free and bound molecules, but the concentration of binding sites, V_{eq} will remain constant. Before the bleach, the fluorescent FtsZ molecules are in equilibrium. Therefore f and b will be F_{eq} and B_{eq} . The ratio of free and bound molecules is then $\frac{F_{eq}}{B_{eq}} = \frac{K_{off}}{K_{on}^*}$.

When the molecules are bleached, overall equilibrium remains unaltered, but the equilibrium of fluorescent molecules is disturbed. At the site of bleaching, the filaments will have low concentration of fluorescent FtsZ. The recovery of fluorescence will be then governed by equation 3, which is the same as derived by Sprague *et al.* (1). The final height of recovery will be $F_{eq} + B_{eq} = 1$ for a data normalised to 1, neglecting the loss of fraction of fluorescent FtsZ molecules due to bleach. This gives $F_{eq} = \frac{K_{off}}{K_{on}^* + K_{off}}$ and $B_{eq} = \frac{K_{on}^*}{K_{on}^* + K_{off}}$. Solving for equation 3 gives us

$b(t) = B_{eq}(1 - e^{-k_{off}t})$. This is the behaviour of FtsZ binding to the filament. Total fluorescence recovery with time would be then

$$rec(t) = F_{eq} + B_{eq}(1 - e^{-k_{off}t}) = 1 - B_{eq}e^{-k_{off}t}.$$

A2. Modelling FtsZ filaments on capillaries.

Twist and curvature of FtsZ helices:

The FtsZ bundles on the glass capillaries wind as a helix with pitch p around the cylindrical capillary of given radius R . The path of the bundle is given by the following arc length parametrization

$$\underline{r}(s) = \left\{ R \cos\left(\frac{\omega s}{\sqrt{R^2 \omega^2 + 1}}\right), R \sin\left(\frac{\omega s}{\sqrt{R^2 \omega^2 + 1}}\right), \frac{s}{\sqrt{R^2 \omega^2 + 1}} \right\}, \text{ where } \omega = 2\pi/p.$$

Since the FtsZ membrane tether always needs to point to the membrane, we can associate a material frame to the curve, where the orthonormal vectors are given by the tangent, the cylinder outward normal and the cross product of the two vectors.

$$e_3(s) = \partial_s r(s) = \left\{ -\frac{R\omega \sin\left(\frac{\omega s}{\sqrt{R^2\omega^2+1}}\right)}{\sqrt{1+R^2\omega^2}}, \frac{R\omega \cos\left(\frac{\omega s}{\sqrt{R^2\omega^2+1}}\right)}{\sqrt{1+R^2\omega^2}}, \frac{1}{\sqrt{1+R^2\omega^2}} \right\}$$

$$e_2(s) = \left\{ \cos\left(\frac{\omega s}{\sqrt{R^2\omega^2+1}}\right), \sin\left(\frac{\omega s}{\sqrt{R^2\omega^2+1}}\right), 0 \right\}$$

$$e_1(s) = e_3(s) \times e_2(s) = \left\{ -\frac{\sin\left(\frac{s\omega}{\sqrt{1+R^2\omega^2}}\right)}{\sqrt{1+R^2\omega^2}}, \frac{\cos\left(\frac{s\omega}{\sqrt{1+R^2\omega^2}}\right)}{\sqrt{1+R^2\omega^2}}, -\frac{R\omega}{\sqrt{1+R^2\omega^2}} \right\}.$$

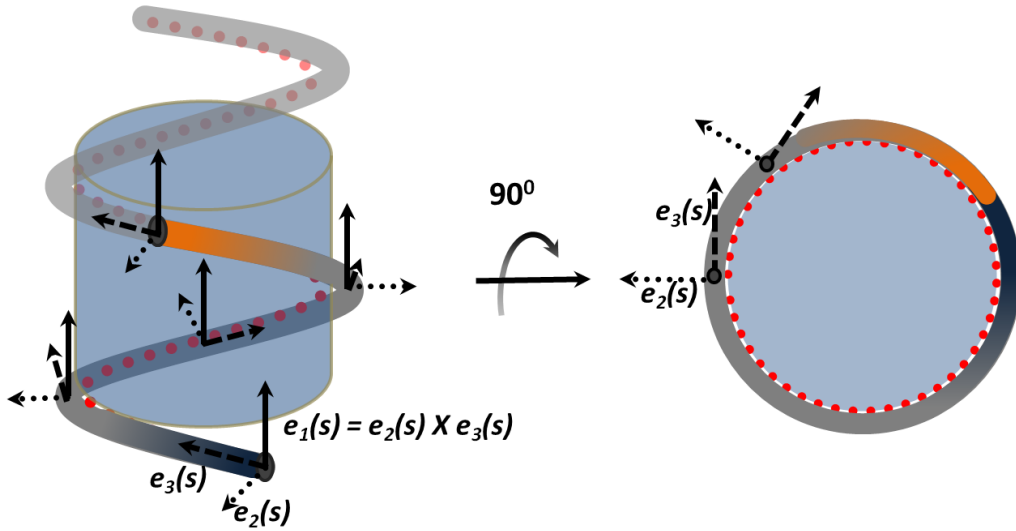


Fig.A2: A material frame of FtsZ filament (grey) with membrane binding sites on N-terminal (inwards), shown by red dots wound on a capillary (blue).

The change of the material frame vectors along the curve is given by an infinitesimal rotation, which is realized by taking the cross product with the vector $\underline{\Omega}$

$$\partial_s e_i(s) = \underline{\Omega} \times e_i(s).$$

$\underline{\Omega}$ of the given curve can be calculated to have the components

$$\Omega_1(R, \omega) = \frac{R\omega^2}{1+R^2\omega^2}, \quad \Omega_2 = 0, \quad \Omega_3(R, \omega) = -\frac{\omega}{1+R^2\omega^2}.$$

The second component Ω_2 happens to be zero for this special choice of a helix. Therefore, the first component Ω_1 is the curvature of the helix, whereas the third component Ω_3 is the twist.

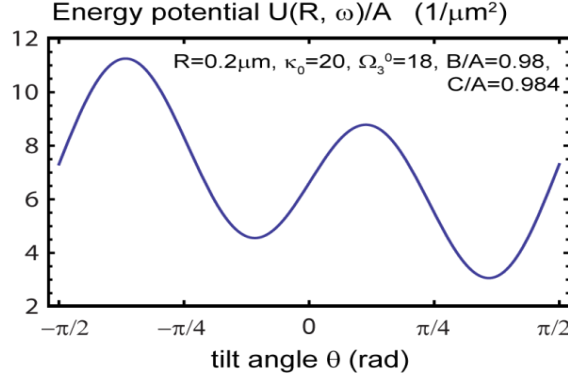


Fig.A3: Scaled conformational energy U of a helix with radius $0.2 \mu\text{m}$, spontaneous curvature $20/\mu\text{m}$, spontaneous twist $18/\mu\text{m}$ and parameters $B/A=0.98$, $C/A=0.984$. The energy minimum is taken at a tilt angle of $\mu_{\min}=1.14$.

Conformational energy of FtsZ helices:

FtsZ polymer bundles will have a preferred curvature κ_0 and twist Ω_3^0 which will be taken if there are no geometrical constraints to the helix. These values will be denoted as spontaneous curvature and twist respectively. The conformational energy of an FtsZ helix on a cylindrical capillary will be minimal for $\underline{\Omega} = (\kappa_0, 0, \Omega_3^0)$. Taylor expansion around this minimum gives the following functional form of the conformational energy:

$$U(R, \omega) = \frac{A}{2}(\Omega_1 - \kappa_0)^2 + B(\Omega_1 - \kappa_0)(\Omega_3 - \Omega_3^0) + \frac{C}{2}(\Omega_3 - \Omega_3^0)^2,$$

Where Ω_1 and Ω_3 are by itself functions of R and ω . $U(R, \omega)$ needs to be positive and therefore $A \cdot C - B^2 > 0$. In the main text, we presented experimental data of FtsZ polymerizing into helices on glass capillaries with given radius (main text, Fig.5.6). Therefore, for these helices, the only adjustable parameter is ω and the taken values are expected to be close to the energy minimum of $U(R_{\text{capillary}}, \omega)$. In (Fig. A4), we give the mean measured helix tilt angle θ of the FtsZ helices which relate to ω by $\theta = \arctan(\omega R)$. Since the measured standard deviation of this tilt angle are moderate (0.1-0.3 rad), we expect that the mean value is close to the angle θ_{\min} that minimizes the energy functional.

Measuring the pitch and the radius of a free FtsZ helix:

We measured the pitch and diameter of FtsZ helices assembled on bilayer. This represents the free structure of FtsZ with minimal surface interactions. FtsZ filaments there are assembled into helices of average pitch 152.9 ± 31.5 nm and average radius 54.6 ± 9.5 nm. These values correspond to a curvature of $\kappa \approx \frac{20}{\mu\text{m}}$ and a torsion of $\frac{18}{\mu\text{m}}$. For FtsZ helices on the capillary, the membrane tether of FtsZ proteins points inward to the membrane coating the capillary. For the free-standing helices on the planar bilayer, this does not need to be true and we cannot be sure about the orientation of the material frame associated to the FtsZ proteins

in the helix. In principle, it is therefore possible that the torsion of the free-standing helices does not equal the twist of the FtsZ polymers. Also the second component of the vector $\underline{\Omega}$, which is the second curvature component, does not need to vanish for a free-standing FtsZ helix. Still, it is suggestive to identify the obtained intrinsic curvature of $\frac{20}{\mu m}$ with the preferred spontaneous curvature κ_0 of FtsZ helices on the capillary and to identify the measured torsion of $\frac{18}{\mu m}$ with their spontaneous twist Ω_3^0 . The excellent fit results that we obtained with these values of κ_0 and Ω_3^0 reconfirm this choice. The remaining parameters B/A and C/A of the scaled potential can be fitted by assuming that the measured average values of the tilt angle θ are the angles at which the conformational energy takes its minimal value. From this fit we obtain B/A=0.98±0.2, C/A=0.984±0.2. (Fitting has been done with the Matlab function "lsqnonlin".)

In the theoretical calculations, we calculated the minimizing or the mean tilt angle in the range $-\pi/2$ and $\pi/2$. The sign of the tilt angle was dropped in the plots. This corresponds to the experimental data acquisition where tilt angles are always considered to be positive due to a lack of information about the orientation of the polymers.

Due to the geometrical confinement on the capillary, the filament tends to assume a helix configuration which deviates from its natural curvature and twist.

Given the conformational energy $U(R, \omega)$ of an FtsZ helix, we can not only determine the angle θ_{min} at which this function takes its minimal value, but also the mean of the tilt angle θ and the standard deviation from the mean

$$\bar{\theta} = \frac{\int_{-\pi/2}^{\pi/2} \theta \exp\left(-\frac{U(R, \omega)}{k_B T}\right) / \int_{-\pi/2}^{\pi/2} \exp\left(-\frac{U(R, \omega)}{k_B T}\right)}{\int_{-\pi/2}^{\pi/2} \exp\left(-\frac{U(R, \omega)}{k_B T}\right)}$$

$$stdev = \frac{\int_{-\pi/2}^{\pi/2} (\theta - \bar{\theta})^2 \exp\left(-\frac{U(R, \omega)}{k_B T}\right) / \int_{-\pi/2}^{\pi/2} \exp\left(-\frac{U(R, \omega)}{k_B T}\right)}$$

From our experimental data, we obtain standard deviations of the measured mean tilt angles between 0.1-0.3 rad. Imposing that thermal fluctuations of the tilt angle give a substantial contribution to the error bars (at least for some of the chosen capillary radii), we estimate the missing parameter of the conformational energy to be $A \approx 10k_B T$, see Fig. A3 for comparison. Assuming a ring configuration ($\omega = \infty$), the derivative of $U(R, \omega)$ with respect to R is $\partial_R U(R, \infty) = \frac{A(R\kappa_0 - 1 - \frac{B}{A}R\Omega_3^0)}{R^3}$

At the point $R=0.5\mu m$, this gives a constrictive force of $\approx 14 \frac{k_B T}{\mu m} \approx 0.06pN$. If the parameter B would vanish, then the force would be larger and give a value of $\approx 3pN$.

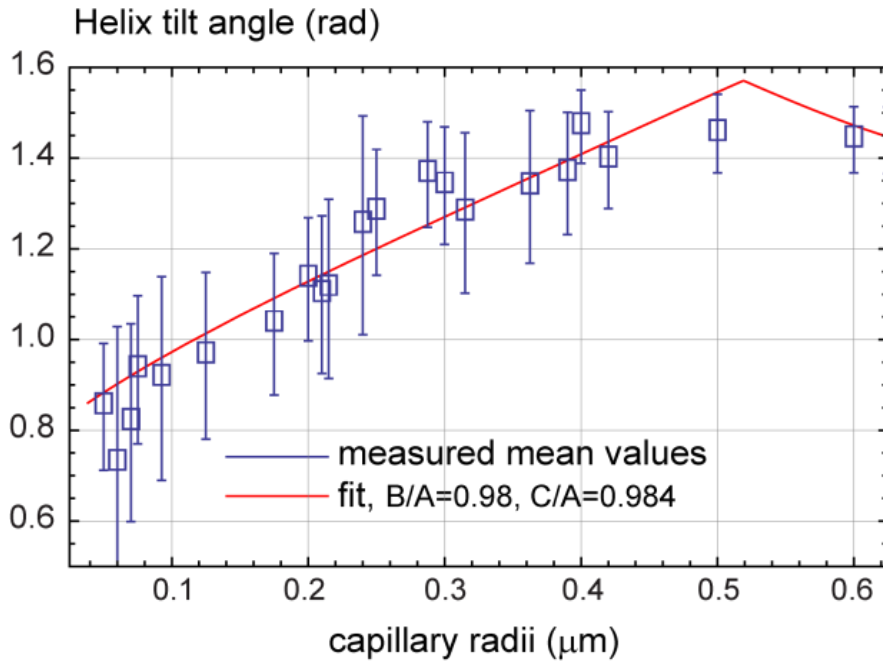


Fig.A4: Measured helix tilt angles of FtsZ helices on glass capillaries. The red line is a fit to the data assuming a spontaneous curvature of $20 \mu\text{m}^{-1}$ and a spontaneous twist $18 \mu\text{m}^{-1}$. The fit yields $B/A=0.98 \pm 0.2$, $C/A=0.984 \pm 0.2$.

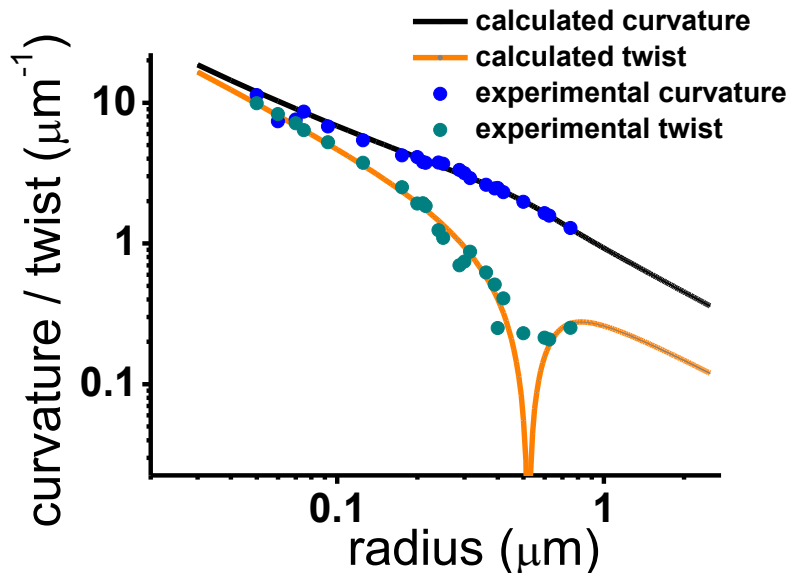


Fig.A5: Curvatures and twists taken by FtsZ filaments on capillaries of different radii. The calculated twist and curvature were obtained from the fit to the helix tilt angles ($B/A=0.98$, $C/A=0.984$).

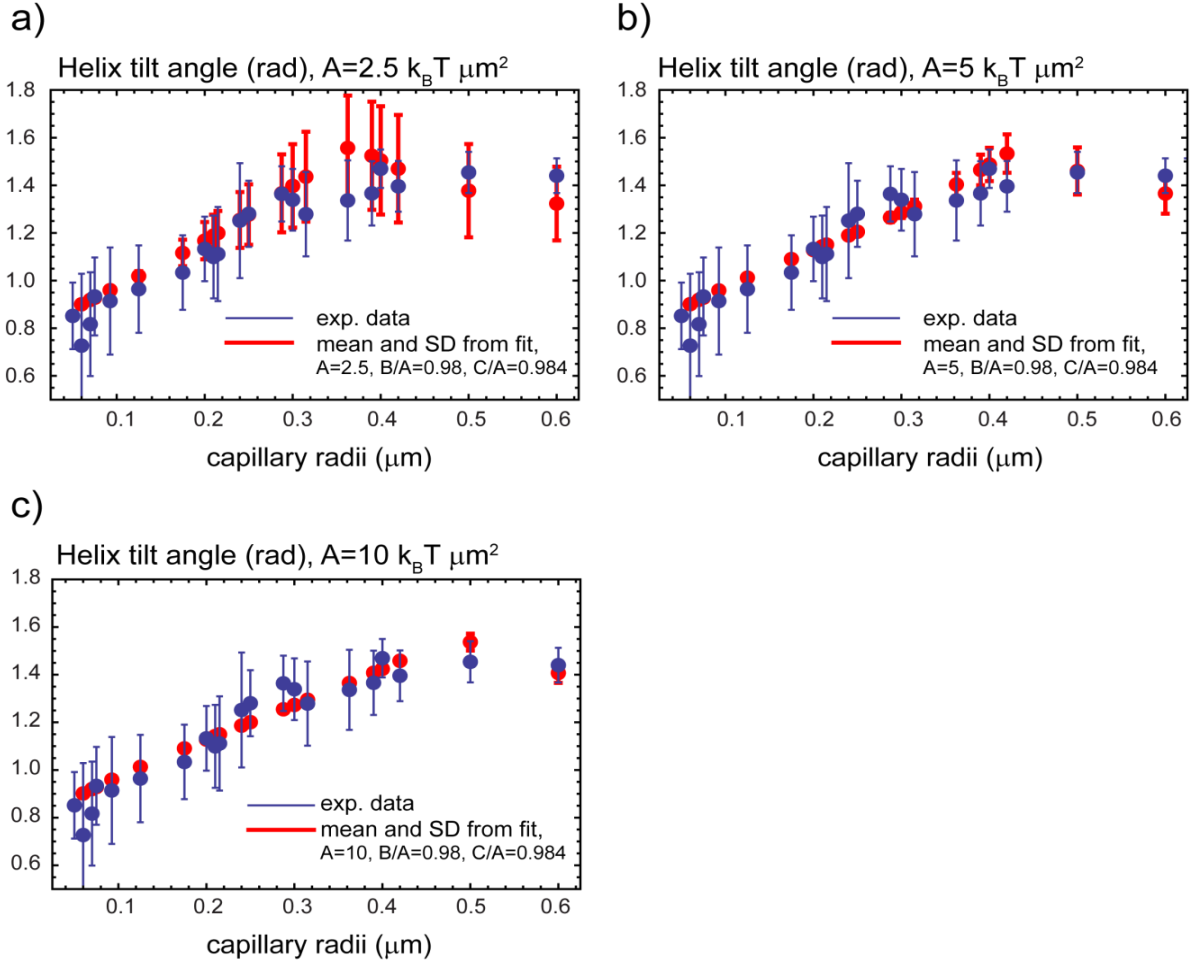


Fig.A6: Experimental data (blue) and mean values with standard deviation obtained from the conformational energy (red) with fit values $B/A=0.98$, $C/A=0.984$ and a) $A=2.5 \text{ k}_B \text{ T } \mu\text{m}^2$, b) $A=5 \text{ k}_B \text{ T } \mu\text{m}^2$ c) $A=10 \text{ k}_B \text{ T } \mu\text{m}^2$. The standard deviation (red data) accounts for the spread due to thermal noise. For smaller capillary radii, the standard deviation due to thermal noise is getting smaller according to the theoretical predictions of the model. For higher noise levels (smaller A), the peak of the data points shifts to the left due to the asymmetric shape of the conformational energy around the minimum.

$A \text{ (k}_B \text{ T } \mu\text{m}^2)$	C/A	B/A	$F \text{ (pN)}$
10	0.984	0.98	~ 0.06
5	0.984	0.98	~ 0.03
10	0.984	0.9	~ 0.3
10	0.984	0	~ 3

Table: Estimated constriction force of the Z ring for different choices of parameters. The constrictive force is largest, when the spontaneous twist or the parameter B vanishes. The assumed spontaneous curvature was $20/\mu\text{m}$ and the spontaneous twist $18/\mu\text{m}$.

Abbreviations:

ADP	Adenosine 3' diphosphate
ATP	Adenosine 3' triphosphate
AFM	Atom Force Microscopy
Cy dyes	Cyanine dyes
DTT	Dithiothreitol
eGFP	enhanced Green Fluorescent Protein
EDTA	Ethylene diamine tetraacetic acid
EM	Electron Microscopy
EM-CCD	Electron Multiplying Charge Coupled Device
FCS	Fluorescence Correlation Spectroscopy
FCCS	Fluorescence Cross Correlation Spectroscopy
FRAP	Fluorescence Recovery After Photobleaching
FRET	Förster resonance energy transfer
FtsZ	Filament thermo sensitive Z
GDP	Guanosine diphosphate
GMPCPP	Guanosine 5'-[(α,β)-methileno] triphosphate
GTP	Guanosine-5'-triphosphate
GUV	Giant Unilamellar Vesicles
HEPES	2-[4-(2-hydroxyethyl) piperazin-1-yl]ethanesulfonic acid
IPTG	Isopropyl- β -D-thiogalactopyranoside
kD	Kilo Dalton 10^3 g/mol
LB	Lysogeny Broth medium
LSM	Laser Scanning Microscope
MTS	Membrane targeting Sequence
NA	Numerical Aperture
NO	Nucleoid Occlusion
NZ	N-terminal of FtsZ
PCR	Polymerase Chain Reaction
SDS-PAGE	Sodium dodecyl sulfate polyacrylamide gel electrophoresis
SEM	Scanning Electron Microscopy
SLB	Supported Lipid Bilayer
STED	Stimulated Emission Depletion microscopy
SUV	Small Unilamellar Vesicles
TCEP	<i>tris</i> (2-carboxyethyl)phosphine
TIRF	Total Internal Reflection Microscopy
Tris	Tris(hydroxymethyl)aminomethane
WACA	Walker A cytoskeletal ATPases
WT-FtsZ	Wild Type FtsZ
YFP	Yellow Fluorescent Protein

Bibliography:

1. Lowe, J. and L.A. Amos, *Evolution of cytomotive filaments: the cytoskeleton from prokaryotes to eukaryotes*. Int J Biochem Cell Biol, 2009. **41**(2): p. 323-9.
2. Bi, E.F. and J. Lutkenhaus, *FtsZ ring structure associated with division in Escherichia coli*. Nature, 1991. **354**(6349): p. 161-4.
3. Mukherjee, A., K. Dai, and J. Lutkenhaus, *Escherichia coli cell division protein FtsZ is a guanine nucleotide binding protein*. Proc Natl Acad Sci U S A, 1993. **90**(3): p. 1053-7.
4. de Boer, P., R. Crossley, and L. Rothfield, *The essential bacterial cell-division protein FtsZ is a GTPase*. Nature, 1992. **359**(6392): p. 254-6.
5. RayChaudhuri, D. and J.T. Park, *Escherichia coli cell-division gene ftsZ encodes a novel GTP-binding protein*. Nature, 1992. **359**(6392): p. 251-4.
6. Erickson, H.P. and D. Stoffler, *Protofilaments and rings, two conformations of the tubulin family conserved from bacterial FtsZ to alpha/beta and gamma tubulin*. J Cell Biol, 1996. **135**(1): p. 5-8.
7. Erickson, H.P., et al., *Bacterial cell division protein FtsZ assembles into protofilament sheets and minirings, structural homologs of tubulin polymers*. Proc Natl Acad Sci U S A, 1996. **93**(1): p. 519-23.
8. Oliva, M.A., S.C. Cordell, and J. Lowe, *Structural insights into FtsZ protofilament formation*. Nat Struct Mol Biol, 2004. **11**(12): p. 1243-50.
9. Lowe, J., *Crystal structure determination of FtsZ from Methanococcus jannaschii*. J Struct Biol, 1998. **124**(2-3): p. 235-43.
10. Mitchison, T.J., *Evolution of a dynamic cytoskeleton*. Philos Trans R Soc Lond B Biol Sci, 1995. **349**(1329): p. 299-304.
11. Mitchison, T.J., *Compare and contrast actin filaments and microtubules*. Mol Biol Cell, 1992. **3**(12): p. 1309-15.
12. Larsen, R.A., et al., *Treadmilling of a prokaryotic tubulin-like protein, TubZ, required for plasmid stability in Bacillus thuringiensis*. Genes Dev, 2007. **21**(11): p. 1340-52.
13. Jenkins, C., et al., *Genes for the cytoskeletal protein tubulin in the bacterial genus Prosthocobacter*. Proc Natl Acad Sci U S A, 2002. **99**(26): p. 17049-54.
14. Schlieper, D., et al., *Structure of bacterial tubulin BtubA/B: evidence for horizontal gene transfer*. Proc Natl Acad Sci U S A, 2005. **102**(26): p. 9170-5.
15. Sontag, C.A., J.T. Staley, and H.P. Erickson, *In vitro assembly and GTP hydrolysis by bacterial tubulins BtubA and BtubB*. J Cell Biol, 2005. **169**(2): p. 233-8.
16. Wickstead, B. and K. Gull, *The evolution of the cytoskeleton*. J Cell Biol. **194**(4): p. 513-25.

17. Artymiuk, P.J., et al., *Three-dimensional structural resemblance between the ribonuclease H and connection domains of HIV reverse transcriptase and the ATPase fold revealed using graph theoretical techniques*. FEBS Lett, 1993. **324**(1): p. 15-21.
18. Dominguez-Escobar, J., et al., *Processive movement of MreB-associated cell wall biosynthetic complexes in bacteria*. Science. **333**(6039): p. 225-8.
19. Garner, E.C., et al., *Coupled, circumferential motions of the cell wall synthesis machinery and MreB filaments in B. subtilis*. Science. **333**(6039): p. 222-5.
20. Bork, P., C. Sander, and A. Valencia, *An ATPase domain common to prokaryotic cell cycle proteins, sugar kinases, actin, and hsp70 heat shock proteins*. Proc Natl Acad Sci U S A, 1992. **89**(16): p. 7290-4.
21. Szwedziak, P., et al., *FtsA forms actin-like protofilaments*. EMBO J. **31**(10): p. 2249-60.
22. Garner, E.C., C.S. Campbell, and R.D. Mullins, *Dynamic instability in a DNA-segregating prokaryotic actin homolog*. Science, 2004. **306**(5698): p. 1021-5.
23. Moller-Jensen, J., et al., *Bacterial mitosis: ParM of plasmid R1 moves plasmid DNA by an actin-like insertional polymerization mechanism*. Mol Cell, 2003. **12**(6): p. 1477-87.
24. Garner, E.C., et al., *Reconstitution of DNA segregation driven by assembly of a prokaryotic actin homolog*. Science, 2007. **315**(5816): p. 1270-4.
25. Orlova, A., et al., *The structure of bacterial ParM filaments*. Nat Struct Mol Biol, 2007. **14**(10): p. 921-6.
26. Ausmees, N., J.R. Kuhn, and C. Jacobs-Wagner, *The bacterial cytoskeleton: an intermediate filament-like function in cell shape*. Cell, 2003. **115**(6): p. 705-13.
27. Cabeen, M.T., et al., *Bacterial cell curvature through mechanical control of cell growth*. EMBO J, 2009. **28**(9): p. 1208-19.
28. Koonin, E.V., *A superfamily of ATPases with diverse functions containing either classical or deviant ATP-binding motif*. J Mol Biol, 1993. **229**(4): p. 1165-74.
29. Sirajuddin, M., et al., *Structural insight into filament formation by mammalian septins*. Nature, 2007. **449**(7160): p. 311-5.
30. Lutkenhaus, J., *Assembly dynamics of the bacterial MinCDE system and spatial regulation of the Z ring*. Annu Rev Biochem, 2007. **76**: p. 539-62.
31. Szeto, T.H., et al., *The MinD membrane targeting sequence is a transplantable lipid-binding helix*. J Biol Chem, 2003. **278**(41): p. 40050-6.
32. Raskin, D.M. and P.A. de Boer, *Rapid pole-to-pole oscillation of a protein required for directing division to the middle of Escherichia coli*. Proc Natl Acad Sci U S A, 1999. **96**(9): p. 4971-6.
33. Raskin, D.M. and P.A. de Boer, *MinDE-dependent pole-to-pole oscillation of division inhibitor MinC in Escherichia coli*. J Bacteriol, 1999. **181**(20): p. 6419-24.

34. Loose, M., et al., *Spatial regulators for bacterial cell division self-organise into surface waves in vitro*. Science, 2008. **320**(5877): p. 789-92.
35. Moller-Jensen, J., R.B. Jensen, and K. Gerdes, *Plasmid and chromosome segregation in prokaryotes*. Trends Microbiol, 2000. **8**(7): p. 313-20.
36. Gerdes, K., J. Moller-Jensen, and R. Bugge Jensen, *Plasmid and chromosome partitioning: surprises from phylogeny*. Mol Microbiol, 2000. **37**(3): p. 455-66.
37. Pratto, F., et al., *Streptococcus pyogenes pSM19035 requires dynamic assembly of ATP-bound ParA and ParB on parS DNA during plasmid segregation*. Nucleic Acids Res, 2008. **36**(11): p. 3676-89.
38. Ebersbach, G. and K. Gerdes, *Bacterial mitosis: partitioning protein ParA oscillates in spiral-shaped structures and positions plasmids at mid-cell*. Mol Microbiol, 2004. **52**(2): p. 385-98.
39. Michie, K.A. and J. Lowe, *Dynamic filaments of the bacterial cytoskeleton*. Annu Rev Biochem, 2006. **75**: p. 467-92.
40. Barilla, D. and F. Hayes, *Architecture of the ParF*ParG protein complex involved in prokaryotic DNA segregation*. Mol Microbiol, 2003. **49**(2): p. 487-99.
41. Golovanov, A.P., et al., *ParG, a protein required for active partition of bacterial plasmids, has a dimeric ribbon-helix-helix structure*. Mol Microbiol, 2003. **50**(4): p. 1141-53.
42. Barilla, D., et al., *Bacterial DNA segregation dynamics mediated by the polymerizing protein ParF*. EMBO J, 2005. **24**(7): p. 1453-64.
43. Marston, A.L. and J. Errington, *Dynamic movement of the ParA-like Soj protein of B. subtilis and its dual role in nucleoid organization and developmental regulation*. Mol Cell, 1999. **4**(5): p. 673-82.
44. Leonard, T.A., P.J. Butler, and J. Lowe, *Bacterial chromosome segregation: structure and DNA binding of the Soj dimer--a conserved biological switch*. EMBO J, 2005. **24**(2): p. 270-82.
45. Hester, C.M. and J. Lutkenhaus, *Soj (ParA) DNA binding is mediated by conserved arginines and is essential for plasmid segregation*. Proc Natl Acad Sci U S A, 2007. **104**(51): p. 20326-31.
46. Thanbichler, M. and L. Shapiro, *MipZ, a spatial regulator coordinating chromosome segregation with cell division in Caulobacter*. Cell, 2006. **126**(1): p. 147-62.
47. Thompson, S.R., G.H. Wadhams, and J.P. Armitage, *The positioning of cytoplasmic protein clusters in bacteria*. Proc Natl Acad Sci U S A, 2006. **103**(21): p. 8209-14.
48. Kiebusch, D., et al., *Localized dimerization and nucleoid binding drive gradient formation by the bacterial cell division inhibitor MipZ*. Mol Cell. **46**(3): p. 245-59.

49. Doolittle, R.F., *The origins and evolution of eukaryotic proteins*. Philos Trans R Soc Lond B Biol Sci, 1995. **349**(1329): p. 235-40.
50. Erickson, H.P., *Evolution of the cytoskeleton*. Bioessays, 2007. **29**(7): p. 668-77.
51. Doolittle, R.F. and A.L. York, *Bacterial actins? An evolutionary perspective*. Bioessays, 2002. **24**(4): p. 293-6.
52. Faguy, D.M. and W.F. Doolittle, *Cytoskeletal proteins: the evolution of cell division*. Curr Biol, 1998. **8**(10): p. R338-41.
53. Becker, E., et al., *DNA segregation by the bacterial actin Alfa during Bacillus subtilis growth and development*. EMBO J, 2006. **25**(24): p. 5919-31.
54. Lutkenhaus, J., *FtsZ ring in bacterial cytokinesis*. Mol Microbiol, 1993. **9**(3): p. 403-9.
55. Lutkenhaus, J. and S.G. Addinall, *Bacterial cell division and the Z ring*. Annu Rev Biochem, 1997. **66**: p. 93-116.
56. Margolin, W., *FtsZ and the division of prokaryotic cells and organelles*. Nat Rev Mol Cell Biol, 2005. **6**(11): p. 862-71.
57. Ishikawa H, K.T., Nagata K, *Encyclopedia of Cell Biology (Asakura Shoten)*. Encyclopedia of Cell Biology (Asakura Shoten). 1950. 159-160.
58. Aarsman, M.E., et al., *Maturation of the Escherichia coli divisome occurs in two steps*. Mol Microbiol, 2005. **55**(6): p. 1631-45.
59. Oliva, M.A., D. Trambaiolo, and J. Lowe, *Structural insights into the conformational variability of FtsZ*. J Mol Biol, 2007. **373**(5): p. 1229-42.
60. Desai, A. and T.J. Mitchison, *Microtubule polymerization dynamics*. Annu Rev Cell Dev Biol, 1997. **13**: p. 83-117.
61. Popp, D., et al., *FtsZ condensates: an in vitro electron microscopy study*. Biopolymers, 2009. **91**(5): p. 340-50.
62. Popp, D., et al., *Suprastructures and dynamic properties of Mycobacterium tuberculosis FtsZ*. J Biol Chem. **285**(15): p. 11281-9.
63. Mingorance, J., et al., *Visualization of single Escherichia coli FtsZ filament dynamics with atomic force microscopy*. J Biol Chem, 2005. **280**(21): p. 20909-14.
64. Adams, D.W. and J. Errington, *Bacterial cell division: assembly, maintenance and disassembly of the Z ring*. Nat Rev Microbiol, 2009. **7**(9): p. 642-53.
65. Addinall, S.G., E. Bi, and J. Lutkenhaus, *FtsZ ring formation in fts mutants*. J Bacteriol, 1996. **178**(13): p. 3877-84.
66. Sun, Q. and W. Margolin, *FtsZ dynamics during the division cycle of live Escherichia coli cells*. J Bacteriol, 1998. **180**(8): p. 2050-6.
67. Stricker, J., et al., *Rapid assembly dynamics of the Escherichia coli FtsZ-ring demonstrated by fluorescence recovery after photobleaching*. Proc Natl Acad Sci U S A, 2002. **99**(5): p. 3171-5.

68. Li, Z., et al., *The structure of FtsZ filaments in vivo suggests a force-generating role in cell division*. EMBO J, 2007. **26**(22): p. 4694-708.
69. Pichoff, S. and J. Lutkenhaus, *Unique and overlapping roles for ZipA and FtsA in septal ring assembly in Escherichia coli*. EMBO J, 2002. **21**(4): p. 685-93.
70. Pichoff, S. and J. Lutkenhaus, *Tethering the Z ring to the membrane through a conserved membrane targeting sequence in FtsA*. Mol Microbiol, 2005. **55**(6): p. 1722-34.
71. Mukherjee, A., C. Saez, and J. Lutkenhaus, *Assembly of an FtsZ mutant deficient in GTPase activity has implications for FtsZ assembly and the role of the Z ring in cell division*. J Bacteriol, 2001. **183**(24): p. 7190-7.
72. Sun, S.X., S. Walcott, and C.W. Wolgemuth, *Cytoskeletal Cross-linking and Bundling in Motor-Independent Contraction*. Curr Biol. **20**(15): p. R649-R654.
73. Allard, J.F. and E.N. Cytrynbaum, *Force generation by a dynamic Z-ring in Escherichia coli cell division*. Proc Natl Acad Sci U S A, 2009. **106**(1): p. 145-50.
74. Erickson, H.P., *Modeling the physics of FtsZ assembly and force generation*. Proc Natl Acad Sci U S A, 2009. **106**(23): p. 9238-43.
75. Lan, G., et al., *Condensation of FtsZ filaments can drive bacterial cell division*. Proc Natl Acad Sci U S A, 2009. **106**(1): p. 121-6.
76. Osawa, M., D.E. Anderson, and H.P. Erickson, *Reconstitution of contractile FtsZ rings in liposomes*. Science, 2008. **320**(5877): p. 792-4.
77. Tamura, M., et al., *RNase E maintenance of proper FtsZ/FtsA ratio required for nonfilamentous growth of Escherichia coli cells but not for colony-forming ability*. J Bacteriol, 2006. **188**(14): p. 5145-52.
78. Dewar, S.J., K.J. Begg, and W.D. Donachie, *Inhibition of cell division initiation by an imbalance in the ratio of FtsA to FtsZ*. J Bacteriol, 1992. **174**(19): p. 6314-6.
79. Dai, K. and J. Lutkenhaus, *The proper ratio of FtsZ to FtsA is required for cell division to occur in Escherichia coli*. J Bacteriol, 1992. **174**(19): p. 6145-51.
80. Leaver, M., et al., *Life without a wall or division machine in Bacillus subtilis*. Nature, 2009. **457**(7231): p. 849-53.
81. Wu, L.J. and J. Errington, *Coordination of cell division and chromosome segregation by a nucleoid occlusion protein in Bacillus subtilis*. Cell, 2004. **117**(7): p. 915-25.
82. Bernhardt, T.G. and P.A. de Boer, *SlmA, a nucleoid-associated, FtsZ binding protein required for blocking septal ring assembly over Chromosomes in E. coli*. Mol Cell, 2005. **18**(5): p. 555-64.
83. de Boer, P.A., R.E. Crossley, and L.I. Rothfield, *A division inhibitor and a topological specificity factor coded for by the minicell locus determine proper placement of the division septum in E. coli*. Cell, 1989. **56**(4): p. 641-9.

84. Szeto, T.H., S.L. Rowland, and G.F. King, *The dimerization function of MinC resides in a structurally autonomous C-terminal domain*. J Bacteriol, 2001. **183**(22): p. 6684-7.
85. Loose, M., K. Kruse, and P. Schwille, *Protein self-organization: lessons from the min system*. Annu Rev Biophys. **40**: p. 315-36.
86. Kovacs, H., et al., *Solution structure of SpoIIAA, a phosphorylatable component of the system that regulates transcription factor sigmaF of Bacillus subtilis*. Proc Natl Acad Sci U S A, 1998. **95**(9): p. 5067-71.
87. van den Ent, F. and J. Lowe, *Crystal structure of the cell division protein FtsA from Thermotoga maritima*. EMBO J, 2000. **19**(20): p. 5300-7.
88. Cordell, S.C., R.E. Anderson, and J. Lowe, *Crystal structure of the bacterial cell division inhibitor MinC*. EMBO J, 2001. **20**(10): p. 2454-61.
89. Hu, Z. and J. Lutkenhaus, *Analysis of MinC reveals two independent domains involved in interaction with MinD and FtsZ*. J Bacteriol, 2000. **182**(14): p. 3965-71.
90. Shen, B. and J. Lutkenhaus, *Examination of the interaction between FtsZ and MinCN in E. coli suggests how MinC disrupts Z rings*. Mol Microbiol. **75**(5): p. 1285-98.
91. Shen, B. and J. Lutkenhaus, *The conserved C-terminal tail of FtsZ is required for the septal localization and division inhibitory activity of MinC(C)/MinD*. Mol Microbiol, 2009. **72**(2): p. 410-24.
92. Dajkovic, A., et al., *MinC spatially controls bacterial cytokinesis by antagonizing the scaffolding function of FtsZ*. Curr Biol, 2008. **18**(4): p. 235-44.
93. Hu, Z., et al., *The MinC component of the division site selection system in Escherichia coli interacts with FtsZ to prevent polymerization*. Proc Natl Acad Sci U S A, 1999. **96**(26): p. 14819-24.
94. Pichoff, S. and J. Lutkenhaus, *Escherichia coli division inhibitor MinCD blocks septation by preventing Z-ring formation*. J Bacteriol, 2001. **183**(22): p. 6630-5.
95. Arumugam, S., G. Chwastek, and P. Schwille, *Protein-membrane interactions: the virtue of minimal systems in systems biology*. Wiley Interdiscip Rev Syst Biol Med. **3**(3): p. 269-80.
96. Misteli, T., *The concept of self-organization in cellular architecture*. J Cell Biol, 2001. **155**(2): p. 181-5.
97. Osawa, M., D.E. Anderson, and H.P. Erickson, *Curved FtsZ protofilaments generate bending forces on liposome membranes*. EMBO J, 2009. **28**(22): p. 3476-84.
98. Rasnik, I., S.A. McKinney, and T. Ha, *Nonblinking and long-lasting single-molecule fluorescence imaging*. Nat Methods, 2006. **3**(11): p. 891-3.
99. Helenius, J., et al., *The depolymerizing kinesin MCAK uses lattice diffusion to rapidly target microtubule ends*. Nature, 2006. **441**(7089): p. 115-9.

100. Haustein, E. and P. Schwill, *Fluorescence correlation spectroscopy: novel variations of an established technique*. *Annu Rev Biophys Biomol Struct*, 2007. **36**: p. 151-69.
101. Kask, P., et al., *Fluorescence-intensity distribution analysis and its application in biomolecular detection technology*. *Proc Natl Acad Sci U S A*, 1999. **96**(24): p. 13756-61.
102. Tamm, L.K. and H.M. McConnell, *Supported phospholipid bilayers*. *Biophys J*, 1985. **47**(1): p. 105-13.
103. Crane, J.M. and L.K. Tamm, *Fluorescence microscopy to study domains in supported lipid bilayers*. *Methods Mol Biol*, 2007. **400**: p. 481-8.
104. Richter, R.P., R. Berat, and A.R. Brisson, *Formation of solid-supported lipid bilayers: an integrated view*. *Langmuir*, 2006. **22**(8): p. 3497-505.
105. Groves, J.T., R. Parthasarathy, and M.B. Forstner, *Fluorescence imaging of membrane dynamics*. *Annu Rev Biomed Eng*, 2008. **10**: p. 311-38.
106. Anderson, D.E., F.J. Gueiros-Filho, and H.P. Erickson, *Assembly dynamics of FtsZ rings in Bacillus subtilis and Escherichia coli and effects of FtsZ-regulating proteins*. *J Bacteriol*, 2004. **186**(17): p. 5775-81.
107. Bramhill, D. and C.M. Thompson, *GTP-dependent polymerization of Escherichia coli FtsZ protein to form tubules*. *Proc Natl Acad Sci U S A*, 1994. **91**(13): p. 5813-7.
108. Lowe, J. and L.A. Amos, *Tubulin-like protofilaments in Ca²⁺-induced FtsZ sheets*. *EMBO J*, 1999. **18**(9): p. 2364-71.
109. Lowe, J. and L.A. Amos, *Helical tubes of FtsZ from Methanococcus jannaschii*. *Biol Chem*, 2000. **381**(9-10): p. 993-9.
110. Yu, X.C. and W. Margolin, *Ca²⁺-mediated GTP-dependent dynamic assembly of bacterial cell division protein FtsZ into asters and polymer networks in vitro*. *EMBO J*, 1997. **16**(17): p. 5455-63.
111. Erickson, H.P., D.E. Anderson, and M. Osawa, *FtsZ in bacterial cytokinesis: cytoskeleton and force generator all in one*. *Microbiol Mol Biol Rev*. **74**(4): p. 504-28.
112. Chen, Y. and H.P. Erickson, *Rapid in vitro assembly dynamics and subunit turnover of FtsZ demonstrated by fluorescence resonance energy transfer*. *J Biol Chem*, 2005. **280**(23): p. 22549-54.
113. Oliva, M.A., et al., *Assembly of archaeal cell division protein FtsZ and a GTPase-inactive mutant into double-stranded filaments*. *J Biol Chem*, 2003. **278**(35): p. 33562-70.
114. Mingorance, J., et al., *Escherichia coli FtsZ polymers contain mostly GTP and have a high nucleotide turnover*. *Mol Microbiol*, 2001. **41**(1): p. 83-91.

115. Gonzalez, J.M., et al., *Essential cell division protein FtsZ assembles into one monomer-thick ribbons under conditions resembling the crowded intracellular environment*. J Biol Chem, 2003. **278**(39): p. 37664-71.
116. Tadros, M., et al., *Activation of the Escherichia coli cell division protein FtsZ by a low-affinity interaction with monovalent cations*. FEBS Lett, 2006. **580**(20): p. 4941-6.
117. Bi, E. and J. Lutkenhaus, *Cell division inhibitors Sula and MinCD prevent formation of the FtsZ ring*. J Bacteriol, 1993. **175**(4): p. 1118-25.
118. Dajkovic, A., A. Mukherjee, and J. Lutkenhaus, *Investigation of regulation of FtsZ assembly by Sula and development of a model for FtsZ polymerization*. J Bacteriol, 2008. **190**(7): p. 2513-26.
119. Mukherjee, A., C. Cao, and J. Lutkenhaus, *Inhibition of FtsZ polymerization by Sula, an inhibitor of septation in Escherichia coli*. Proc Natl Acad Sci U S A, 1998. **95**(6): p. 2885-90.
120. Trusca, D., et al., *Bacterial SOS checkpoint protein Sula inhibits polymerization of purified FtsZ cell division protein*. J Bacteriol, 1998. **180**(15): p. 3946-53.
121. Rothfield, L., A. Taghbalout, and Y.L. Shih, *Spatial control of bacterial division-site placement*. Nat Rev Microbiol, 2005. **3**(12): p. 959-68.
122. Nogales, E., et al., *Tubulin and FtsZ form a distinct family of GTPases*. Nat Struct Biol, 1998. **5**(6): p. 451-8.
123. Romberg, L. and T.J. Mitchison, *Rate-limiting guanosine 5'-triphosphate hydrolysis during nucleotide turnover by FtsZ, a prokaryotic tubulin homologue involved in bacterial cell division*. Biochemistry, 2004. **43**(1): p. 282-8.
124. Chen, Y. and H.P. Erickson, *FtsZ filament dynamics at steady state: subunit exchange with and without nucleotide hydrolysis*. Biochemistry, 2009. **48**(28): p. 6664-73.
125. Mateos-Gil, P., et al., *Depolymerization dynamics of individual filaments of bacterial cytoskeletal protein FtsZ*. Proc Natl Acad Sci U S A. **109**(21): p. 8133-8.
126. Dai, K., et al., *Mutations in ftsZ that confer resistance to Sula affect the interaction of FtsZ with GTP*. J Bacteriol, 1994. **176**(1): p. 130-6.
127. Shih, Y.L. and L. Rothfield, *The bacterial cytoskeleton*. Microbiol Mol Biol Rev, 2006. **70**(3): p. 729-54.
128. Horger, I., et al., *FtsZ bacterial cytoskeletal polymers on curved surfaces: the importance of lateral interactions*. Biophys J, 2008. **94**(11): p. L81-3.
129. Paez, A., et al., *Simple modeling of FtsZ polymers on flat and curved surfaces: correlation with experimental in vitro observations*. PMC Biophys, 2009. **2**(1): p. 8.
130. Andrews, S.S. and A.P. Arkin, *A mechanical explanation for cytoskeletal rings and helices in bacteria*. Biophys J, 2007. **93**(6): p. 1872-84.

131. Fischer-Friedrich, E., B.M. Friedrich, and N.S. Gov, *FtsZ rings and helices: physical mechanisms for the dynamic alignment of biopolymers in rod-shaped bacteria*. *Phys Biol*. **9**(1): p. 016009.
132. Yu, X.C. and W. Margolin, *FtsZ ring clusters in min and partition mutants: role of both the Min system and the nucleoid in regulating FtsZ ring localization*. *Mol Microbiol*, 1999. **32**(2): p. 315-26.
133. Fu, G., et al., *In vivo structure of the E. coli FtsZ-ring revealed by photoactivated localization microscopy (PALM)*. *PLoS One*. **5**(9): p. e12682.
134. Chen, Y., et al., *A rapid fluorescence assay for FtsZ assembly indicates cooperative assembly with a dimer nucleus*. *Biophys J*, 2005. **88**(1): p. 505-14.
135. Huecas, S., et al., *Energetics and geometry of FtsZ polymers: nucleated self-assembly of single protofilaments*. *Biophys J*, 2008. **94**(5): p. 1796-806.
136. Turner, D.J., et al., *The Mechanics of FtsZ Fibers*. *Biophys J*. **102**(4): p. 731-8.
137. Hamon, L., et al., *Mica surface promotes the assembly of cytoskeletal proteins*. *Langmuir*, 2009. **25**(6): p. 3331-5.
138. Rothfield, L., S. Justice, and J. Garcia-Lara, *Bacterial cell division*. *Annu Rev Genet*, 1999. **33**: p. 423-48.
139. Goley, E.D., et al., *Imaging-based identification of a critical regulator of FtsZ protofilament curvature in Caulobacter*. *Mol Cell*. **39**(6): p. 975-87.
140. Angert, E.R. and R.M. Losick, *Propagation by sporulation in the guinea pig symbiont Metabacterium polyspora*. *Proc Natl Acad Sci U S A*, 1998. **95**(17): p. 10218-23.
141. Robinow, C. and E.R. Angert, *Nucleoids and coated vesicles of "Epulopiscium" spp.* *Arch Microbiol*, 1998. **170**(4): p. 227-35.
142. Yoshida, Y., et al., *Isolated chloroplast division machinery can actively constrict after stretching*. *Science*, 2006. **313**(5792): p. 1435-8.
143. Osteryoung, K.W. and J. Nunnari, *The division of endosymbiotic organelles*. *Science*, 2003. **302**(5651): p. 1698-704.
144. Sato, M., et al., *Conserved relationship between FtsZ and peptidoglycan in the cyanelles of Cyanophora paradoxa similar to that in bacterial cell division*. *Planta*, 2007. **227**(1): p. 177-87.
145. Yoshida, Y., et al., *Chloroplasts divide by contraction of a bundle of nanofilaments consisting of polyglucan*. *Science*. **329**(5994): p. 949-53.
146. Wang, X. and J. Lutkenhaus, *Characterization of the ftsZ gene from Mycoplasma pulmonis, an organism lacking a cell wall*. *J Bacteriol*, 1996. **178**(8): p. 2314-9.
147. Fraser, C.M., et al., *The minimal gene complement of Mycoplasma genitalium*. *Science*, 1995. **270**(5235): p. 397-403.
148. Sprague, B.L., et al., *Analysis of binding reactions by fluorescence recovery after photobleaching*. *Biophys J*, 2004. **86**(6): p. 3473-95.

Acknowledgements:

I would like to thank my PhD advisor, Prof. Petra Schwille, for guiding me through the project during the last four years. I express my gratitude for having faith in me through difficult times. She has also been very supportive and has given me the freedom to pursue various projects without objection. She has been a great mentor during the last four years.

I also thank Prof. Joe Howard and Dr. Stephan Grill, who, as my thesis committee members, have been great critics which eventually laid the trail for the work in the thesis. I hope that I could be as critical and practical in my scientific career someday.

I thank Prof. Harold Erickson and Prof. William Margolin for the plasmids used extensively in this thesis. I would also like to thank Prof. William Margolin, Prof. David Sheratt, Dr. Paola Bissichia and Prof. German Rivas for discussions on the project during their visits to Dresden.

I would also like to thank Dr. David Drechsel, who came to rescue for something I never did in my life: protein purification. I also thank him for various insights and chats on the project. Dr. Thomas Kurth was very helpful with the electron microscopy. I would like to express my gratitude and appreciation for Dr. Zdenek Petrasek, who was very helpful in analysis of the results, and in various discussions. I thank him for his persistence to work with me even after a dozen dead ends. I would also like to thank Dr. Elisabeth Fischer-Friedrich, who worked with me on the modelling of curved filaments.

I would like to thank all the technicians in the lab – Karin Crell, Ellen, Anke, Sabine and Sarah, without whom the work wouldn't have proceeded at the pace it has. I would also like to thank Dr. Ariadna Martos, who was very helpful with all the discussions, and managing the protein purifications in the lab. It was great pleasure working with her on the FtsA-FtsZ project.

I would like to thank my 2iC – Grzegorz Chwastek, who performed the AFM measurements almost single handily. It was also a great joy to write a review with him at a time when we thought we were aimless. It was a great pleasure having Carina Schäfer, now Ehrig, as a diploma student working on the curved substrate. It was also a joy working with Robert Weinmeister and Paul Müller and sharing the optical setup.

I would also like to thank the organisers, funders and various scientists of the Physiology course at Woodshole, especially Dyche Mullins, Clare Waterman, David Odde and James Nelson who've taught me, and inspired me in many ways.

I would like to thank Dr. Eugene Petrov for his frequent company to beer hours. His wicked humour will be forever etched in my memories. I also express my gratitude for taking interest in various scientific details of my PhD project, as well as other interesting facts of life. I would also like to thank Dr. Thomas Weidemann and Dr. Remiguisz Worch for general discussions, help and advices with various things. I thank all the earlier members on the Schwille group – Dr. Jonas Ries, Dr. Salvatore Chiantia

and Dr. Ana Garcia, who were very welcoming and helpful during my early months in the lab. I thank all the members of Schwille lab for being very helpful and ensuring a fun-filled time during my stay here. I thank Christoph and Janine for translating the abstract.

Without Annett Dümmler, life in Dresden wouldn't have been as easy; I express my thanks to her for helping me with a variety of things – apartments, random bills and other issues. I will forever cherish the memories of the longest bike ride I ever had over the hills of Dresden, hikes on Sächsische Schweiz, cross country skiing to the Czech border for beer and the football world cup at the Fährgarten by the Elbe.

I would like to thank my long list of friends in Dresden – Remi and Guciu with whom I had my first spiritual session in Dresden. I can never forget the taste of pickled cucumber for my entire life. I thank Guciu for all the voltages exchanged. I am grateful to him for turning what could have been a cold lonely winter into a very warm, joyable affair by inviting us to his family in Dzierżewice, Poland. I thank Sundar, Erdinc, Jens, Carina, Viktoria, Alex and Maya for being the support system in Dresden and ready to help whenever needed. It was also a pleasure enjoying futsal with the league.

I would also like to thank 'Ring of Fire', the ultimate Frisbee group - playing with them through the last four years was a great pleasure. I am glad I started playing Ultimate and I am thankful to Ana for introducing me to it.

As ever, my thesis would have been incomplete without being proof read by Angika. I would like to thank Angika and Kamalika who read this thesis even as they were busy with their own graduate studies. I also thank them for sending numerous scientific articles inaccessible here. I thank many other friends (the list is long, you know who you are!) for being there, hosting me during my visits and helping out in need. I am sure the gratitude can be expressed later in the right spirits.

No words are enough for my hard working parents, who have sacrificed half of their lives raising me, educating me and doing everything they could. Love and affection from my parents and Karthic continues to inspire me. Life wouldn't have been half as easy without my dear wife, who continues to stand by me and stand me even if I was irritable many times. We both have learnt a lot about life, found great friends in here and Dresden. Dresden will always be a cherished part of our lives.

Erklärung entsprechend §5.5 der Promotionsordnung

Hiermit versichere ich, dass ich die vorliegende Arbeit ohne unzulässige Hilfe Dritter und ohne Benutzung anderer als der angegebenen Hilfsmittel angefertigt habe; die aus fremden Quellen direkt oder indirekt übernommenen Gedanken sind als solche kenntlich gemacht. Die Arbeit wurde bisher weder im Inland noch im Ausland in gleicher oder ähnlicher Form einer anderen Prüfungsbehörde vorgelegt.

*Die Dissertation wurde im Zeitraum vom **August 1, 2008** bis **July 30, 2012** verfasst und von **Prof. Dr. Petra Schwille, TU Dresden, Biotechnologischen Zentrum der TU Dresden** betreut.*

Meine Person betreffend erkläre ich hiermit, dass keine früheren erfolglosen Promotionsverfahren stattgefunden haben.

Ich erkenne die Promotionsordnung der Fakultät für Mathematik und Naturwissenschaften, Technische Universität Dresden an.

Declaration according to §5.5 of the doctorate regulations

I herewith declare that I have produced this paper without the prohibited assistance of third parties and without making use of aids other than those specified; notions taken over directly or indirectly from other sources have been identified as such. This paper has not previously been presented in identical or similar form to any other German or foreign examination board.

*The thesis work was conducted from **August 1, 2008** to **July 30, 2012** under the supervision of **Prof. Dr. Petra Schwille, TU Dresden at Biotechnology Center of the TU Dresden**.*

I declare that I have not undertaken any previous unsuccessful doctorate proceedings.

I declare that I recognize the doctorate regulations of the Fakultät für Mathematik und Naturwissenschaften of the Technische Universität Dresden.

Senthil Arumugam

